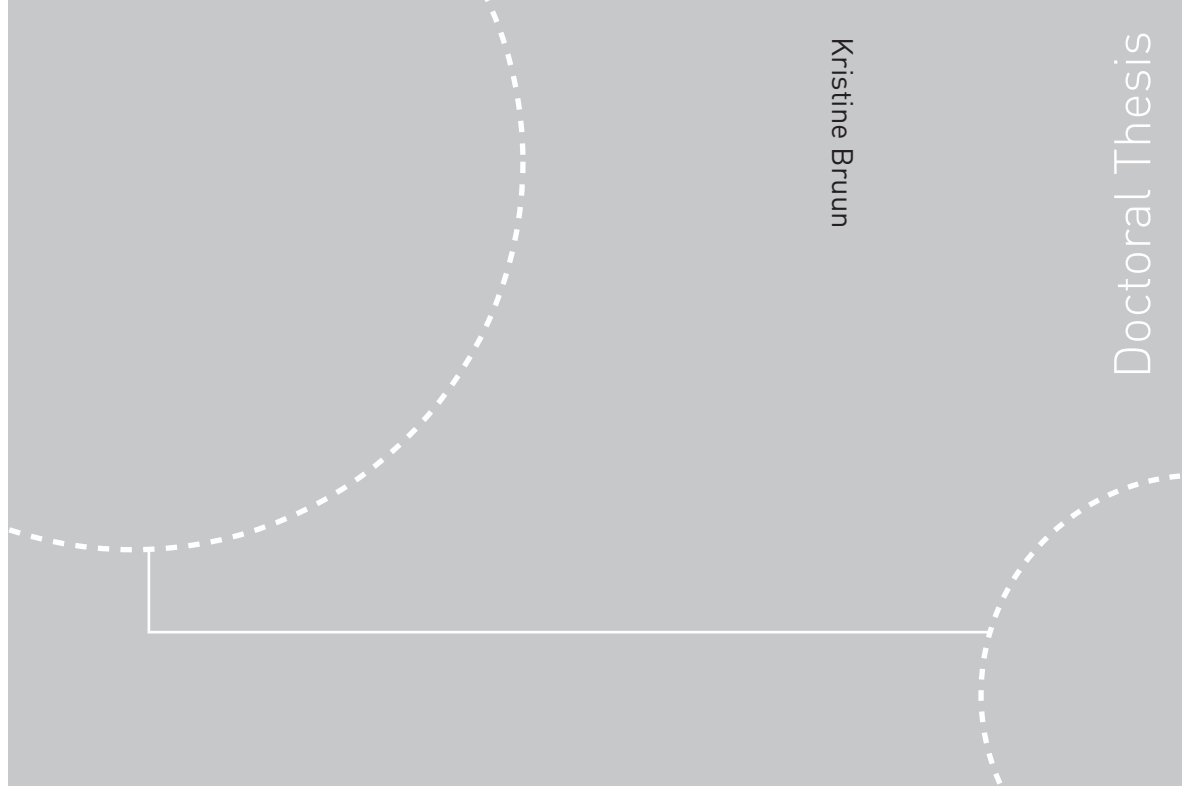


Doctoral theses at NTNU, 2009:161

Kristine Bruun

Bond Graph Modelling of Fuel Cells for Marine Power Plants



ISBN 978-82-471-1715-6 (printed ver.)
ISBN 978-82-471-1716-3 (electronic ver.)
ISSN 1503-8181

Doctoral theses at NTNU, 2009:161

NTNU
Norwegian University of
Science and Technology
Thesis for the degree of
philosophiae doctor
Faculty of Engineering Science and Technology
Department of Marine Technology



Kristine Bruun

Bond Graph Modelling of Fuel Cells for Marine Power Plants

Thesis for the degree of philosophiae doctor

Trondheim, September 2009

Norwegian University of
Science and Technology
Faculty of Engineering Science and Technology
Department of Marine Technology



NTNU

Norwegian University of
Science and Technology

NTNU
Norwegian University of Science and Technology

Thesis for the degree of philosophiae doctor

Faculty of Engineering Science and Technology
Department of Marine Technology

©Kristine Bruun

ISBN 978-82-471-1715-6 (printed ver.)
ISBN 978-82-471-1716-3 (electronic ver.)
ISSN 1503-8181

Doctoral Theses at NTNU, 2009:161

Printed by Tapir Uttrykk

Abstract

There is a constant search for alternative solutions improving the fuel efficiency and environmental impact of marine power plants. Fuel cells are regarded as a potential future candidate for significantly reducing pollution from such systems. In this thesis a bond graph template for mathematical modelling of fuel cells is developed. To show the applicability of this template, models of a solid oxide fuel cell (SOFC) system are implemented and simulations carried out. The models are intended for analyses of marine power production in overall ship system applications.

The models developed in this thesis can simulate the transient behaviour of a SOFC. These models are developed from fundamental physical relations, resulting in an improved understanding of the high temperature fuel cell, its possibilities and limitations, in the overall power plant. Fuel cells increase the system complexity, and the template provides an important tool for evaluating system performance under various operating conditions.

Main findings of this thesis are;

- Bond graphs are identified as a good tool for the multi-domain nature of fuel cell modelling. Pseudo-bond graphs are chosen to model thermofluid properties while true bond graphs are the choice for electrochemical and electrical domains.
- A new bond graph element (*R*-field) is developed, enabling a straight forward conversion between the thermofluid and electrochemical domains.
- By expanding the lumped model approach, a new type of model is developed enabling simulations of distributed characteristics inside the fuel cell. Typical distributed variables of interest are pressure, temperature and concentration of gas components.
- The bond graph tool strongly supports the model implementation process when evaluating different ways of representing electrochemical losses. The resulting models are of complete integral causality, lending themselves to computationally efficient system simulations.

Component models of the gas supply system is also developed and implemented, permitting simulations of the fuel cell stack under realistic operating conditions. Both the fuel cell template and the support system components provide a basis for implementing other types of fuel cells using the bond graph language.

Acknowledgements

This thesis is submitted to complete the requirements for the degree of philosophiae doctor (PhD) at the Norwegian University of Science and Technology (NTNU). The research was funded by The Norwegian Research Council as part of the project Energy Efficient All-Electric Ship (EEAES), and carried out at the Department of Marine Technology in the period from August 2003 through September 2008.

First of all I want to express sincere gratitude to my supervisor Associate Professor Eilif Pedersen for guiding me through these years of research. Our discussions were particularly important helping me see the value of my contributions and setting direction for the final result. I would also like to thank my colleagues at Tyholt for their friendship and support during my time there. Special thanks to Tom Arne Pedersen for constructive discussions on modelling and simulation.

Completion of this thesis was made possible by the support from my parents Berit and Thorleif, and parents-in-law Eva and Rolf. Their willingness to spend their leisure looking after our daughter Lill Synnøve was an enormous help. Gratitude also goes to my current employer Det Norske Veritas for their patience with my situation.

Finally, I want to thank my husband Martin Ludvigsen for convincing me to do a PhD. Your constant support and ability to understand the inevitable frustration of research is continuously appreciated.

Oslo, April 2009

Kristine Bruun

Contents

ABSTRACT	I
ACKNOWLEDGEMENTS	III
NOMENCLATURE	VII
CHAPTER 1 INTRODUCTION	1
1.1 MARINE POWER PLANTS.....	2
1.1.1 Electric propulsion	2
1.1.2 Prime movers.....	3
1.1.3 Combined power plants.....	5
1.1.4 Status of fuel cells in marine applications	7
1.2 PROJECT DESCRIPTION	10
1.3 MAIN CONTRIBUTIONS	11
1.4 ORGANISATION OF THE THESIS.....	11
CHAPTER 2 DYNAMIC MODELLING OF PRIME MOVERS	13
2.1 ENGINE MODELLING FOR MARINE APPLICATIONS	13
2.2 FUEL CELL MODELLING, SOFC	15
CHAPTER 3 MODELLING THEORY	19
3.1 DYNAMIC MODELLING OF THERMOFLUID PROCESSES	19
3.1.1 Languages for model implementation	21
3.2 BOND GRAPHS FOR THERMOFLUID SYSTEMS.....	23
3.2.1 Bond graphs for chemical reactions	29
3.2.2 Bond graphs for electrochemical reactions	34
CHAPTER 4 BOND GRAPH MODELLING OF A SOFC STACK	37
4.1 SYSTEM DESCRIPTION	37
4.2 THE SOLID OXIDE FUEL CELL MODEL.....	41
4.2.1 Gas supply model	43
4.2.2 Heat transfer model.....	46
4.2.3 Electrochemical model	48
4.2.4 Resulting bond graph model.....	55
4.3 DISTRIBUTED FUEL CELL MODEL.....	60
4.4 SUPPORT SYSTEM MODELS	64
4.4.1 Ejector	64
4.4.2 Reformers.....	65
4.4.3 Valve	67

4.4.4	Afterburner	67
4.4.5	Heat exchanger.....	69
4.4.6	Electric output power	70
4.5	CONTROL OF SOFC SYSTEMS.....	71
CHAPTER 5 SIMULATIONS.....		73
5.1	THE DESIGN CASE.....	74
5.2	STEADY STATE PERFORMANCE	76
5.2.1	Lumped model.....	76
5.2.2	Distributed model.....	78
5.3	TRANSIENT SIMULATIONS.....	85
5.3.1	Behaviour of single cell models.....	85
5.3.2	Total system behaviour.....	92
5.3.3	Distributed characteristics at part load.....	97
CHAPTER 6 CONCLUSIONS AND FURTHER WORK.....		101
6.1	CONCLUSIONS	101
6.2	FURTHER WORK	102
BIBLIOGRAPHY.....		105
APPENDIX A THE BOND GRAPH METHOD		A1
APPENDIX B MODEL PARAMETERS		B1
APPENDIX C THERMODYNAMIC RELATIONS.....		C1
C.1	THERMAL PROPERTIES.....	C1

Nomenclature

Abbreviations

AC	Alternating current
ADT	Air delivery tube
AES	All electric ship
AFC	Alkaline fuel cell
CC	Combined cycle
CDL	Charge double layer
CFD	Computational fluid dynamics
CODAG	Combined diesel and gas turbine
COGES	Combined gas turbine and steam turbine-electric
CPP	Combined power plant
DC	Direct current
FEM	Finite element method
HTFC	High temperature fuel cells
IC	Internal combustion
IMO	International maritime organization
LNG	Liquid natural gas
MCFC	Molten carbonate fuel cell
MEA	Membrane electrolyte assembly
NS	Not specified
ODE	Ordinary differential equations
PDE	Partial differential equations
PEM	Polymer electrolyte membrane
SOFC	Solid oxide fuel cell
SOFC/GT	SOFC in combination with gas turbine
TPB	Triple phase boundary

Variables

A	[J]	Helmholtz free energy
A	[J/mol]	Affinity for gas mixture
A	[m ²]	Area, cross sectional
A_{el}	[m ²]	Active surface area of fuel cell
c_v	[J/kgK]	Heat capacity, constant volume
c_p	[J/kgK]	Heat capacity, constant pressure
c_i	[-]	Mass fraction of component i
\mathbf{c}	[-]	Vector of mass fractions

C	[NS]	Bond graph capacitance factor
C_d	[-]	Flow coefficient, nozzle equation
d	[m]	Diameter
d_{hyd}	[m]	Hydraulic diameter
$D_{i,j}$	[m ² /s]	Binary diffusion coefficient of component i through gas j
$D_{K,i}$	[m ² /s]	Knudsen diffusion coefficient for component i
$D_{eff,i}$	[m ² /s]	Effective diffusion coefficient for comp. i through electrode
e	[NS]	Effort, bond graph power variable
E	[J]	Energy
E_{act}	[J/mol]	Activation energy for chemical reaction
\dot{E}	[W]	Energy flow
f	[NS]	Flow, bond graph power variable
f_l	[-]	Friction factor
F	[N]	Force
F	[C/mol]	Faraday constant (96485.3)
g	[J/mol]	Molar Gibbs energy
G	[J]	Gibbs free energy
h	[W/m ² K]	Heat transfer coefficient
h_i	[J/mol]	Molar enthalpy of component i
H	[J]	Enthalpy
\dot{H}	[W]	Enthalpy flow
i	[A]	Current
I	[NS]	Bond graph inertia factor
j	[A/m ²]	Current density
j_0	[A/m ²]	Exchange current density
J	[mol/s]	Chemical reaction rate
J_i	[mol/m ² s]	Molar flux of component i
k	[W/mK]	Thermal conductivity, heat exchanger
k_f	[-]	Forward reaction rate coefficient
k_b	[-]	Backward reaction rate coefficient
$K_{ig,e}$	[-]	Equilibrium constant, ideal gas mixture
K	[-]	Empiric constant
l	[m]	Length, axial direction
m	[NS]	Bond graph transformer modulus
m	[kg]	Mass
\dot{m}	[kg/s]	Mass flow
\dot{m}_i	[kg/s]	Mass flow of component i
M_i	[kg/mol]	Molar mass of component i
n	[-]	Charge transfer number (n=2 for a oxygen ion)
n	[mol]	Moles

\dot{n}_i	[mole/s]	Molar flow of component i
n_{cells}	[-]	Number of cells
Nu	[-]	Nusselt number
P	[NS]	Generalised momentum
P	[-]	Number of products of a chemical reaction
p_j	[-]	Molecule name of product j of a chemical reaction
P	[Pa]	Pressure
P_0	[Pa]	Reference pressure (1 bar=1e ⁵ Pa)
$P_{i/j}$	[Pa]	Partial pressure component i or j
P	[W]	Power
P	[m]	Wetted perimeter
PR	[-]	Degree of prereforming
q	[NS]	Generalised displacement
\dot{Q}	[W]	Heat flow
r	[NS]	Bond graph gyrator modulus
r	[-]	Number of reactants of a chemical reaction
r_i	[-]	Molecule name of reactant i of a chemical reaction
r_{por}	[m]	Pore radius
r_i	[m]	Inner radius of tube
r_o	[m]	Outer radius of tube
R	[NS]	Bond graph resistance factor
R	[J/moleK]	Universal gas constant (8.3144)
R_{re}	[-]	Reynolds number
R_{Ω}	[Ω]	Ohmic resistance factor
R_d	[Ω]	Degradation factor
s_i	[J/moleK]	Molar entropy of component i
S	[J/K]	Entropy
\dot{S}_{sen}	[W/K]	Irreversible entropy
t_i	[m]	Thickness solid/gas layer i
T	[K]	Temperature
u	[m/s]	Velocity
U	[J]	Internal energy
v	[m/s]	Velocity
v_{ri}	[-]	Stoichiometric constant of chemical reaction, reactant i
v_{pj}	[-]	Stoichiometric constant of chemical reaction, product j
V	[m ³]	Volume
V_i	[m ³]	Diffusion volume for component i
V	[V]	Voltage
V_r	[V]	Reversible voltage
\dot{V}	[m ³ /s]	Volume flow

\dot{W}	[J/s]	External work
y_i	[-]	Molar fraction
z	[-]	Charge transfer number ($z=4$ for a oxygen molecule)

Greek letters

β	[-]	Charge transfer coefficient
Δ	[-]	Difference between two variables
ε	[-]	Surface emissivity
$\varepsilon_{A/C}$	[-]	Porosity anode/cathode
$\gamma_{A/C}$	[-]	Empiric factor anode/cathode
μ_i	[J/mole]	Chemical potential of component i
μ	[kg/ms]	Dynamic viscosity
η	[V]	Overvoltage/ voltage loss
ρ	[kg/m ³]	Mass density
σ_B	[W/m ² K ⁴]	Stefan-Boltzmann constant ($5.67 \cdot 10^{-8}$)
λ	[W/mK]	Thermal conductivity
δ	[m]	Thickness of electrodes, electrolyte or interconnect
$\tau_{A/C}$	[-]	Tortuosity anode/cathode

Indexes

0	Reference state conditions	<i>in</i>	Input to element
<i>act</i>	Activation	<i>I</i>	Interconnect
<i>A</i>	Anode	<i>j</i>	Component j
<i>ADT</i>	Air delivery tube	<i>loss</i>	Loss
<i>Air</i>	Air	<i>MEA</i>	Membrane electrolyte assembly
<i>B</i>	Bulk (uniform volume)	<i>out</i>	Output from element
<i>C</i>	Cathode	<i>r</i>	Reforming reaction
<i>conv</i>	Convection	<i>r</i>	Reversible
<i>d</i>	Downstream	<i>recycle</i>	Recycled gas
<i>diff</i>	Diffusion	<i>rad</i>	Radiating heat
<i>el</i>	Electrical	<i>s</i>	Shift reaction
<i>Exh</i>	Exhaust	<i>tot</i>	Total
<i>E</i>	Electrolyte	<i>TPB</i>	Triple phase boundary
<i>Fu</i>	Fuel	<i>u</i>	Upstream
<i>gas</i>	Gas	<i>wall</i>	Solid wall
<i>HE</i>	Heat exchanger	Ω	Ohm
<i>i</i>	Component i		

Chapter 1

Introduction

This thesis considers methods to evaluate the performance of new components in marine power plants. Modern technology has reached a high level of energy efficiency for conventional machinery systems. However, the rate of this development has diminished as we approach the physical limits of some of the existing technologies. Engineers therefore seek to investigate alternative components and configurations. At the same time, ship-owners and advanced shipyards are placing great emphasis on the cost-effectiveness and reliability of new machinery systems. Hence, methodology for performance evaluation is essential when introducing new solutions.

Machinery arrangements found on board most vessels today can be divided in two main categories. The first category has a two-stroke low-speed diesel engine with a directly driven propeller. The second category has medium-speed four-stroke diesel engines connected to the propeller through gears and shafting. Even though these diesel engine technologies can achieve efficiencies slightly above 50%, their environmental impact is significant. Efforts to lower emissions of sulphur and nitrogen oxides have had high priority, but in general these methods lower the overall energy efficiency (AEA 2008). For diesel engines, significant improvements or alternative solutions must therefore be introduced to meet forthcoming environmental regulations in shipping (IMO 2008).

Alternative machinery arrangements will consist of components such as gas engines, gas- and steam-turbines, free-piston engines or fuel cells. New types of fuels will also be introduced to reduce emissions. Efficiency can be improved by for example cogeneration of heat, or by combining multiple components with different power characteristics. Electric propulsion facilitates the introduction of such solutions. The fuel cell promise high energy efficiency, and is one of few components with a zero-emission potential, but suffer from being an immature technology. More research on the physical behaviour of fuel cells in marine power plants is therefore necessary.

The main contribution of this thesis is a template for mathematical modelling of fuel cells. Resulting models are capable of simulating the dynamic behaviour of fuel cells in a machinery system. A solid oxide fuel cell is implemented for simulations

of its physical behaviour. The bond graph method is used for model implementation, resulting in a well defined framework for future developments.

1.1 Marine power plants

In this context, a marine power plant is defined as the power production and main distribution of power on board a seagoing vessel. Engines are prime movers converting power from chemical energy to the mechanical energy of rotating shafts. This energy is utilised by propellers and support systems such as water and lube oil pumps, or converted to electricity by generators. Thermal energy from exhaust gas and cooling water may be utilised for heating purposes onboard, improving the efficiency of the power plant.

1.1.1 Electric propulsion

Electric propulsion systems distribute power to the propeller through electric cabling, allowing for more flexibility in design of ship machinery arrangements. Other advantages with electric propulsion are; optimized loading of prime movers, reduced maintenance, reduced vulnerability to single failure and less noise and vibrations (Ådnanes 2003). The idea is more than 100 years old, but has gained increased focus due to improvements within the electric generator and motor technology. The concept of all electric ship (AES) has been subject to extensive research during the last decades, particularly in military applications (Little, Young et al. 2003).

Costs related to design and installation of electric propulsion are higher than for conventional systems. Today, increased investment costs can only be justified for vessels with a need for multiple prime movers. Large variations in power demand or specific requirements for redundancy can typically cause such needs. Comprehensive research is ongoing to lower component costs and improve system efficiency of electric propulsion systems. The project “Energy Efficient All Electric Ship” addresses questions regarding design and optimization of the energy production and consumption systems onboard (EE-AES 2003). Optimised energy management can increase system efficiency as outlined in (Radan 2008). Increased system understanding can be achieved through development of mathematical models (Pedersen 2009). New ways to integrate and control large consumers such as propellers may also increase the benefits of electric propulsion (Smogeli 2006).

Alternative designs for mechanical and thermal power production also have potential for increasing the market share of electric propulsion in ships. It is hard to perform better than the diesel engine in terms of mechanical or electrical efficiency. However, alternative concepts can be able to compete in terms of optimising overall thermal efficiency. Figure 1.1 gives a schematic description of the total power plant in an electric propulsion system, and shows how a range of configurations are possible. For vessels having special requirements regarding vibration or noise levels, fast power response or special restrictions on emissions, electric propulsion will allow for a more optimal machinery arrangement.

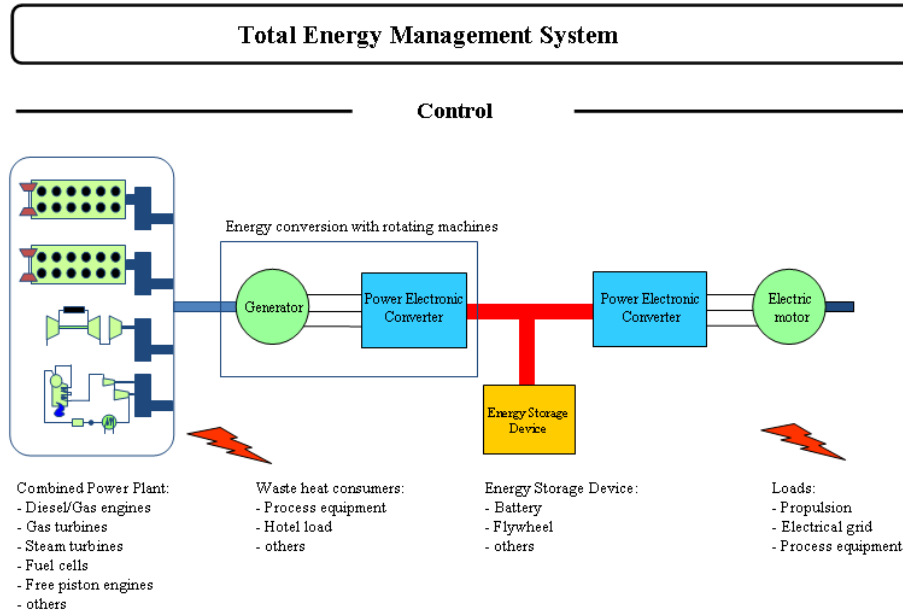


Figure 1.1 Overall power plant for electric propulsion (EE-AES 2003)

1.1.2 Prime movers

For centuries, diesel engines have been the prime choice due to high efficiency over a wide operating range, relatively compact design and mature, reliable technology for marine applications. Their ability to run on readily available and cheap fuel has also limited the introduction of alternative power plant concepts for marine applications. Slow response, lower efficiency at part-load, mechanical problems due to vibration and problems with meeting future regulations on emissions are drawbacks of this technology. Thus, designers seek new alternatives for the onboard power production.

Gas combustion results in less emission of nitrogen oxides, sulphur and particles. Gas engines are therefore an attractive alternative for vessels operating in coastal areas. These engines are usually modified diesel engines, and the main modification is that self-ignition must be replaced by using spark plugs or a pilot flame. The dual-fuel engine, with the ability to operate on both gas and diesel fuel, is an attractive gas engine. This concept helps reducing emissions without making the vessel completely dependent on gas supply (Levander 2001).

Gas turbines have a lower efficiency than internal combustion (IC) engines. The high power density of these engines still establish them as the preferred choice to meet the demands of power generation for the electric warship (Little, Young et al. 2003). In commercial vessels, gas turbines are only seen as a good alternative for high-speed vessels where low power-weight ratio is more important than high efficiency. Turbines also have a strong advantage over IC engines when it comes to vibration and noise, important factors in cruise ships, war ships and research

vessels. Gas turbines significantly reduce both NO_x emissions and visible smoke, and have been chosen for ships operating in areas with strict environmental requirements. Recent technology developments make diesel engines able to compete in terms of emission levels. The EnviroEngine of Wärtsilä, featuring common rail injection and possibilities of direct water injection and selective catalytic reduction, is claimed to be capable of the same performances (Levander 2001).

Steam turbines were outdistanced by the diesel engine in the middle of the 20th century. LNG(liquid natural gas)-carriers burning cargo boil-off gas are the only recent applications of steam turbines. The efficiency is low, and for new LNG-ships dual-fuel engines or the combined cycle power plant described below are preferred. New modifications to the steam turbine cycle have been purposed, significantly increasing the efficiency to the level of dual-fuel engines (MarineProp 2008a). However, factors such as lack of trained people will still limit the number of new installations.

Even though the first fuel cell was developed by Sir William Robert Grove in 1843 it is still an immature technology. The increased focus on pollution from the transport sector introduces a growing interest for this technology. Fuel cells operate by converting fuel directly to electric energy through electrochemical reactions. Reactions occur on the interfaces between anode and cathode electrodes and the electrolyte, more details are given in chapter 4. No combustion or moving parts are involved in the energy conversion. This results in some positive properties for a marine power plant; low exhaust emissions, high thermal efficiency, no vibrations, insignificant noise, good part-load performance and low operating- and maintenance costs (Yuan, Sun et al. 2004).

Dynamic properties, fuel flexibility and hence their appropriateness for different power plants depend on the fuel cell design. The electrolyte determines the possibility of ions and molecules to diffuse through the membrane, thus defining the fuel cell type. This affects their operational temperatures and pressures as well as ability to handle specific fuels. The most common fuel cell types are listed in Table 1.1. Values for efficiency, temperature and output power diverge between different sources, and the table gives a summary of common values found in literature, see e.g. (DOE 2008) or (MarineProp 2008b).

Proton exchange membrane (PEM) fuel cells running on pure hydrogen can follow fast changes in power demand and compete with the diesel engine when it comes to start-up and shutdown times. In addition, hydrogen as fuel enables ship operation with no pollution to air. Research developing PEM fuel cells have been extensive and offer the most mature fuel cell technology. Some major obstacles for introducing PEM fuel cells are; the availability of hydrogen in ports, and technical possibilities, rules and procedures for handling hydrogen in a safe manner on board. These problems seem unrealistic to overcome in a short time frame, and particularly for long distance applications other fuel cell alternatives are regarded as more suitable. PEM fuel cells are only seen relevant for short distance operation where frequent fuelling is possible. An example designed in the Netherlands is a

harbour tug (50 ton bollard pull) with electric propulsion powered by fuel cells and diesel generators. A 200 kW PEM fuel cell with battery back-up is intended for stand by operation, and a diesel generator bank will allow optimal operation in service (WWM 2008).

Table 1.1 Typical characteristics of four common fuel cell types

Fuel cell type	Electrolyte	Efficiency	Temperature	Reactants	Output
Proton exchange membrane (PEM)	Polymer membrane	35-40%	70-90 °C	H ₂ , O ₂	<1kW-300kW
Phosphoric acid (PAFC)	Phosphoric acid	35-40%	~210 °C	H ₂ , O ₂	10kW-1MW
Molten carbonate (MCFC)	Potassium carbonate	45-50%	~650 °C	H ₂ , O ₂ , CO	10kW-1MW
Solid oxide (SOFC)	Zirconium ceramic	45-50%	750-1100 °C	H ₂ , O ₂ , CO	10kW-3MW

High temperature cells (HTFCs) represent solutions better fit for ship operation. As shown in Table 1.1, HTFCs can run on fuels with carbon content such as natural gas or pre-reformed diesel. There are two main classes of HTFCs available; the molten carbonate fuel cell (MCFC) and the solid oxide fuel cell (SOFC). Several large scale units of MCFCs have been delivered, but problems related to electrode corrosion have so far limited their durability, and successful commercialization now seems less likely (Young 2007). SOFCs are more promising but not fully developed, introduction of megawatt-scale power plants are planned by several companies before 2010. Development of reasonably priced material of high durability is the key technical challenge also for SOFCs.

1.1.3 Combined power plants

The possibilities of combined power plants (CPP) for a better utilization of energy resources on board has been a main focus for recent research (EE-AES 2003). In this context the CPP concept is used to describe a system that combines at least two of the prime movers introduced in section 1.1.2. The CPP can meet requirements not attainable for a component alone, and has potential for a high performance over a wide range of operating conditions. Such a flexible plant represents large opportunities, but also poses a challenge when it comes to power management and process optimisation.

Combined cycle (CC) power plants utilize exhaust heat recovery from gas turbines to produce steam for a steam turbine driven generator. Figure 1.2 shows a CC power plant proposed for a ship with electric propulsion, usually termed COGES (combined gas turbine and steam turbine-electric), for which efficiencies in excess of 50% is claimed (NavalArch 2004b). Steam turbine cycles are rather complex and occupy large volumes and are therefore not a good alternative unless steam is

required for heating purposes. In (Stapersma 1999) gas turbines configurations that can achieve efficiencies above 50% are outlined, making them competitive with CC systems.

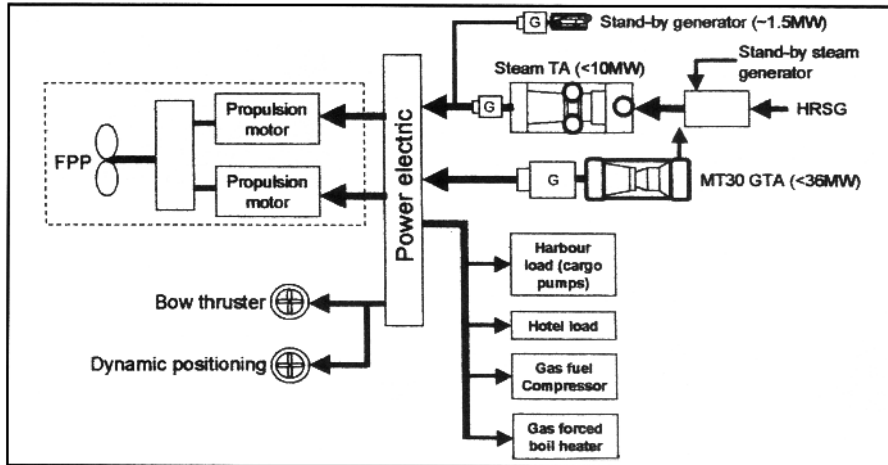


Figure 1.2 A COGES power system proposed for an LNG carrier (NavalArch 2004b)

Several combined systems are proposed exploiting the advantages of both diesel engines and gas turbines. The large cruise liner Queen Mary 2 came into service January 2004 with a CODAG (combined diesel and gas turbine) power plant. The ship has four medium-speed diesel engines, each producing 16,8 MW. In addition two 25 MW gas turbines are installed. The turbines will be fired up when a power boost for faster ship speed is needed, or when approaching environmentally-sensitive areas such as Alaska or in ports (NavalArch 2004a).

The concept “Hybrid Propulsion” from automotive industry has also been introduced for ships. Hybrid propulsion systems combine traditional engines and batteries for power supply. Many prime movers have low fuel efficiency at part load, or limited ability to tolerate load fluctuations. The main engine will run at maximum power and recharge the batteries at conditions close to full load. At part load, the batteries can provide the required power while engines are unloaded. This can save fuel and facilitate clean operation in sensitive areas. So far introduction of proper batteries has been limited by excessive space requirements and high prices.

For all new concepts, the fuel saving potential depends on the operating profile of the ship. A range of ships could profit from introducing alternative engine layouts. However, profits are often small compared to the uncertainties and costs associated with introducing new technology. The above concepts have to some extent been tested and found attractive only for a small range of ships. Fuel cell technology on the other hand is an immature technology yet to prove its applicability for marine propulsion. The environmental potential is high and encourages further investigation of its capabilities.

Power plants combining high temperature fuel cells with turbines or IC engines are regarded the most realistic alternatives for large scale introduction of fuel cells in

ships (Greig 2003). For main propulsion, combined systems such as SOFC and gas turbine (high exhaust temperatures from cell) or MCFC and steam turbines (intermediate exhaust temperatures from cell) are possible replacements for traditional diesel engine configurations. Estimated values are as high as 80% for the thermal efficiency of such a hybrid system (Winkler and Lorenz 2002). The major challenges with HTFC technology are long start up times, slow transient response and low tolerance of temperature variations across membrane materials. Control strategies to minimize thermal fluctuations are developed for combined plants, although making their operation quite complex (Stiller 2006).

The first introductions of fuel cells in ship are more likely to be auxiliary power units, or base load units in combination with traditional gas or dual fuel engines. Even though these solutions are not optimal in terms of system efficiencies, they are still attractive in terms of reducing emissions, especially in port and for stand-by operation.

Although the traditional diesel engine power plants for marine applications will hold a strong market position in years to come, modifications and alternative concepts will increase in complexity. For owners and classification societies ways to prove reliability and availability of such systems will become increasingly important. Efficient methods to develop mathematical models suitable for assessment of systems at design stage are therefore required.

1.1.4 Status of fuel cells in marine applications

Fuel cells have a great potential in ship applications, but still suffers from being a rather immature technology. At present the power density of fuel cells is low, there are issues related to fuel storage and flexibility, costs are high and no larger projects can prove their reliability in a marine environment (Sattler 2000). With a conservative shipbuilding industry in mind, the fuel cell is still years from being a realistic alternative. Even though most actors wait for fuel cells to prove themselves in other areas first, a range of research projects are still initiated trying to prepare for introduction of fuel cells in ships. In the following, an attempt is made to describe the current status on research and implementations of fuel cells for marine applications.

Due to their silent operation and the emerging regulations against IC engines on rivers and lakes, there are high expectations to fuel cells in small scale applications such as pleasure boats, sailboats, ferries and water taxis. Market surveys (Adamson 2005; Butler 2008) reveal a small range of such experimental installations planned and operated. Examples are the MTU sailboat No1 (20 kW cell) and the Voller Energy Group sailboat who crossed the Atlantic in 2007 (1 kW cell). In California a 18 passenger water-taxi powered by four 1,5 kW PEM fuel cells is operated. A hybrid hydrogen barge powered by a 1 kW PEM fuel cell and batteries, is operated by the University of Birmingham investigating hydrogen storage in metal powder. In Norway a project by Vestfold University College has rebuilt an old pleasure boat to run on hydrogen by installing two 1.2 kW PEM fuel cells.

Military research has for a long period had focus on fuel cells, primarily due to the low noise signatures achievable (Greig 2003). According to (Siuru 2007), the only operating large scale hydrogen at sea projects are U212 class submarines built by the German HDW. These are powered by PEM fuel cells running on hydrogen stored in metal hydride powder. In addition to the advantage of low noise, the exhaust from PEM fuel cells is cold and not detectable to enemies. Fuel cells are therefore an important part of the “all electric warship”-vision, where a major part of the components shall be driven by electricity. The “Navy Shipboard Fuel Cell Program” of the U.S. Navy focus on cells in a marine environment by investigating issues such as salt air, shock requirements and load sharing. A 625 kW MCFC has been successfully installed and operated on shore. Results are related to developing packing and plant design. Under the same program PEM fuel cell research has been focusing on process control, and research on SOFC integration is also planned (Nickens 2006). Due to worldwide operation requiring fuel flexibility, research also focus heavily on onboard reforming of diesel fuel, as the European project DESIRE (Krummrich, Tuinstra et al. 2006).

The EU-project FCSHIP (2002-2004) carried out a number of projects looking at possible future fuel cell applications in ships. The prime focus was evaluating safety and operational demands, as well as assessing economical and environmental potentials and limitations, of the fuel cell for marine applications. Major obstacles found were that the high volume, weight and price at the moment are far from the end users requirements. In addition, dependency and storage of pure hydrogen are regarded as challenges for marine environment and regulations. The research pointed at the need for improved simulation models to investigate the dynamic behaviour of fuel cells. There is also a lack of experience with fuel cells operating in a marine environment. Thus a need for full-scale demonstrations of total systems was identified to assure the quality of energy production. The project concluded that fuel cells have a large environmental potential, and that there are no unsolvable safety issues concerned with operating fuel cells on ships (FCSHIP 2004).

FELICITAS is an EU-project running from 2005 to 2008 focusing on development of fuel cells for heavy duty transport on road, rail and marine applications. For marine applications the development of Rolls Royce’s planar SOFC is the main activity (FELICITAS 2006). Other activities are developing an external fuel reformer, acquiring operational data from marine systems and conducting reliability assessments. Another EU-project named METHAPU will run from 2006-2009 (METAPHU 2009). The scope is to prove the use of methanol on board cargo vessels to support the introduction of necessary regulations allowing the use of methanol as a marine fuel. A SOFC fuelled by methanol was planned to be installed onboard a car-carrier in 2009, but delays are reported.

Also other projects plan to meet the demand for large scale or commercial demonstrators. The first commercially used fuel cell passenger ship was put into service on the Alster Lake in Hamburg August 2008. The ferry, taking 100

passengers, is powered by two 50 kW fuel cells with a battery pack for peak loading. In Iceland the SMARTH₂ project has replaced the diesel generator in a whale-watching ship with a fuel cell. At the moment three main companies are looking at adapting high temperature fuel cells for marine applications; MTU CFC Solution (MCFC), Wärtsilä Corporation (planar SOFC) and Rolls Royce (planar SOFC). In addition Germanischer Lloyd cooperates with HDW Fuel Cell Systems to develop PEM fuel cells previously installed on submarines for operation in surface vessels.

FellowSHIP is a Norwegian collaboration working to “Develop system solutions that make it possible to utilise current fuel cell technology in ships”. The project involves development, design, building and testing of marine solutions for a MCFC. Installation of a 330 kW stack is planned on board a supply ship in 2009 as auxiliary power unit for a dual-fuel machinery system (FellowSHIP 2009). A hybrid solution of MCFC and steam turbines as a totally new machinery configuration is also designed and found technically feasible. In this patented system the steam boiler and turbines will handle dynamic operating requirements, resulting in stable operating conditions for the fuel cell. Other challenges approached in the project are development of suitable power electronics and dynamic modelling and simulation.

Safety and reliability of fuel cells in ships have been addressed in (Tronstad and Byrknes 2003). To combine the requirement for low thermal transients with major power transients and meeting safety requirements for emergency shutdown are identified as the main challenges of systems including HTFCs. There is also a fear that ship vibration might accelerate cracking, and that salt in process air might not be compatible with the cathode materials. These possible failure modes represent typical scenarios evaluated when developing classification rules. For fuel cells such rules and guidelines can be found in (DNV 2008) and (GL 2003).

A fuel cell system will have higher investment costs, but is expected to have lower operational costs, than traditional diesel engine systems. (Sødal 2003) estimates a price development for marine fuel cell power, and argues that the technology is far from reaching a competitive level. At present (2008) LNG prices are low compared to marine diesel oil. (Mangset 2008) therefore estimates fuel cells to be competitive at investment costs only twice the cost of diesel engine installations. This is regarded achievable in a shorter time frame. Possible future regulations on pollution might also help the fuel cell system being competitive. (Sødal 2003) emphasise that a fuel cell design offer less flexibility towards future vessel operating profiles, a factor that can play a major role for ship-owners investments.

The main obstacles for high temperature fuel cells in ships can be summed up as dimensions, weight and costs as well as the limited ability to handle transient loads. Research and development result in constant reductions of these obstacles as technology matures. Optimized plant design, and control algorithms developed to handle all operational conditions of a marine power plant, can ensure suitable operating conditions for new solutions. Proper mathematical models will aid the development process and contribute to facilitate successful introduction in ship

applications. Such models must be detailed enough to represent the actual physical processes involved in power production. However, the models must also be suitable for system simulations to show their dynamic interaction with the overall power plant.

1.2 Project description

The introduction above describes how the complexity of machinery systems increases, introducing a need for improved design tools. The main objective for this PhD-project is to simplify dynamic performance evaluations of new power plant concepts at design stage. To reach this goal, existing tools and methods for modelling and simulation must be evaluated and possibly improved. The resulting methodology should simplify the development of component models for simulations of both steady state and transient performance of power plants.

Such tools will aid the development process by;

- Proving the conceptual design of alternative power plant configurations. This is achieved through simulations of components and overall system behaviour in all operational conditions.
- Facilitating the development of sophisticated control systems. Proper models will allow for monitoring of a range of component variables during virtual testing of control algorithms.
- Improving the physical understanding with respect to limitations of involved components. This is essential knowledge when performing safety and reliability assessments with the overall goal to minimise system failures and component malfunction during introduction of new technology.

Therefore, access to advanced dynamic models of prime movers for power plant performance simulations is essential. Fuel cells are identified as components where proper models are lacking and the need for efficient measures to communicate operational capabilities are required. The high temperature solid oxide fuel cells are pointed out as relevant for large scale introduction in ships, and model development for an SOFC is presented in this thesis.

Power plants in general and fuel cells in particular involve a range of physical domains; mechanical, chemical, thermal, fluid and electrical. A method for multi-domain modelling is thus essential in order to develop models within a well defined framework. This will allow efficient generation of models with consistent interface to other power plant components. According to literature, the bond graph language for model implementation has shown its capability for these purposes. An important goal for this PhD-project is to investigate how bond graphs are suited to structure previous models and know-how developed for fuel cell modelling.

1.3 Main contributions

The main contribution of this thesis is a flexible template for mathematical modelling of fuel cells. The template is based on a bond graph framework appropriate for simulation of system behaviour. All models are open for further development to allow for an increased level of details to be included.

A new energy consistent way of combining pseudo bond graphs with true bond graphs is developed as an important part of this framework. Pseudo-bond graphs represent the processes of mass flow and thermodynamics, while true bond graphs represent the electrochemical reactions. Based on a standard lumped model representation of the fuel cell, distributed characteristics are studied. Each lump is divided in multiple repeated sections along the cell. This feature is particularly important for high temperature fuel cells with internal reforming.

A model of a solid oxide fuel cell stack is developed. The development process demonstrates the advantage of a bond graph template when discussing and comparing different model implementations. The resulting models are of complete integral causality allowing for stable and computationally efficient system simulations.

The models of the fuel cell and its system components are important contributions to a component model library supporting design of future marine power plants.

1.4 Organisation of the thesis

The remainder of the thesis is organized as follows:

Chapter 2 is a literature study providing background for development of fuel cell models for marine power plant simulations.

In chapter 3 the most relevant methodologies used in dynamic modelling of power systems are discussed. This discussion provides the background for adapting the bond graph framework to support fuel cell modelling.

The development of a mathematical model for the solid oxide fuel cell (SOFC) is outlined in chapter 4 together with basic models of the support system components in a high temperature fuel cell stack.

Chapter 5 present the results of simulations carried out to verify the different model implementations arrived upon in chapter 4.

Conclusions and suggestions for further work are the contents of chapter 6.

An introduction to the bond graph method can be found in Appendix A. Parameters for the simulations in chapter 5 are listed in Appendix B, and Appendix C describe how thermal properties of gases are implemented in the simulation model.

Chapter 2

Dynamic modelling of prime movers

A high number of publications exist that present a range of models for simulating the behaviour of power plant components. A study of some important contributions to modelling typical engines for marine power plant simulations is included here. This study provides a basis for discussing proper complexity levels of prime mover models in system simulations.

The solid oxide fuel cell is a component subject to commercialisation; therefore no easy access to performance data is available for the cell studied in depth in chapters 4 and 5. Model development and verification is therefore based on a literature study of models already published. The main publications serving as basis for the model development in this thesis are described below.

Flexible and reusable models for a component library are not trivial to make. A variety of engine designs exist and for specific engines it is difficult to obtain necessary parameters. The various model implementations and complexities are therefore discussed further when developing a framework for fuel cell modelling in chapter 3. The objective is to make a fuel cell model that can be included in an overall tool for power plant design and evaluation, for example as presented in (Pedersen 2009).

2.1 Engine modelling for marine applications

As described in chapter 1 most vessels are powered by diesel engines, thus models published for marine power plant simulations are mainly diesel engine systems. In (Gjerde 1999) different ways of modelling the prime mover of electric power systems in ships is discussed. A model based on physical parameters is evaluated against an empirical model where combinations of time constants describe the diesel engine. The latter is considered sufficient when analysing the power system from an electric or control point of view and is applied by for example (Hansen, Ådnanes et al. 2001). If the goal is to analyse dynamic behaviour of the prime mover itself, or the resulting forces acting on the machinery from the total system, more detailed models are necessary. This also applies if the power plant models shall be used for energy management calculations or estimation of emissions. Then more advanced thermodynamic models are essential.

(Woodward and Latorre 1984), (Boot, Klein Woud et al. 1991), (Carrera and Rizzuto 1997) and (Hetet, Inozu et al. 1999) all discuss different mathematical models of diesel engines for use in computer simulations of marine propulsion transients. For total system simulations a simple empirical transfer function as mentioned above is common. Another approach used for engine design is detailed modelling of the complete diesel engine process, calculating all relevant parameters for each crank angle. The first type of models allows for fast simulation, but requires great amounts of test data for validation. Engine performance information is limited due to no computation of thermodynamic cycles. Models such as CFD approaches describing fluid dynamics in detail are regarded superfluous for a system approach. The aim is always to include in a model just enough of its internal characteristics to predict external characteristics accurately under all operating circumstances. The need for empirical data should also be put to a minimum as the ideal engine model should base all its equations on the principles of combustion, heat transfer, fluid flow and mechanical dynamics. Thus the abovementioned authors find thermodynamic models of intermediate complexity most appropriate for system simulations.

(Carrera and Rizzuto 1997) uses a medium complexity model described in (Boot, Klein Woud et al. 1991) for simulation of mechanical and thermodynamic performances of a ship propulsion plant during transients such as slam-start and crash stop. In (Campora and Figari 2003) full-scale validation of an equivalent model is presented. Other relevant transient cases are as simulated in (Hetet, Inozu et al. 1999); sequential turbo charging (including compressor surge), extreme load conditions (ice) and conditions causing severe pollutant emissions. In (Chesse, Chalet et al. 2004) the model of (Hetet, Inozu et al. 1999) is simplified for real-time simulation appropriate for training simulators. In (Haller 2001) an integrated diesel-electric propulsion system for an ice-breaker is simulated in order to optimize sizing of diesel engines and pods to handle all relevant transient operations. In this work, a detailed dynamic model of the electronic governor and hydraulic actuator are considered sufficient for the analyses, and the engines are described by performance maps.

(Kyrtatos, Theotokatos et al. 2001) and (Kyrtatos, Theodossopoulos et al. 1999) use engine models based on physical relations to improve the control scheme of marine diesel engines. The simulation code is thus used as a substitute for the engine testing required for designing new engine controllers. In (Kyrtatos, Theotokatos et al. 2001) an on board measurement project verifying the code is described.

(Pedersen and Engja 2000) presents a library for modelling diesel engine transient performance using bond graphs. Sub-models for the engine processes, the cylinder model with combustion and valves, the air and exhaust receivers, the air cooler, the turbocharger (turbine and compressor) and the exhaust system are outlined. All models are based on thermodynamic principles and are well suited for system integration. The level of complexity reflects the models named “intermediate thermodynamic models” introduced above. The graphical representation gives

advantages similar to object-oriented modelling where the level of complexity for subsystems can easily be adjusted according to intended application. Bond graphs represent both the physical and the computational structure of a model; a great advantage for controller development. Other bond graph models based on the same structure and available for a power plant library are for example; the gas turbine (Pedersen 2001), hydraulic systems (Pedersen and Engja 2008), boilers and refrigeration systems (Moksnes 1997; Thoma and Ould-Bouamama 2000), shafting systems (Bruun, Pedersen et al. 2005) and compressors (Engja 1985). Recently a library for all electric ship simulations was published by (Pedersen 2009). A bond graph framework for thermodynamic modelling of fuel cells will be of grate value to this collection.

2.2 Fuel cell modelling, SOFC

Awaiting successful commercialisation, solid oxide fuel cells are subject to extensive research and development activities. Detailed physical models are used during component design and performance evaluation involving multi-dimensional distributed representations at cell level. They can help overcome technological challenges such as choosing appropriate materials for membranes, and estimating correct dimensions of gas flow channels; all reducing the need for and supporting the choice of required physical testing. The goal is to increase efficiency and durability of SOFCs to a competitive level. Heavy computational efforts are needed to solve complex thermofluid and electrochemical phenomena, and such models are regarded superfluous when investigating system integration. (Thorud 2005) points out the value of such models for SOFCs since there is a lack of experimental data available. Important contributions to modelling part-load performance of solid oxide fuel cells on a fairly detailed level, while still allowing for system integration, can be found in for example (Selimovic 2002) and (Campanari and Iora 2004).

At the other end of the scale are dynamic models applied for controller development. Most are based on lumped approaches, treating each gas channel or solid membrane as volumes with uniform physical properties (Sedghisigarchi and Feliachi 2004; Kandepu, Imsland et al. 2007; Xi, Sun et al. 2007). In some cases fuel cells are simply modelled as an equivalent electric circuit. Parameters and dynamic response of such models must be verified against measurements or more detailed models.

The first significant contribution to models for dynamic performance evaluation of solid oxide fuel cells was presented in (Achenbach 1994); accounting for both multidimensional and time dependent effects of thermal properties in a planar SOFC. The model shows how the effect of internal reforming strongly affects operating conditions, and it is found important to include distributed characteristics in the model. Kinetic relations presented for electrochemical and reforming reactions are claimed to be preliminary, with need for improvement as knowledge increases. However, the results presented here are widely used in new

SOFC models, thus revealing the lack of accessible experimental results for this technology.

(Haynes 2002) presents a model for dynamic simulation of a tubular SOFC whose inlet fuel conditions remain unchanged during load variations. The purpose is to find the fuel cell response when not slaved to the response of gas supply systems. Dynamic response is found to improve with initial conditions of lower fuel utility or higher voltage. The model is based on a one-dimensional approach, including changes in gas composition and electrochemical reactions along the cell. Thermal and electrical development is decoupled in the simulation due to different time scales, and a steady state electric production is assumed when calculating the thermal development. This may not be justified during conditions such as start-up, where a model representing total dynamic behaviour is necessary.

Two models of different complexities are evaluated in (Iora, Aguiar et al. 2005). For the low complexity model, assumptions such as constant flow properties reduced the complexity and significantly reduced the computational effort. Nevertheless, nearly equivalent simulation results with the high complexity model were achieved for several important operational conditions. For high current densities deviation between the models becomes significant. The importance of evaluating the valid area for assumptions is emphasised in the paper. A framework that arrange for further refinement or simplification of the model implementation depending on desired analyses will be beneficial.

For such cases it will be beneficial to have a framework that enables further refinement or simplification of the implementation of different physical phenomena for the representation to correspond with the desired analyses.

(Qi, Huang et al. 2005) presents a detailed state space model for a finite volume representation of solid oxide fuel cells. In (Qi, Huang et al. 2006) the model is applied to a cross-sectional slice of the tubular SOFC. The wider the slice is in the tangential direction, the closer one comes to a lumped representation of the cell, but distributed characteristics are lost. To show distributed characteristics (Qi, Huang et al. 2008) extend the finite volume models throughout the cell. The resulting set of partial differential equations (PDEs) is transferred by analytical simplifications to a state space model suitable for controller design. The finite volumes may also result in a set of ordinary differential equations (ODEs) more convenient for control development, but according to (Qi, Huang et al. 2008) the set of ODEs will be too large. A range of assumptions must be taken to simplify the PDEs using the approach in (Qi, Huang et al. 2008). (Kandepu, Imsland et al. 2007) suggest a distributed representation by repeating the lumped model in sections, but does not show a proper way to distribute current between each lump.

(Thorud 2005) develops a quasi-2D model of a tubular SOFC; thermofluid properties of gas flows are calculated in axial direction, while chemical reactions and heat flows are calculated in radial direction. The model is calibrated against available data from a Siemens Westinghouse cell, and an assessment of the dynamic capabilities of a SOFC/GT power plant is carried out. (Stiller 2006)

improves some components in the system model and evaluate a range of control strategies for such a power plant. (Stiller 2006) provides a well structured and detailed presentation of each component model, thus found well suited as a main source for the model representation developed in this thesis.

Models investigating properties of specific phenomena occurring in solid oxide fuel cells are for example (Haberman and Young 2006), presenting models for chemical reaction rates, or (Wagner, Schnurnberger et al. 1998) who uses impedance measurements to establish an equivalent circuit for the electrochemical reactions. In (Todd and Young 2002) the accuracy and reliability of methods applied to predict properties of SOFC gas mixtures are evaluated.

Above publications show how distributed characteristics have great influence on SOFC dynamic behaviour. Models including such characteristics easily become computationally heavy, and decoupling of dynamics or ignoring physical phenomena of less importance to the ones studied are common approaches. Lumped models are used for controller development; these cannot represent the distributed characteristics of possible importance when choosing the correct control scheme. A goal for future model development must be to represent all dynamics relevant for controller development without excessive computational effort, while monitoring actual physical behaviour of processes inside the cell. Such models can enhance both system design and control development.

Being a tool for multi-domain modelling, bond graphs should be well suited for fuel cell modelling at a system level, particularly for control-plant models. Examples of bond graph implementations of fuel cell models are (Benbouzid, Fouquet et al. 2003), (Benbouzid, Dauphin-Tanguy et al. 2004), (Saisset, Fontes et al. 2006) and (Hung, Lin et al. 2008); all for PEM fuel cells. (Saisset, Turpin et al. 2002), (Bruun and Pedersen 2007) and (Vijay, Samantaray et al. 2008) apply bond graphs to modelling of a SOFC. All the bond graphs are fairly consistent when it comes to modelling the electrochemical and electrical phenomena in the fuel cells. More difficult it seems to agree upon a consistent way of treating the exchange of energy between thermofluid and electrochemical domains. When multiple gas components and phases are present the models become rather specialised for assumptions such as the ideal gas approach. The model presented in (Bruun and Pedersen 2007), and elaborated further in this thesis, suggest a general framework for bond graph modelling of distributed characteristics of fuel cells.

Chapter 3

Modelling theory

Models for simulation of power plants are of increasing importance when designing new complex propulsion systems. Modelling systems containing power production from thermofluid processes proves to be a challenging task. They involve a high degree of nonlinear relations, and there is a need for consistence in interaction between different physical domains.

This chapter discuss different ways to implement such models, arriving at the bond graph method as the preferred tool for creating appropriate simulation models. The application of this method to the thermofluid, chemical and electrochemical domains important in fuel cell modelling will be elaborated. A general introduction to the bond graph method can be found in Appendix A.

3.1 Dynamic modelling of thermofluid processes

Time development of multiple physical phenomena must be represented when simulating the dynamic response of prime movers in a power plant. In general, the energy in the system is converted from chemical to thermal energy and further to mechanical and electrical energy; in the remaining discussion referred to as a multi-domain process. The thermofluid concept is used to describe phenomena related to the energy transported by fluids (liquids, gases and vapours), and involves both thermodynamics and fluid mechanics. When the complexity of power plant systems increase, and a focus is put towards reducing pollution, thermofluid processes become important to include also in system simulations. The behaviour of fluids and gases in changing conditions also involving chemical reactions is complex. It is therefore important to find a proper method to represent components, whose dynamics are based on thermofluid processes, in overall system models.

Low complexity models are based on stationary measurements, experimental data or empirical correlations, linking together the main variables of the engine; fuel input and power output. In system analysis, prime movers are often represented by one or several time constants based on empirical data. Transfer functions implementing these time constants are widely used for controller design and optimization. Transfer functions may also result from Laplace transformation of a system of ordinary differential equations with time as the free variable (Egeland

and Gravdahl 2002). The origin and level of details of these equations can vary. (Kyrtatos, Theotokatos et al. 2001) describe how time constants and transfer functions for diesel engines can be successfully obtained from detailed models based on physical parameters rather than from empiric engine data. Low complexity models might represent the dynamics of interest for a component. However, their ability to monitor time development of variables inside the component and to refine parts of the model is somewhat limited.

High complexity models describe in detail the spatial variation of thermofluid processes inside each component, requiring a detailed physical description and high computational effort. Such fluid dynamic models are often used when investigating details of the flow fields inside cylinders or through intake and exhaust ports. This modelling approach is based on the fundamental equations of fluid dynamics and commonly called CFD-analysis (Computational Fluid Dynamics). The models consist of partial differential equations for conservation of mass, momentum, energy, and component concentration. Engine designers use the results to reveal details of the different load cycles that engine components must endure. The finite element method (FEM) is applied for detailed analysis of heat transfer and mechanical endurance of system components. A variety of engine designs exist. It is difficult to obtain all parameters of relevance to allow for detailed model implementation of specific engines. Detailed component models of engines are therefore not trivial to include in a general simulation library. In addition, system simulations will be slow due to the computational efforts required.

The objective of this thesis is to develop models for system simulations, enabling analysis of how prime movers interact with surrounding systems. The models must be able to predict main variables, ranging from overall power output and fuel utilisation to properties such as local temperature, density and pressure development, and the effect of changing external operating conditions. Possible phase changes, flow rates and chemical reactions for the fluids might also be important. Thermodynamic models can describe the development of such properties, typical relations used in these models can be found in e.g. (Moran 1998) and (Bejan 2006).

Thermodynamic models use a lumped approach based on energy and mass conservation in control volumes. The control volumes are described as reservoirs where energy and mass present in the volumes can change with time. Flows between the reservoirs are driven by the difference in energy and mass levels. These models are based on a combination of physical relations and empirical data. To define all relevant variables of the control volumes conservation of mass and energy must be calculated. In addition, a state equation for the gas mixture and an equation to find gas composition must be calculated, see e.g. (Moksnes 1997; Bejan 2006). Different empirical relations are developed to account for heat transfer across system boundaries.

Thermodynamic control volume models are mainly developed to represent equilibrium states of a system. For initial system design, such models are used for optimization of dimensions and layout. The models can also be used as basis for

transient simulations estimating the systems dynamic response to external load changes and internal failures. This implies monitoring the change of a systems state over time, non-equilibrium systems. In most cases the thermodynamics are slowly varying and local pseudo-equilibrium can be assumed, allowing standard relations to be applied. Inside each control volume, intensive properties like temperature, pressure and chemical potentials are assumed uniform (Karnopp 2000). To circumvent these assumptions non-equilibrium thermodynamics must be applied. Its formulas are largely based on empiric observations and no additional physical insight about relations between rates and variables is gained (Bejan 2006). Such an approach is thus believed to be superfluous from a system point of view.

3.1.1 Languages for model implementation

As described above, thermodynamic models typically predict temperature and pressure variations inside control volumes. Interface to other domains such as chemical and mechanical processes are important in system design. There are several projects aimed at making standards in modelling and simulation. Their main objective is to simplify the communication of mathematical objects between different computer programs and users. This will enable distribution of model libraries for a range of applications, particularly useful to researchers dealing with multi-domain models and control algorithms.

A broad choice of software exists for model implementation and simulation, most intended for one type of analysis or physical domain. General purpose software such as MATLAB/Simulink and ACSL are widely used, but based on a signal flow standard making them less appropriate for multi-domain modelling. Software and techniques for more general physical system modelling exist, such as gPROMS, 20sim, VHDL-AMS and Dymola, but are in general used by smaller groups, see (Mattsson, Elmqvist et al. 1998) and references therein. Modelica and VHDL-AMS are attempts to make standards enhancing the use of such general system modelling tools and are therefore given further attention here.

Modelica is an object-oriented modelling language developed as an international effort to facilitate exchange of models and model libraries. The language is designed to allow component-oriented modelling of complex physical systems, e.g. systems containing mechanical, electrical, electronic, hydraulic, thermal, control, electric power or process-oriented subcomponents (Fritzson, Aronsson et al. 2007). The Modelica project was initiated in 1996 and free libraries for different research fields are continuously added. Their objects can easily be used in simulation environments built on the Modelica standard. Models are implemented and equations are generated in a non-causal way to make the objects as general and independent as possible. Model processing therefore gives a set of ordinary and differential algebraic equations that might be quite complex and even redundant, but still solvable with the appropriate numerical method (Borutzky 2002).

VHDL-AMS is another multi-domain language. It is developed as an analogue and mixed-signal extension to the VHDL discrete modelling standard for electronic hardware by IEEE (Christen and Bakalar 1999). The definition of the standard

allows one to build simulation models of physical components and subsystems belonging to multiple domains. Packages covering electronic, thermal, mechanical systems etc are under development. The analogue models are based on a lumped system description which enables implementation of thermodynamic systems.

Signal flow modelling is by far the most used representation for control design and analysis. Block diagrams representing the state equations for a system and implemented in for instance a MATLAB/Simulink (www.mathworks.com) environment can be found for most physical systems, as for fuel cells in (Pukrushpan, Stefanopoulou et al. 2004). Due to feedback loops in a signal flow model the limited possibility to separate different sections of a system is regarded as a drawback (Blunier and Miraoui 2008). In (Blunier and Miraoui 2008) an introduction to the VHDL-AMS language is found and applied to a typical fuel cell model. The language is compared to three different multi-domain approaches; equivalent circuit diagrams, signal flow diagrams and the bond graph approach. Both bond graphs and the VHDL-AMS language assign causality before generating equations and can provide graphic interpretation of controllability and observability. They also allow validation and development of different properties or sections of a model. Also block diagram structures contain causal information, while a Modelica model offers no such information.

VHDL-AMS and Modelica are standards primarily aimed at enhancing software development and model exchange. They facilitate reuse of model knowledge, but the low level physics of each component might still be difficult to comprehend. The tools may be regarded more relevant to software and library developers than modelling at component level (Broenink 1997) and therefore less valuable as an aid for the modeller when trying to describe interactions within the physical system. In the present work the modelling process is the prime focus and the bond graph language is chosen. A more thorough introduction to the method and its possibilities is given in the remaining sections of this chapter.

Bond graph is a method developed to enhance interconnection of various physical models, facilitating multidisciplinary communication by recognising the exchange of energy as the unifying concept for dynamic systems (Karnopp 2000). It has been used since the sixties to enhance the modelling process, particularly in mechatronics. It is a graphical tool showing the energy exchange between elements representing model properties. Applying causality to the graph enables an automatic generation of first order differential equations, appropriate for efficient system simulation.

The low level graphical representation of computational causality between different system properties, allows the modeller to reveal and solve for example singularities and invertibility in the formulating stage (Samantaray and Bouamama 2008). This makes the bond graph tool attractive to modellers seeking to develop stable and efficient models for integration in total system simulations. Bond graphs are relatively easy accessible for new users since they are developed from a cross-disciplinary engineering point of view. In addition to computational causality, bond graphs have the big advantage of being energy consistent by nature as power

continuity is expressed explicitly. However, Modelica and VHDL-AMS can handle discontinuities such as switches and variable structure models in a more efficient way than bond graphs (Borutzky 2002).

As opposed to block diagrams showing flow directions of each signal, bond graph is similar to network models in using energy flow to connect elements. Two variables are in general needed to describe an energy flow. Development of object-oriented models are enhanced by applying energy to describe the interconnection between subsystems or elements in a graphical presentation (Egeland and Gravdahl 2002). Bond graphs are as shown in (Borutzky 2002) essentially an object-oriented modelling method, but a direct transfer to languages such as Modelica and VHDL-AMS is not straight forward. The reason is them being based on generalized network theory where the power variables are related to ports instead of bonds. This makes summation of the power variables inconsistent between the three languages. With some special adaptations described by (Borutzky 2002) bond graph method is nevertheless proven suitable for generating models in Modelica libraries, as for example the thermofluid models by (Cellier 2008).

It is not common to include details of thermal development in overall multi-domain system models. Therefore there exist relatively few publications applying bond graphs for modelling thermofluid systems. Standard variables in thermodynamic modelling do not fit well with bond graph terminology and have also limited the number of applications. In the remainder of this thesis it is shown how the benefits of bond graph modelling can be applied to thermofluid systems.

3.2 Bond graphs for thermofluid systems

A bond graph is essentially a mathematical model of the energetic structure of a system presented in a graphical notation form. The elemental physical properties of a system is identified and represented by ideal elements representing sources, accumulation, transfer and dissipation of energy. These elements are connected by graphical lines representing energy flow of the system. A set of first order differential equations appropriate for numerical simulation of the system can be generated from this graphical representation. An introduction to the bond graph method can be found in Appendix A.

The fundamental relations of thermodynamics are based on the 1st and 2nd laws of thermodynamics, (3.1) and (3.2). The change in internal energy, U , is a sum of the heat, Q , the work, W and the energy of mass flowing across system boundaries. For a system consisting of a number of chemical components the energy in mass flows are represented by the enthalpy h of each component and the number of moles flowing, n . The summation variable n is the number of components flowing into the system while m represents the number of components in the output flow. If no chemical reactions occur inside the system, n equals m . S_{gen} is the irreversible entropy generated when energy is transformed from one condition to another.

$$\frac{dU}{dt} = \dot{Q} - \dot{W} + \sum_{i=1}^n h_i \dot{n}_i - \sum_{i=1}^m h_i \dot{n}_i \quad (3.1)$$

$$\dot{S}_{gen} = \frac{dS}{dt} - \frac{\dot{Q}}{T} + \sum_{i=1}^n s_i \dot{n}_i - \sum_{i=1}^m s_i \dot{n}_i \geq 0 \quad (3.2)$$

The relations describe a system in equilibrium with its environment. Assuming also quasi-static changes, volume as the only external variable acting on the system and integrating the system over a small time period, the relation takes the form of equation (3.3), see (Bejan 2006) for details. Gibbs free energy per mole of a component is commonly denoted by the chemical potential μ_i , equation (3.4).

$$dU = TdS - PdV + \sum_{i=1}^n \mu_i dn_i - \sum_{i=1}^m \mu_i dn_i \quad (3.3)$$

$$\mu_i = h_i - Ts_i \quad (3.4)$$

The above equation is called the fundamental relation in energy representation, and the resulting state equations are (3.5)-(3.7). Rewriting (3.3) one can find the fundamental relation in entropy representation and the corresponding state equations.

$$T = \left(\frac{\partial U}{\partial S} \right)_{V, n_1, \dots, n_n} \quad (3.5)$$

$$P = - \left(\frac{\partial U}{\partial V} \right)_{S, n_1, \dots, n_n} \quad (3.6)$$

$$\mu_i = \left(\frac{\partial U}{\partial n_i} \right)_{S, V, n_n \neq n_i} \quad (3.7)$$

The basic bond graph notation for thermal systems is to use temperature and pressure as effort variables and entropy change and volume change as flow variables. (Thoma 1971) was of the first to represent such models. This seems plausible since the product of each pair is power, but some challenges exist. First of all a thermodynamic state must be specified by $2+n$ independent and intensive variables, (Bejan 2006), where n is the number of mass components flowing across the system boundaries. An element calculating the state must therefore have at least two input variables, a single bond is not sufficient unless we deal merely with heat conduction through matter at rest.

A multiport C -field representing the accumulation of energy in a closed system is shown in Figure 3.1. When no mass flows across system boundaries $n=0$ and the state equations for the C -field are showed in (3.5) and (3.6). The hydraulic and thermal effects are treated by separate bonds. Internal equilibrium between components is assumed, closed systems with a change in composition due to chemical reactions are treated in the next chapter.



Figure 3.1 Thermal multiport C -field

Losses due to irreversibility in mechanical or electric systems cause production of entropy. This can be represented by two-port resistors between the respective domains, Figure 3.2.



Figure 3.2 Two-port thermal resistor

The transfer of heat through a system can also be described by this resistor, with temperature and entropy as power variables both on the input and output bonds. Acting as a heat source to the thermal domain, this element is frequently called an RS -element (Cellier 1991). Since the element still represents direct relations between efforts and flows, we choose not to introduce a new element for this purpose, but keep the basic R -element. Being power conservative elements one might also think of replacing the R -fields with TF or GY elements, but this is not done due to irreversible properties. The one port resistor is not present in a system model that account for thermal energy changes.

Two main arguments exist against using the above approach. First, the use of entropy flow and accumulation gives nonlinear relations for the state equations that are not commonly used in thermodynamic engineering analyses. Secondly, when dealing with thermofluid processes the hydraulic and thermal energies cannot be decoupled. The variables for thermal flux do not describe the accompanying mass transfer and are only applicable for conduction through matter at rest. In addition, for a compressible flow the volume flow might change through an element and mass flow is a more appropriate variable.

As discussed in (Pedersen 2001) an equilibrium state for a system can also be characterised by the extensive variables internal energy, volume and number of moles of each chemical component present in a mixture. These extensive variables can be used to find the entropy S , a fundamental relation equivalent with the internal energy U from which all thermodynamic properties can be derived. The Helmholtz free energy (A), the enthalpy (H) and Gibbs free energy (G) are other common variables used to monitor energy changes in a thermodynamic system. They can all be derived by Legendre transformation of equation (3.3), assuming different constraints on the system (e.g. constant p or T). The most appropriate variables simplifying the modelling process must be chosen when applying the bond graph technique to model such systems.

$$\begin{aligned}
 U &= f(S, V, n_1 \dots n_i) & A &= f(T, V, n_1 \dots n_i) \\
 S &= f(U, V, n_1 \dots n_i) & H &= f(S, P, n_1 \dots n_i) \\
 & & G &= f(T, P, n_1 \dots n_i)
 \end{aligned}$$

Pseudo-bond graphs were introduced by (Karnopp 1979) replacing the entropy with total heat as the flow variable. The unit for heat flow is power and the product of the effort and flow variables is no longer consistent with true bond graphs, thereof the pseudo notation. There are two main reasons for choosing to deviate from the standard definition; the resulting relations are more consistent with the traditional engineering approach to thermodynamics, and an extension to accommodate compressible flow effects is simplified. True bond graphs and a Lagrangian description is still regarded feasible for heat flow problems and systems where constant mass is contained within the system. Pseudo-bond graphs are preferred when an Eulerian control volume approach is used (Karnopp 2000). This is the common engineering approach. As pointed out in (Thoma and Ould-Bouamama 2000), most bond graphers use some kind of pseudo-bond graph to describe systems with compressible gas flow.

Pseudo-bond graphs use four variables and two parallel bonds to represent the power flow between each element, Figure 3.3. This gives a close connection to true bond graphs as junction structures and basic elements are unchanged, but special attention must be made when connecting to true bond graphs to assure a power consistent graph. The variables proposed by (Karnopp 1979) are pressure and temperature as efforts and the corresponding mass or volume and total energy, heat or enthalpy as flow variables, Figure 3.3. Volume flow may be appropriate for incompressible systems, while mass flow is preferred for the remaining systems. Heat radiation, convection and conduction may well be described with heat as the flow variable. For mass flow the accompanying energy can be described by the enthalpy flow. External work can also cause energy change in a fluid, and the total energy is preferred as the flow variable in this thesis.

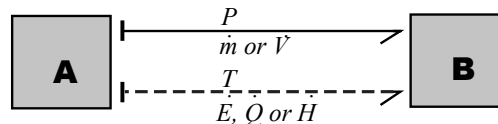


Figure 3.3 Definition of pseudo-bonds

Because bond graphs are developed for lumped parameter models, a thermodynamic control volume is a good place to start describing the method. Figure 3.4 defines the variables and directions associated with energy change in a control volume and the corresponding pseudo-bond graph. A true hydraulic bond represents the possible volume change as input to the C-field. For a constant volume this bond can be ignored. The upper zero junction of Figure 3.4 represents the summation of mass flows in the volume. The lower zero junction represents the summation of energy flows according to equation (3.3). A modulated flow source must be applied to connect the true bond graph to the pseudo-bonds. This flow source represents the energy change due to external work applied by the surrounding system. A volume change is the external work in Figure 3.4. The flow source from thermal pseudo-bonds can represent heat flow into the control volume. The pair of pseudo-bonds in and out of the θ -junctions represents the energy associated with mass flow.

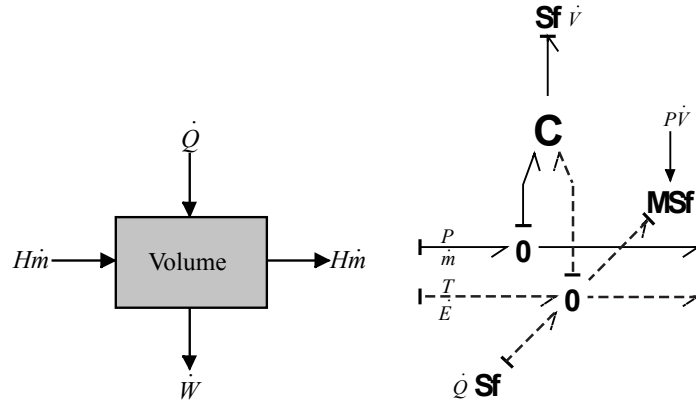
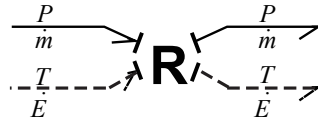


Figure 3.4 Pseudo-bond graph of accumulation in control volume

Constitutive equations for the C -field are found in (3.8). The type of state functions to be applied depends on the system. For gases the ideal gas or perfect gas laws are the simplest relations. Other state equations exist for describing for example two-phase behaviour or fluid systems, examples can be found in e.g. (Moksnes 1997) or (Smith 2005).

$$\begin{aligned} P &= f_p(m, E, V) \\ T &= f_r(m, E, V) \end{aligned} \quad (3.8)$$

R -fields are implemented to represent the rate of change in energy and mass flows between each control volume, Figure 3.5. The element can also represent flow through restrictions such as a nozzle or a valve. Flow rates are set as function of pressure ratio, temperatures and parameters such as friction factors and geometric data (3.9). The flow is always in the direction of decreasing pressure.


 Figure 3.5 Pseudo-bond graph, R -field

$$\begin{aligned} \dot{m}_{in} &= \dot{m}_{out} = f(\Delta P, T_{in}, f, d, l) \\ \dot{E}_{in} &= \dot{E}_{out} = f(\dot{m}, T, h) \end{aligned} \quad (3.9)$$

The integration of temperature as an effort variable has no physical relevance, thermal inertia is not defined and an I -field equivalent with the C -field does not exist. Possible inertia in a thermofluid system is only related to the hydraulic part and is not very relevant in a system where only the gas phase is present. In (Moksnes 1997) it is shown how inertia for water flow can be implemented by pseudo-bond graphs.

Several applications of the pseudo-bond graph exist in literature. Some of them are; models of heat conduction within a system (Aesoy and Engja 1994) and (Engja

1985), compressors (Engja 1985), engines (Pedersen and Engja 2000), continuously stirred tank reactor (Heny, Simanca et al. 2000) and process control (Samantaray and Bouamama 2008). (Benbouzid, Fouquet et al. 2003; Benbouzid, Dauphin-Tanguy et al. 2004), (Saisset, Turpin et al. 2002; Saisset, Fontes et al. 2006) and (Bruun and Pedersen 2007) all apply variants of pseudo-bond graphs for fuel cell modelling.

A different approach to modelling thermodynamic systems has been introduced by (Brown 1991); convection bond graphs. The new convection bond has two effort variables and one flow variable to fix the thermodynamic state of a system. The main intention is to keep the graph structure and power flow as in true bond graphs. A new element for heat transfer is introduced, junctions are redefined and macro elements are used to enable a good representation. These deviations from standard bond graph representation might be the reason why few applications of the convection bond graphs by other authors can be found in the literature.

(Greifeneder 2001) tries to keep the definition of power bonds as in Figure 3.1 as well as avoiding the common assumptions of quasi-stationary or flow equilibrium conditions. A bus bond is defined assembling the three bonds for thermal, volume and mass flows, each representing one term on the right hand side of equation (3.3). Compared to the methods introduced above, this approach claims a more realistic treatment of energy exchange between the three energy forms involved in fluid flow. To enable the use of linear state equations new bond graph macro-elements are introduced describing the storage and exchange of energy and mass. This makes the models difficult to read and follow even for experienced bond graphers. The authors have produced a Modelica library “ThermoBondLib” with components based on the above bond graph development (Cellier 2008) making the models more accessible to other users.

(Pedersen 1999) and (Pedersen 2001) showed how pseudo-bond graphs can be extended to account for multicomponent and multi-phase gas mixtures. The hydraulic and thermal bond is kept as for a single component flow, and one mass fraction bond is added for each extra component i , Figure 3.6. Variables chosen are mass flows for each component and partial pressure or mass fraction as effort variables, equations (3.8) and (3.9) must be extended to account for mass composition. Junction structures and basic elements are kept consistent with the pseudo-bond graph introduced above.

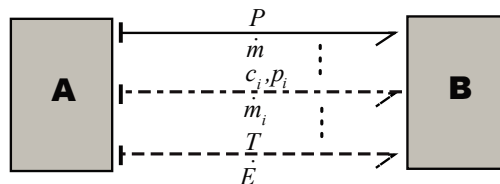


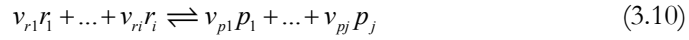
Figure 3.6 Pseudo-bonds for multicomponent flow

Major strengths of the pseudo-bond graph are that the variables chosen are familiar to the engineering community, that thermodynamic data exist and that

frequently used state equations can be applied. Thermodynamic data are in general found from equilibrium analysis built on static systems and are therefore not always well suited for dynamic models. Iteration in thermodynamic data tables becomes necessary as systems grow in complexity with a number of gases and phases. Pseudo-bond graphs allow one to choose the variables most appropriate for such iteration (Moksnes 1997). (Brown 2002) introduce ways to avoid the iteration procedures in finding state variables. Methods applied to the convection bond graphs are also well suited for pseudo-bond graphs and this contribution might improve system simulations.

3.2.1 Bond graphs for chemical reactions

A general reaction between i chemical reactants with molecule name r_i forming j products with name p_j can be expressed by (3.10). The number of each molecule participating in a reaction is noted by the stoichiometric constants of reaction, v . The double arrow indicates that a reaction can move in any direction. The system has reached equilibrium when net concentrations of reactants and products are constant.



Applying Legendre transformation on equation (3.3) the energy potential of a chemical reaction is described by the Gibbs free energy (3.11) of a closed volume. For reactions to occur spontaneously the change in Gibbs free energy must be negative, at equilibrium the Gibbs free energy is zero.

$$dG = VdP - SdT + \mu_{r_1}dn_{r_1} + \dots + \mu_{r_i}dn_{r_i} - \mu_{p_1}dn_{p_1} - \dots - \mu_{p_j}dn_{p_j} \quad (3.11)$$

If reactions are assumed to occur at constant temperature and pressure we have a quasi-equilibrium approach. The mixture is in equilibrium with its environment and the chemical potential, μ , and the number of moles, n , of each component governs whether a reaction occurs spontaneously or not. Chemical potentials and molar flows are therefore obvious choices describing chemical reactions in bond graph notation. (Brown 2006), (Thoma and Ould-Bouamama 2000), (Karnopp 1990) all model chemical and electrochemical reactions by bond graph using these variables.

In (Karnopp 1990) the dynamics of chemical reactions are described by the reaction rate J and the affinity A defined by a mixture of the chemical potentials, molar flows and the stoichiometric coefficients v_i , according to (3.12). The coefficients v_i are negative for reactants.

$$A = -\sum_{i=1}^{r+p} v_i \mu_i \quad \dot{n}_i = v_i J_i \quad (3.12)$$

The product of J and A is the irreversible loss of Gibbs free energy during a chemical reaction, equation (3.13). In bond graph notation an R -element is generally used to set the reaction rate J (the flow variable) as function of the

affinity A (the effort variable). The loss of energy can be accounted for by a thermal bond as described later in this section.

$$A \cdot J = -\frac{d}{dt}G = \sum_{i=1}^r \mu_i \dot{n}_i - \sum_{j=1}^p \mu_j \dot{n}_j \quad (3.13)$$

Whether the reaction is endothermic or exothermic is found from the enthalpy of reaction being the sum of the change in Gibbs free energy and the entropy production (3.14). If the absolute value of the Gibbs free energy is larger than the entropy production, the enthalpy change is negative and heat is released (an exothermic reaction). If the enthalpy change is positive we have an endothermic reaction.

$$dh = dg + Tds \quad (3.14)$$

A true bond graph representation of equation (3.11) will be an extension to Figure 3.1 with a number of power bonds equivalent to the number of reactants and products involved in the reaction. Figure 3.7 shows the bond graph for the general reaction of eq. (3.10). The reaction rate J is here set by a flow source. As shown later this representation will be altered depending on whether it is a chemical or an electrochemical reaction.

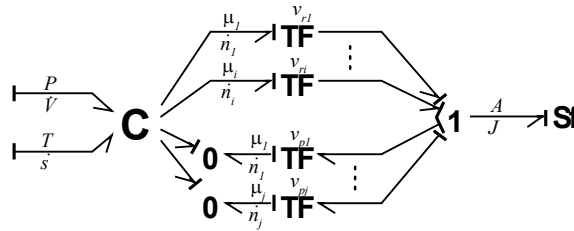


Figure 3.7 Chemical reaction by true bond graphs

As discussed in the previous chapter thermodynamic variables are not so easily found with internal energy as the state equation. Using true bond graphs and the Gibbs free energy state equation results in a mixed causality C -field (Karnopp 1990). To avoid this we have chosen to treat the gas dynamic relations by pseudo-bond graphs. A way to connect the pseudo-bonds with chemical bonds is elaborated below and shown in Figure 3.8.

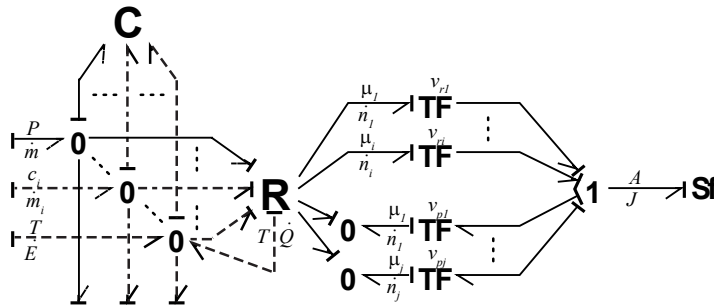


Figure 3.8 Mix of thermofluid pseudo-bonds and true chemical bonds

The interaction between pseudo-bonds and the chemical bonds is represented by an R -field. Essentially this is an energy conserving transformation of the pseudo-bond variables in a gas volume to chemical or electrochemical power variables. The constitutive equations for the R -field are derived assuming constant pressure, temperature and volume for each time step during simulation of the chemical reaction. The entropy and enthalpy for pure components at the current temperature and pressure is used according to equation (3.15) to calculate the chemical potential for each component. This connects the effort inputs P , c_i and T to the output μ on the chemical side.

$$\mu_i = h_i(T, c_i) - Ts_i(T, P, c_i) \quad (3.15)$$

In Figure 3.8 two thermal power-bonds are used to represent the total energy flow, equation (3.16), caused by the reactions. The upper bond represents the change in enthalpy and the lower bond the entropy production due to the overall change in molar composition.

$$\dot{E}_{tot} = \sum_{i=1}^{r+p} h_i \dot{n}_i - T \sum_{i=1}^{r+p} s_i \dot{n}_i \quad (3.16)$$

Conservation of mass through the element gives relation (3.17) between the mass and molar flow variables of the R -field, M_i is the molecular weight.

$$\sum_{i=1}^{r+p} \dot{m}_i = \sum_{i=1}^{r+p} \dot{n}_i M_i \quad (3.17)$$

(Gawthrop 1999) argues that the mixing of true bond graphs and pseudo-bonds done in for instance the thermodynamic accumulator of Figure 3.4 is “conceptually awkward and can lead to erroneous bond graphs if great care is not taken.” He introduces a two-port energy-conserving component, the “flow-to-power converter” FP , joining true bonds with pseudo-bonds. The FP -element is used to create three new macros; components being pseudo-bond graphs internally and true bond graphs externally. He uses standard relations “hiding” them from the remaining bond graph. The elements are developed for non-flow thermodynamic processes and are therefore simple and linear. The R -field above has essentially the same functionality, and some might prefer naming it a FP -field. Due to nonlinear relations, the variable numbers of bonds and the mix of pseudo-bond with true bond graph an R -field is chosen to represent these relations. This is consistent with the pseudo-bond graph R -field of Figure 3.5 representing general relations between effort and flows, with no losses present.

Chemical reaction rate

Reaction rates are usually not available analytically. Kinematic expressions based on the “mass-action law” still exist. The law states that the measurable net reaction rate is a sum of the forward and aft reaction rates of the reactants and products in a mixture (Auslander, Oster et al. 1972). It is found that most experimental results can be fitted to an expression similar to equation (3.18) where k_f and k_b are the

forward and backward reaction rate coefficients. The partial pressures P_i can be given in terms of total pressure and molar fraction y_i .

$$J = k_f \prod_{i=1}^r (P_i)^{\nu_i} - k_b \prod_{j=1}^p (P_j)^{\nu_j} \quad (3.18)$$

$$P_i = y_i P$$

When temperature and pressure of an ideal gas mixture is known, the composition of a system in equilibrium will apply to equation (3.19) (Bejan 2006). This expression is equivalent to the affinity of equation (3.12) being zero. An equilibrium constant is defined as function of temperature, equation (3.20). At this temperature the reactions will approach a specific molar concentration for each reactant and product.

$$-\sum_{i=1}^{p+r} \nu_i \mu_i(T, P_0) = RT \ln \left(\left(\frac{P}{P_0} \right)^{\sum \nu_i} \prod_{i=1}^{p+r} y_i^{\nu_i} \right) \quad (3.19)$$

$$K_{ig,e}(T) = \left(\frac{P}{P_0} \right)^{\sum \nu_i} \prod_{i=1}^{p+r} y_i^{\nu_i} = e^{\frac{-\sum \nu_i \mu_i(T, P_0)}{RT}} \quad (3.20)$$

The overall reaction rate J is zero at equilibrium. The ratio between the reaction rate coefficients of equation (3.18) will then be expressed by (3.21), a relation between the concentration of the components corresponding to the equilibrium constant for $P_0=1$ atm.

$$\frac{k_f(T)}{k_b(T)} = \prod_{i=1}^{r+p} (P_{i,e})^{\nu_i} = P^{\sum \nu_i} \prod_{i=1}^{r+p} y_{i,e}^{\nu_i} = K_{ig,e}(T) \quad (3.21)$$

Based on the above expressions, equation (3.22) express the reaction rate in an ideal gas mixture (Haberman and Young 2006). Actual values for the partial pressures are used. When these values become equal to the partial pressures at equilibrium, $P_{i,e}$, the reaction rate is zero. Coefficients for chemical reaction rates are typically expressed by an Arrhenius equation, (3.23), where K is an empiric constant and E_{act} is the activation energy.

$$J = k_f(T) \left(\prod_{i=1}^r (P_i)^{\nu_i} - \frac{1}{K_{ig,e}(T)} \left(\prod_{j=1}^p (P_j)^{\nu_j} \right) \right) \quad (3.22)$$

$$k_f(T) = K e^{\frac{-E_{act}}{RT}} \quad (3.23)$$

The derivation above shows that the flow variable J is not commonly expressed as a function of the effort variable A . The reaction rate expressions do therefore not fit well with bond graph terminology. One alternative is to represent the reaction rate for a chemical equation by a modulated R -element as shown in Figure 3.9. Pressure and a concentration vector are signal inputs from the pseudo-bond graph. The total mass and energy inside the control volume remains unchanged if no

work is extracted from the chemical reactions (no electrochemical work). Thermal bonds representing the change in Gibbs free energy and the entropy production are therefore included to transport the energy back to the pseudo-bond side. The change of temperature in a gas volume due to chemical reactions becomes a function of the difference between enthalpy of the gas mix flowing into and out of the volume.

The detailed bond graph of Figure 3.9 is rather messy and might seem superfluous. Concentration, temperature and pressure are variables of a pseudo-bond graph, and the above relations can easily be implemented in a pseudo-bond R -field representing the rate of change in gas composition, Figure 3.10. Information lost when omitting the true bond graph is a graphical way of monitoring the chemical potentials and molar flows of a reaction. (Lefèvre and Barreto 1985) also suggests a similar way of using chemical concentration as the effort variable describing chemical reactions by pseudo-bonds.

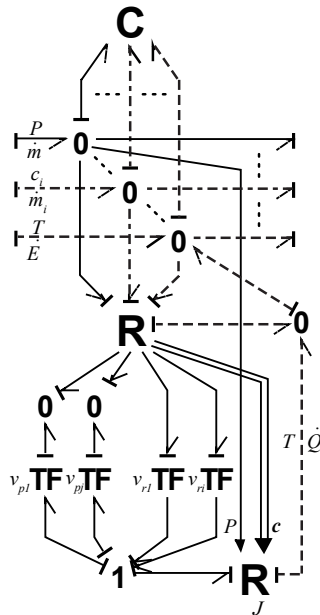


Figure 3.9 Reaction rate by true BG

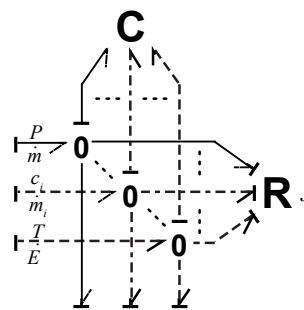


Figure 3.10 Reaction rate by pseudo BG

The reaction rate of equation (3.18) is further elaborated in (Auslander, Oster et al. 1972) to be expressed by the affinity of the reactants A_r and products A_p in equation (3.24). Signal bonds setting pressure and gas composition are no longer needed as input to the R , but a modulated R -element is still required to separate the affinities of reactants and products. The corresponding graph can be found in Figure 3.11.

$$J = k_f e^{-\sum v_i^f \mu_i^0 / RT} \left[e^{A_r / RT} - e^{A_p / RT} \right] \quad (3.24)$$

In (Couenne, Jallut et al. 2008) an alternative bond graph representation of chemical reaction rate is shown by using vector bonds from the C -field of Figure 3.7 to the reaction rate. A vector TF -field implements the stoichiometric coefficients relating flow rates to reaction rates and chemical potentials to the affinities. The bond graph is used to model reactions in a perfectly mixed gas phase autoclave.

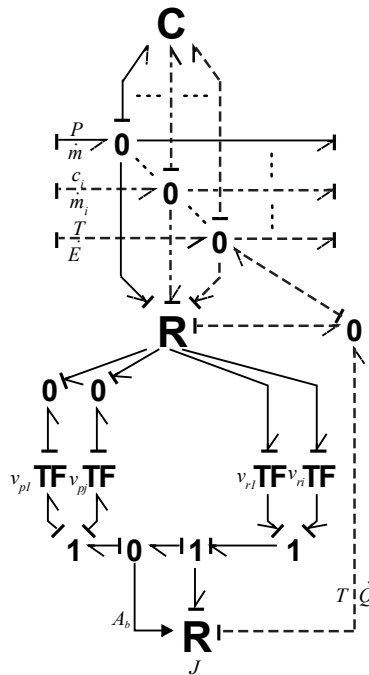


Figure 3.11 Reaction rate by (Auslander, Oster et al. 1972)

When the pseudo-bond graph method is used to describe gas and heat flows traditional elaborations of the reaction rate can easily be implemented in the R -field of Figure 3.10 and this approach is preferred for future model implementation.

3.2.2 Bond graphs for electrochemical reactions

An electrochemical reaction occurs when a transfer of charges in the form of electrons must be present for the reaction between components to happen. Typical examples are; electrolysis where electrical power must be supplied for reactions to proceed, and batteries or fuel cells which both can deliver electrical power to a consumer. The basic principle is shown for a fuel cell in Figure 3.12. A multiple of ions can diffuse between the electrodes, and a number of reactions can be combined. Whether the products are released on the anode or the cathode side depends on the nature of the reaction. General relations for reactions at the anode and cathode side are presented in(3.25), a more detailed description is given for a solid oxide fuel cell in chapter 4.

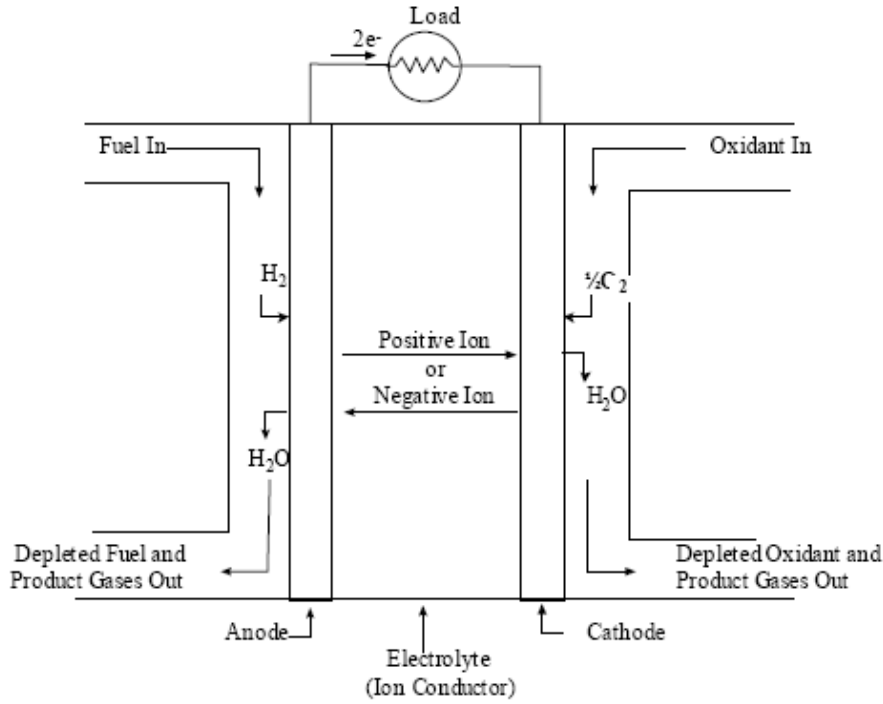
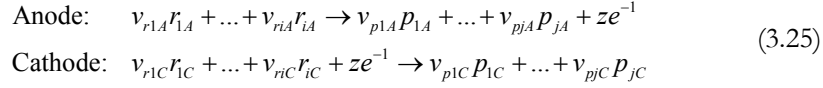


Figure 3.12 Electrochemical reaction in a fuel cell (EG&G 2004)

Electrochemical reactions are modelled by recognizing the relation between the current (electron flow) and the reaction rate (molar flow) as dependent only on Faraday's constant F (the charge of one mole of electrons) and the charge transfer number z (number of electrons per reaction). The same holds for the relation between change in Gibbs free energy and the voltage as described by the equations in (3.26).

$$\begin{aligned}
 i &= zFJ_{el} & V_r &= \frac{-\Delta g}{zF} \\
 -\Delta g &= v_i\mu_{rA} + v_i\mu_{rC} - v_i\mu_{pA} - v_i\mu_{pC}
 \end{aligned} \tag{3.26}$$

When no external power is supplied or released from the reactions, we have equilibrium and open circuit voltage between the electrodes, represented by V_r in equation (3.26). When a cell is loaded the reaction has to overcome the activation energy at both anode and cathode and the output voltage is lowered by these activation losses. Also losses due to ion and electron transport occur and are modelled as ohmic losses. Losses are traditionally represented as overvoltages, η , and the thermal energy produced by these losses is expressed according to equation (3.27).

$$\eta i = \dot{Q} \quad (3.27)$$

Equations (3.26) are implemented by *TF*-elements and a centred *I*-junction in the bond graph of Figure 3.13. The product of z and F is the transformer modulus between chemical and electrical domains. As for ordinary chemical equations the stoichiometric coefficient is used as transformer modulus to set the relative amount of each component participating in the reaction. Losses are implemented by two-port *R*-elements assuring a energy conserving model. Their causal implementations depend on the nature of the relevant reaction as some phenomena might dominate others. Further discussion of this and presentation of alternative causal representations are left for chapter 4.

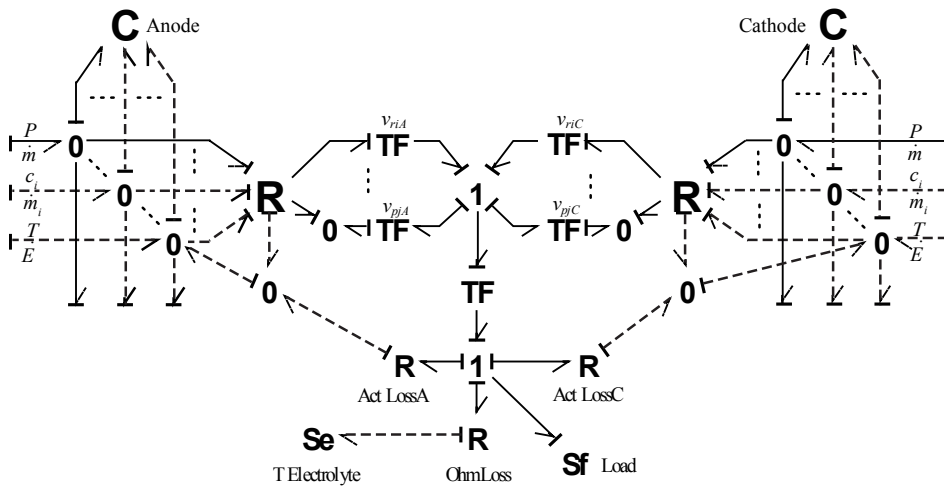


Figure 3.13 Bond graph of electrochemical reaction

C-fields represent accumulation of mass and energy in the anode and cathode gas channels. The *R*-fields are based on the one described in Figure 3.8 representing the relation between pseudo-bond variables and true bond graph variables. In addition, the diffusion losses caused by mass transport to the reaction site can be implemented here. Due to entropy production not all the energy in the mass flow to the reaction site is obtainable as electrochemical work, equation (3.14). This is implemented together with the diffusion loss as the thermal output bond from the *R*-field.

Reactions occur at the interface between one of the electrodes and the electrolyte, and ions diffuse between the two electrodes as shown in Figure 3.12. Since we have a reaction between two control volumes a net change of mass and energy in each control volume can occur. For the SOFC presented next, oxygen ions are transported from the cathode to the anode side. This is accounted for in the model by the mass and energy variables of the corresponding pseudo-bonds into the *R*-fields.

Chapter 4

Bond Graph Modelling of a SOFC stack

In section 1.1.4 the high temperature fuel cell is introduced as one of the most promising fuel cell alternatives for marine vessels. When introducing such a new component in complex machinery systems, the dynamic behaviour of power-interfaces across multiple physical domains must be studied. Mathematical models enabling these analyses are therefore developed for a solid oxide fuel cell (SOFC) stack.

This system is implemented using the bond graph framework introduced in chapter 3. First, a lumped model of the single fuel cell is developed. Next, the possible expansion to a distributed model is presented. Models of the other components included in a typical SOFC power plant are also developed. Only general model descriptions are documented; parameters and simulations for a case implementing and testing these models are presented in chapter 5.

4.1 System description

Basic fuel cell

A single fuel cell is a small unit producing power through electrochemical reactions, typically a reverse electrolysis of hydrogen and oxygen with water as product. The absorption and release of electrons sets up an ideal voltage, V_r , of approximately 1.0 V between two electrodes. Subtracting losses described further in chapter 4.2.3, this voltage can be utilized by the surroundings when current, i , is drawn from the cell. Ideal electrical power, P_r , from a single cell can be expressed by equation (4.1), where dG is the change in Gibbs free energy of formation for the chemical reaction.

$$P_r = V_r i = -dG = -(g_{H_2O} - g_{H_2} - 1/2 g_{O_2}) \dot{n} \quad (4.1)$$

The last expression in (4.1) is specific for a hydrogen fuelled fuel cell, where g is the molar Gibbs energy and \dot{n} is the molar flow of the reacting components.

A number of cells are joined by interconnect material in a serial circuit, and the voltage from each cell is added to produce overall stack power. The nature of reactions and ion transport in anode, cathode and through the electrolyte are different for each fuel cell type, Table 1.1. The basic operation of a fuel cell was shown in Figure 3.12.

The power density of a fuel cell depends on the rate of electrochemical reactions. High rates are achieved by making the electrodes flat with large surfaces and thin electrolytes in-between. An important performance criterion for a fuel cell is therefore the current density; the number of electrons per m² electrode at optimal operating point. More detailed introductions to fuel cells can be found in e.g. (Larminic and Dicks 2003) or (EG&G 2004).

The solid oxide fuel cell

The solid oxide fuel cell operates at high temperatures (600-1000°C) giving high reaction rates and enabling operation on natural gas as fuel. Each SOFC consists of two porous electrodes, the anode (Ni-ZrO₂ cermet) and the cathode (Sr-doped LaMnO₃), separated by a solid ceramic electrolyte (usually Y₂O₃-stabilized ZrO₂), (EG&G 2004). Anode, cathode and electrolyte are often described by the collective term MEA (membrane electrolyte assembly). Different designs for the MEA are purposed and tested for SOFCs. The tubular design of SiemensWestinghouse (Siemens 2007) is modelled in the present thesis. Here the MEAs are formed as tubes, Figure 4.1, where air flows inside the tube and up along the cathode. Between a stack of connected tubes fuel is supplied along the anode surfaces, flowing in the same direction as cathode air.

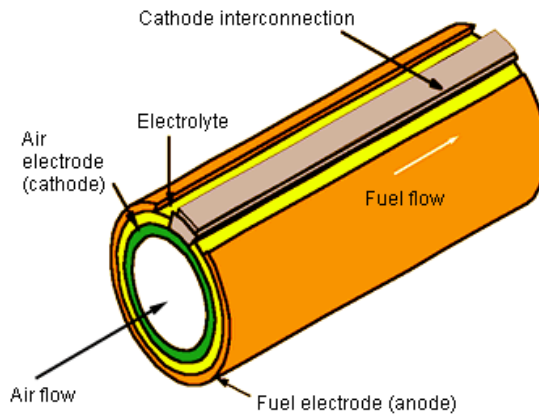
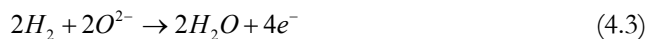


Figure 4.1 Siemens cylindrical-tube SOFC Technology (Siemens 2007)

Reactants diffuse through the porous electrodes to the triple phase boundaries (TPB) where electrode and electrolyte allow for the electrochemical reactions to take place, see Figure 4.2. A reduction of oxygen in air occurs at the cathode side (4.2). Oxygen ions are conducted through the electrolyte. An oxidation of fuel (4.3) occurs on the anode side, releasing electrons that are forced through an electric circuit.



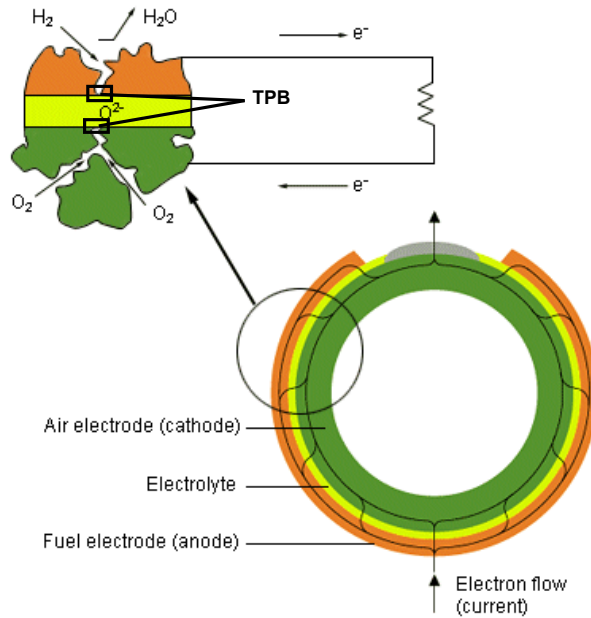


Figure 4.2 The current path through the membrane assembly (Siemens 2007)

More detailed descriptions of operation and design of this and other solid oxide fuel cell types can be found in (Singhal 2003).

Fuel reforming

It is common to use methane as fuel in SOFCs. The methane needs to be transformed into carbon monoxide and hydrogen through a reforming process. This process includes a combination of steam reforming of methane and the water gas shift reaction, equations (4.4) and (4.5). Steam from the electrochemical reactions together with the high operating temperatures enables these reactions.



Pre-reformers are included in the process plant, but some reforming will also occur inside the anode gas channel. The pre-reforming process is divided in two stages, one adiabatic and one where heat is supplied from the fuel cell stack. This is necessary due to the endothermic nature of the reforming process.

Carbon monoxide can also react electrochemically with oxygen ions and add to the power production according to equation (4.6).



Under the conditions present at the anode of an SOFC, the oxidation of carbon monoxide is much slower than hydrogen oxidation. The shift reaction will therefore dominate the transformation to carbon dioxide, and direct oxidation is ignored in the model (Selimovic 2002).

The stack and process plant

Figure 4.3 describes the basic operation of a tubular SOFC stack and its main process components.

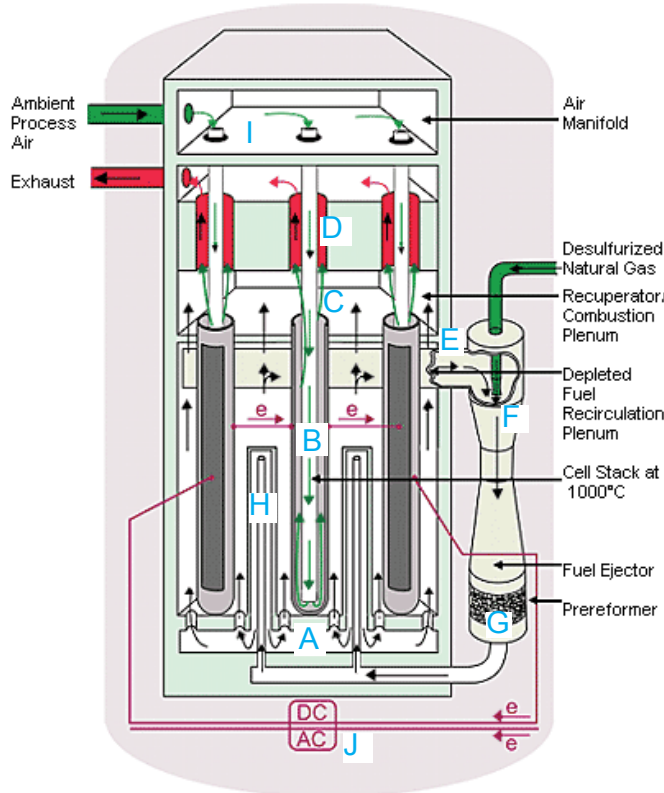


Figure 4.3 Basic operation of an SOFC stack (Siemens 2007)

Inside the stack fuel is supplied as a gas flowing between the tubes (A), along the anode surfaces. At the cathode side oxygen is supplied by an air flow through air delivery tubes (ADT) (B). The air exits the ADT at the bottom of each tube, allowing air and fuel to flow in the same direction. Outside the tubes steam, carbon dioxide and heat is transported away as products of the reactions. Air exiting the tubes is mixed with the anode gas flow in afterburners (C) where complete combustion can be assumed and the exhaust contains only oxygen, nitrogen, steam and carbon dioxide. The exhaust heat is utilized in tubular heat exchangers to increase the temperature of air entering the tubes (D).

Some of the anode gas is recycled (E) in order to keep the steam to carbon ratio high enough, typically in the area of 2-3, allowing for a specified degree of pre-reforming. Fresh fuel is induced in an ejector at high pressure (F) to increase the pressure of the recycled anode gas. Fresh fuel and the recycled gas enter a pre-reformer (G). Pre-reforming also occurs inside the stack catalyzed by heat from the electrochemical reactions (H). Air must also be supplied at an increased pressure

level (I) driving the flow through the system. This can be provided by a compressor or a further integration with gas or steam turbines, a system not treated here. Power electronics must be supplied to convert the DC (direct current) output from the stack (J).

4.2 The solid oxide fuel cell model

Two main alternatives exist for dynamic modelling of a single fuel cell; a lumped approach using volumes with uniform pressure, temperature and concentrations for each gas channel, or a distributed model modelling the distributed nature of these variables along the cell. The first approach is common in overall system models and for control purposes (Kandepu, Imsland et al. 2007). In the work used as basis for the present thesis (Thorud 2005; Stiller 2006) a distributed model is developed by a quasi-2D approach (radial and axial direction for heat flow in solids, only axial direction for gas flows). Their model includes 40 mesh points in axial direction and three in radial direction.

In the present model the distributed nature of the cells is modelled as an extension to the lumped approach by simply dividing the gas channels and membranes in multiple control volumes, a repeated finite volume approach. This approach poses some challenges when modelling the electrochemical part of the system as will be discussed in ch. 4.3. A similar approach is also used by (Qi, Huang et al. 2006) who present the state space model for one finite slice of a tubular SOFC.

Figure 4.4 shows how a tubular SOFC can be divided into control volumes. Three control volumes enclose gas transport; one at the anode side (V_{fuel}), one at the cathode side (V_{air}) and one inside the air delivery tube (V_{ADT}). The remaining control volumes enclose the solid walls and membranes; one for the MEA ($V_{s,MEA}$) and one for the ADT ($V_{s,ADT}$). The basic phenomena to be modelled are gas-transport, chemical and electrochemical reactions and heat transport through both gas and solid materials.

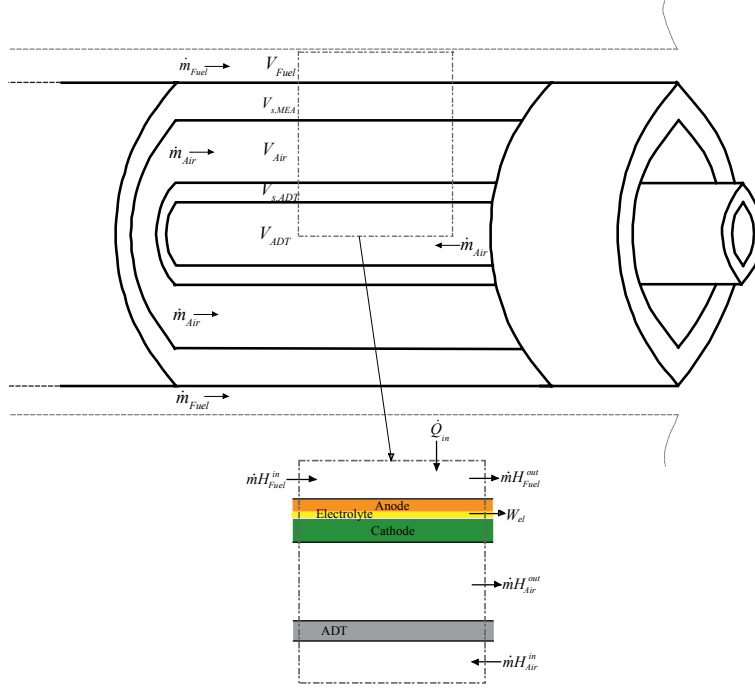


Figure 4.4 Control volumes, tubular SOFC

Conservation of energy and mass across the system boundaries are important aspects of the model. The first law of thermodynamics, (4.7), can describe the energy conservation for the single cell model. Here h denotes the specific molar enthalpy of each component i , and \dot{n} is the molar flow.

$$\frac{dE}{dt} = \dot{Q} + \dot{W}_{el} + \sum_{i,in} \dot{n}_i h_i - \sum_{i,out} \dot{n}_i h_i = 0 \quad (4.7)$$

The energy transferred from the gas channels either as electrical work, \dot{W}_{el} , or radiation heat, \dot{Q} , according to equation (4.8). Chemical potential of a gas component is denoted by μ_i and can express the change in Gibbs energy. The remaining energy will be transported out of the volume through the gas flow, and can be expressed by equation (4.9).

$$\begin{aligned} \dot{W}_{el} &= iV = -\Delta g \dot{n} - \dot{Q}_{loss} \quad (-\Delta g = 2\mu_{H_2} + \mu_{O_2} - 2\mu_{H_2O}) \\ \dot{Q} &= -\dot{Q}_{rad} \end{aligned} \quad (4.8)$$

$$\sum_{i,out} \dot{n}_i h_i = \sum_{i,in} \dot{n}_i h_i - (2\mu_{H_2} + \mu_{O_2} - 2\mu_{H_2O}) \cdot \dot{n} + \dot{Q}_{loss} - \dot{Q}_{rad} \quad (4.9)$$

Energy in and out of the fuel cell as a control volume is shown in the dotted frame of Figure 4.4. Heat transport is defined positive in to and electrical work is positive out of the volume. The enthalpy, H , of fuel and air express the energy of the mass, m , flowing across the system boundaries.

A control of the mass flowing into and out of the system should be applied to assure that the implementation conserve total mass of the system, equation (4.10).

$$\dot{m}_{Air,i} + \dot{m}_{Fu,i} = \dot{m}_{Air,o} + \dot{m}_{Fu,o} = \dot{m}_{Exh} \quad (4.10)$$

In the following subchapters general component models valid for finite volume representations are described. The special causal considerations needed when representing the cell by repeated finite volumes are presented in chapter 4.3.

4.2.1 Gas supply model

At the anode side fuel is supplied as a gas flow between the tubes, and steam, carbon dioxide and heat is transported away as products of the reactions. In addition to electrochemical reactions the reforming reaction (4.4) and the shift reaction (4.5) will change the gas composition in the anode gas flow. At the cathode side the ADT supplies heated air at the bottom of the tube. Air transports oxygen to the reactions as well as provide cooling for the stack.

Gas flow

Each gas volume is modelled by the pseudo-bond *C*-field introduced in chapter 3. Control volumes modelled as *C*-fields set the pressure, temperature and concentration of the gas flows. Pseudo-bond *R*-fields are implemented to model the flux of mass and energy in and out of each control volume, as shown in Figure 4.5. In SOFCs the gases flow at low velocities and can thus be modelled as plug flows with no gas dynamics included.

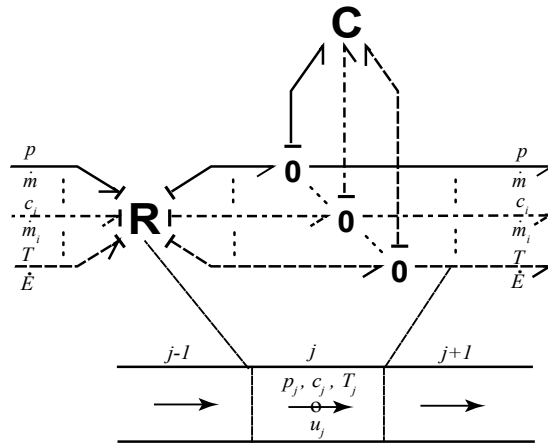


Figure 4.5 Pseudo-bond graph description of gas flow

In the anode flow of cells fuelled by methane, carbon monoxide, methane, steam and carbon dioxide are represented by separate pseudo-bonds for each mass fraction, c_i . The amount of hydrogen is found by subtracting these components from the total mass. On the cathode side only one mass fraction bond, for nitrogen, is included. The amount of oxygen is found by subtracting the nitrogen from the total mass.

Disregarding start-up and shut-down (requires special procedures), a SOFC system operates in a limited temperature and pressure area. The model is therefore implemented based on the ideal gas assumption. Constant heat capacities, $c_{v,i}$, around the operating temperature are also assumed, avoiding an iterative temperature equation (perfect gas). The constitutive laws for the pressure, P , mass fractions, c_i , and temperature, T , of each C-field then becomes:

$$P = \frac{mT}{V} \sum_{i=1}^N c_i R_i \quad (4.11)$$

$$c_i = \frac{m_i}{m} \quad (4.12)$$

$$T = \frac{E - E_0}{m \sum_{i=1}^N (c_i c_{v,i}(T_{0h}))} + T_{0h} \quad (4.13)$$

Here V is the volume, R_i the gas constant, E is the total energy and E_0 is the energy at a the temperature T_{0h} . T_{0h} is the temperature for which the value of the heat capacity c_v is found. N is the number of components in the gas mixture.

The constitutive laws of the R -fields are elaborated from a widely used relation for pressure loss, ΔP , in a straight channel based on experimental results, equation (4.14) (Overli 1978).

$$\Delta P = \left(f_l \frac{l}{d_{hyd}} \right) \frac{1}{2} \rho u^2 \quad (4.14)$$

The pressure loss is a function of the hydraulic diameter, d_{hyd} , the gas density ρ and the velocity u . A friction factor, f_l , for laminar flow based on the Reynolds number, R_{re} , is used to rewrite the pressure drop according to (4.15) where μ is the viscosity, l is the length of each volume and A is the cross sectional area.

$$\begin{aligned} f_l &= \frac{64}{R_{re}} \quad R_{re} = \frac{\rho u d_{hyd}}{\mu} = \frac{\dot{m} d_{hyd}}{A \mu} \\ \Rightarrow \Delta P &= \frac{64}{2} \frac{l}{A d_{hyd}^2} \frac{\dot{m} \mu}{\rho} \end{aligned} \quad (4.15)$$

Thermodynamic properties are based on upstream pressure, temperature and gas composition. The flow direction is always set equal to the direction of pressure drop. Equations (4.16) and (4.17) calculate the resulting mass and energy flows through the border of a control volume.

$$\dot{m} = \frac{A d_{hyd}^2}{32l} \frac{(P_u - P_d) \rho(P, T, \mathbf{c})_u}{\mu(P, T, \mathbf{c})_u} \quad (4.16)$$

$$\dot{E} = \sum_{i=1}^N \dot{m}_i h_i(T_u) \quad (4.17)$$

Change in gas composition

The shift reaction rate is modelled as described in section 3.2.1, with the resulting equation (4.18) for molar production of hydrogen. The constant k_{fs} is set as high as possible, without causing numerical problems, to assure equilibrium condition at all times (Stiller 2006). The equilibrium coefficients, K_{ps} based on equilibrium values, and K_{as} , based on actual values, depend on temperature, pressure and chemical potentials, equation (4.19) (Haberman and Young 2006).

$$J = \dot{n}_{H_2} = k_{fs} \left(P_{H_2O} P_{CO} - \frac{P_{H_2} P_{CO_2}}{K_{ig,e}} \right) \quad (4.18)$$

$$K_{ig,e} = e^{\frac{-(\mu_{H_2}^0 + \mu_{CO_2}^0 - \mu_{H_2O}^0 - \mu_{CO}^0)}{RT}} \quad (4.19)$$

The reforming rate of methane can be modelled using the same approach. Inside the SOFCs this reaction occurs on the anode surface catalyzed by nickel-cermet materials. In literature there is described some uncertainty regarding this reforming rate as discussed in (Selimovic 2002). The empiric relation most frequently referred to, based on Arrhenius law and developed by (Achenbach 1994), is adopted here, eq. (4.20). A_{el} is the active area of the fuel cell.

$$J = \dot{n}_{H_2} = 3 \cdot 4274 e^{\frac{-82000}{RT}} y_{CH_4} \frac{P}{10^5} A_{el} \quad (4.20)$$

As introduced in section 3.2, R -fields attached to the zero junctions of the control volume C -fields are used to model the change in gas composition caused by chemical reactions, Figure 4.6. The R -field calculates and sets the rate of a chemical reaction based on the current temperature, pressure and gas composition in the volume. The reforming reaction is endothermic and the shift reaction is exothermic. No work or heat transfer to the surroundings are caused directly by these chemical reactions, and the change in free energy is accounted for by the enthalpy flow in and out of the control volume, see equation (4.7). Zero energy therefore flow on the thermal bonds of Figure 4.6. Conservation of mass for each reaction can be controlled by monitoring the bonds representing net mass flow into the R -fields.

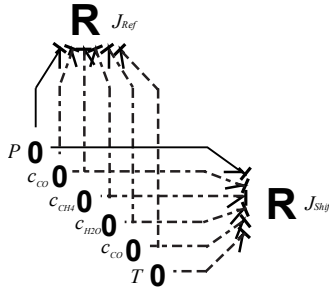


Figure 4.6 Chemical reactions in anode channel

4.2.2 Heat transfer model

In high temperature fuel cells it is critical to monitor thermal gradients across the solid materials, as high thermal gradients might damage the cell. A model representing heat flows inside the cell is therefore included. This model calculates heat exchange between the gas channels, and account for heat released from the electrochemical reactions inside the MEA. Also heat exchange between the cathode air flow and the ADT is modelled. Figure 4.7 shows the different convection, conduction and radiation phenomena included in the model. All heat flows occur in radial direction of the fuel cell tube. Heat loss to the surroundings is represented by conduction to an imaginary wall of the fuel channel. In a real stack this will be replaced by heat exchange with a neighbouring fuel cell.

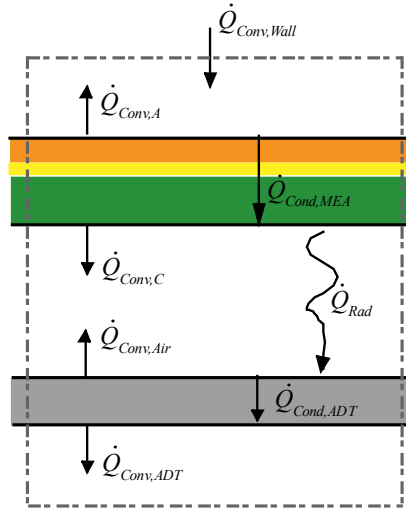


Figure 4.7 Heat flows in fuel cell

Convection between solid walls and gas flows is described by the well known equation (4.21) with the heat transfer coefficient h set by equation (4.22), (Incropera and DeWitt 2002).

$$\dot{Q}_{conv} = hA(T_{gas} - T_{wall}) \quad (4.21)$$

$$h = \frac{Nu\lambda}{d_{hyd}} = \frac{Nu\lambda}{4A/P} \quad (4.22)$$

Hydraulic diameter, d_{hyd} , is defined by flow cross sectional area, A , and wetted perimeter P . The Nusselt number, Nu , and the thermal conductivity, λ , can for some cases be treated as constants. This assumption is validated in chapter 5.

Radiation between the solid walls can be described by equation (4.23) where the heat transfer is set by Stefan-Boltzmann law with the constant σ_B and the surface emissivity ε .

$$\dot{Q}_{rad} = \varepsilon\sigma_B A(T_{wall1}^4 - T_{wall2}^4) \quad (4.23)$$

In the above models, the heat conduction through the solid is represented by a single heat capacity setting the temperature. The capacity constant is set by equation (4.24).

$$C = A\rho c_v l$$

$$\Rightarrow T = \frac{1}{C} \int \dot{Q} dt \quad (4.24)$$

Figure 4.8 shows the bond graph model implemented for the control volume representation in Figure 4.7. Heat flows are output from *R*-elements, calculated based on temperature inputs from each side. The implementation assures a positive heat flow from warm to cold independent of power bond directions. The heat capacities are included in *C*-elements setting the temperature and fixing the causality of the model.

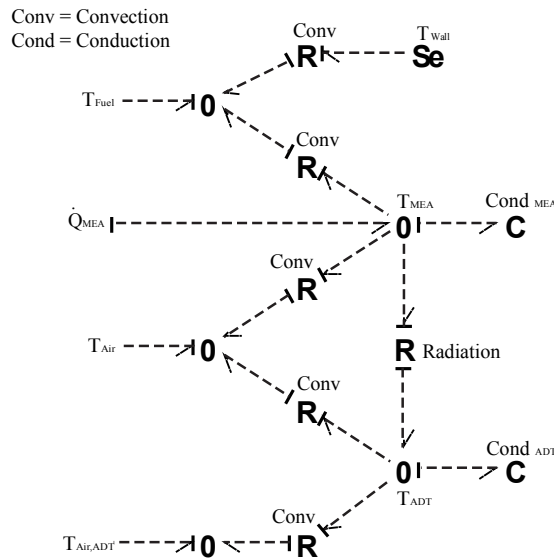


Figure 4.8 Bond graph of heat flows through MEA and ADT

The instant thermal conductivity and the Nusselt number can also be implemented as variables (Qi, Huang et al. 2006). Convection *R*-elements of Figure 4.8 then need to be modulated, either by these variables calculated in other elements, or by a composition vector together with the instantaneous mass flow and gas density.

A distributed 1 dimensional (1D) heat conduction model can be implemented through a modal presentation as shown in (Engja 1985). Using a modal representation enables detection of transient temperature gradients across the solid membranes. No major difference in overall dynamic behaviour of the current model was found when implementing this representation, so distributed heat conduction was not included in the final models. This lumped capacity approach is also supported by (Haynes 2002).

A distributed model will be implemented to show the temperature variations along the cell. In this case, heat flows in radial direction shown in Figure 4.8 are repeated for each section. Conduction in the axial direction of the solids will also occur, but is assumed ignorable compared to the heat transported with the gas flows. If 3D characteristics along the cell are of interest, the model can be extended as discussed in (Engja 1985).

The purpose of the present model will be to monitor if and for how long critical temperature gradients occur across the membranes of each cell. They will occur where the temperature differences are highest. This will always be across the membranes and along the gas flow direction of the cell, and this quasi-2D model is believed to be sufficient.

4.2.3 Electrochemical model

As introduced earlier, the power from a fuel cell is produced through electrochemical reactions at the triple phase boundaries. There is a net transport of mass (oxygen ions) from the cathode side to the anode side, as well as a net energy transport from both gas volumes. Mass flows into the MEA control volume are expressed in (4.25).

$$\begin{aligned}\dot{m}_A &= \dot{m}_{H_2} - \dot{m}_{H_2O} = \dot{n}_{H_2} (M_{H_2} - M_{H_2O}) \\ \dot{m}_C &= \dot{m}_{O_2} = M_{O_2} \dot{n}_{O_2} \\ \dot{m}_{N_2} &= \dot{m}_{CO} = \dot{m}_{CH_4} = \dot{m}_{CO_2} = 0\end{aligned}\quad (4.25)$$

Energy transport from the anode and cathode gas volumes can be expressed by the enthalpy, equation (4.26).

$$\begin{aligned}\dot{E}_A &= \dot{n}_{H_2} (h_{H_2} - h_{H_2O}) = \dot{n}_{H_2} (\mu_{H_2} - \mu_{H_2O}) - T_A \dot{n}_{H_2} (s_{H_2} - s_{H_2O}) \\ \dot{E}_C &= \dot{n}_{O_2} h_{O_2} = \dot{n}_{O_2} \mu_{O_2} - T_C \dot{n}_{O_2} s_{O_2}\end{aligned}\quad (4.26)$$

Only the Gibbs free energy of equations (4.26) can be transformed to electric work. In the model, heat due to entropy production, equation (4.27), remains at the anode and cathode surfaces.

$$\dot{Q}_A = \dot{n}_{H_2} (s_{H_2} - s_{H_2O}) \quad \dot{Q}_C = \dot{n}_{O_2} s_{O_2}\quad (4.27)$$

The power available for electric work is given in equation (4.28).

$$\dot{W}_{el,A} = \dot{n}_{H_2} (\mu_{H_2} - \mu_{H_2O}) \quad \dot{W}_{el,C} = \dot{n}_{O_2} \mu_{O_2}\quad (4.28)$$

Actual output potential is limited by three main losses affecting the electrochemical process. These are the ohmic, the diffusion, and the activation losses described more closely in the following sections. Figure 4.9 shows how the activation losses dominate when current density is low, and diffusion (concentration) losses dominate at high current densities. The ohmic resistance is nearly linearly dependent on the current density.

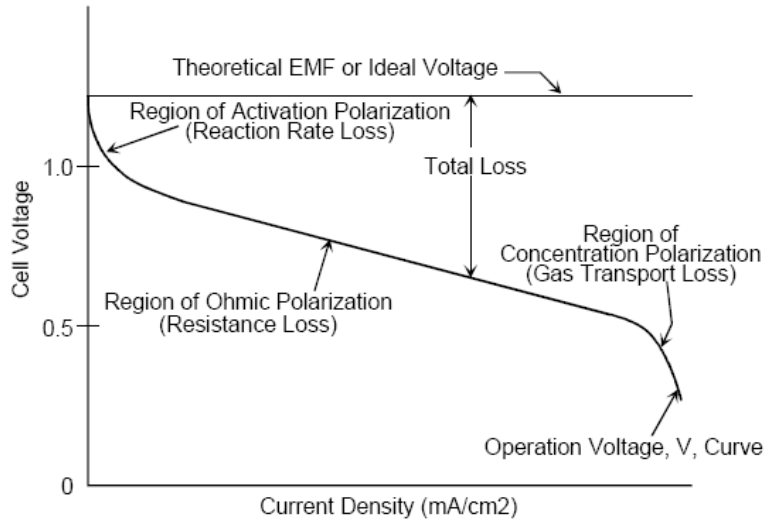


Figure 4.9 Voltage losses as function of current density (EG&G 2004)

Normally the losses (frequently also named overpotentials or polarisation) are implemented as voltage drops in a fuel cell model. With a bond graph model, one has the possibility to implement these losses in their actual physical domains. This can be beneficial when solving causal issues in a simulation model.

Following the relations outlined in section 3.2.2, a basic bond graph model of the electrochemical reactions in an SOFC is shown in Figure 4.10. These reactions result in an expression for available Gibbs energy, and a corresponding charge transfer number, as in equation (4.29).

$$-\Delta g = 2\mu_{H_2} + \mu_{O_2} - 2\mu_{H_2O} \Rightarrow z = 4 \quad (4.29)$$

The transfer between pseudo-bond variables and chemical potential are as described for the R -field in section 3.2. This is implemented in the same R -field as the diffusion losses for transport through the membranes. The loss of entropy from the reaction is added to the diffusion losses, and represented by thermal bonds out of the R -fields on the anode and cathode side. T_A and T_C are the surface temperatures of the anode and the cathode. Ohmic losses are shown at the electrical side, while the activation losses are left out for now. Ways to implement the three main losses in a fuel cell model is outlined below.

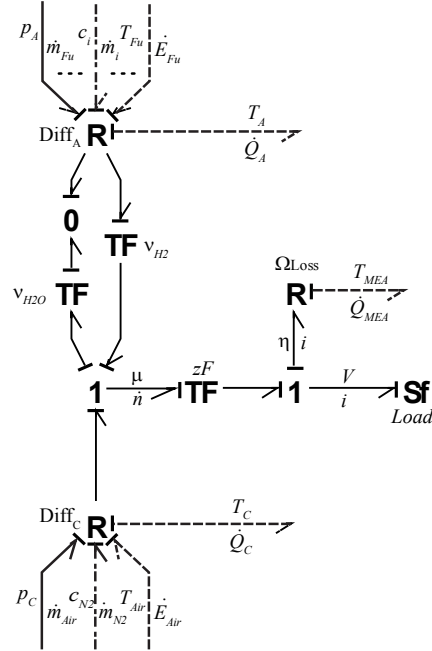


Figure 4.10 Electrochemical reactions

Ohmic losses

Ohmic losses are caused by the resistance towards electric charge flow in the membrane materials. Also the interconnecting material between the cells causes resistance and thereby loss of useful power.

The ohmic losses are frequently treated as a linear relation between the current drawn from the cell and the lost voltage, η_Ω (4.30). Here an expression developed for a tubular cell is adopted from (Stiller 2006). The material densities for anode, cathode and electrolyte, $\rho_{A,C,E}$, are slightly temperature dependent giving a nonlinear resistance factor, R_Ω , (4.31). In eq. (4.30) a degradation factor, R_d , is also included as the resistance may increase with pollutions of the membrane.

$$\eta_\Omega = (R_\Omega(T) + R_d)i \quad (4.30)$$

The resistance factor in (4.31) is expressed by the thickness δ of the MEA layers, the tube length l and the circumferential lengths of interconnect and electrolyte l_I and l_E .

$$R_\Omega(T) = \frac{1}{l} \left(\frac{\left(\left(\frac{\rho_A}{\delta_A} \right)^2 + \left(\frac{\rho_C}{\delta_C} \right)^2 \right) \cosh(J_E) + \frac{\rho_A \rho_C}{\delta_A \delta_C} (2 + J_E \sinh(J_E))}{2 \sqrt{\frac{1}{\rho_E \delta_E} \left(\frac{\rho_A}{\delta_A} + \frac{\rho_C}{\delta_C} \right)^{3/2}} \sinh(J_E)} + \frac{\sqrt{\rho_I \delta_I \frac{\rho_C}{\delta_C}}}{2 \tanh(J_I)} \right) \quad (4.31)$$

Equation (4.32) gives the variables used for the materials, and (4.33) the expression for the variables J_E and J_I .

$$\begin{aligned}\rho_A &= 1.053 \cdot 10^{-8} T_{MEA}^{\frac{1150}{T_{MEA}}} & \rho_C &= 2.381 \cdot 10^{-8} T_{MEA}^{\frac{1200}{T_{MEA}}} \\ \rho_E &= 2.994 \cdot 10^{-5} e^{\frac{10300}{T_{MEA}}} & \rho_l \delta_l &= 2 \cdot 10^{-7} \Omega m^2\end{aligned}\quad (4.32)$$

$$J_E = \frac{l_E}{2} \sqrt{\frac{1}{\rho_E \delta_E} \left(\frac{\rho_A}{\delta_A} + \frac{\rho_C}{\delta_C} \right)} \quad J_l = \frac{l_l}{2} \sqrt{\frac{1}{\rho_l \delta_l} \frac{\rho_A}{\delta_A}} \quad (4.33)$$

The equations are implemented in a two-port R -element, Figure 4.10, with one electric and one thermal bond. Input variables are current on the electric side and MEA temperature from the thermal side. Output variables are voltage drop η and heat flow \dot{Q} , (4.34). Since relation (4.30) is linear, causality on the electric side can be altered.

$$\dot{Q}_{loss} = \eta_{\Omega}(T_{MEA})i \quad (4.34)$$

Diffusion losses

Fuel must be transported from the gas volumes to the reaction sites. Anode and cathode materials hinder the diffusion process, and available energy is lost due to a lower concentration of fuel at the reaction sites. The rate at which gas flows through the materials must be modelled to find the concentration difference.

Fick's first law, (4.35), is an empirical relation defining the diffusion of component i through a component j at steady state. The molar flux J_i is the amount passing through an area normal to the z -direction of diffusion per time increment. The total flux is also dependent on convection, represented by the second term in equation (4.36) a relation assuming an ideal gas mixture and constant temperature and pressure throughout the diffusion path.

$$J_i = -D_{i,j} \frac{d(y_i / v_i)}{dz} \quad (4.35)$$

$$J_i = -D_{eff,i} \frac{P}{RT} \frac{dy_i}{dz} + y_i J_{tot} \quad (4.36)$$

Diffusion loss coefficients, D , for equation (4.35) can be expressed by the Fuller correlation in (4.37), where V_i are diffusion volumes specific for each molecule (Poling, O'Connell et al. 2001). This relation only holds for binary diffusion, and no proper relations really holds for diffusion of multicomponent mixtures. A mixing rule can be applied to estimate a modified diffusion coefficient, equation (4.38). For diffusion through membranes the constants are also modified by the Knudsen coefficient expressed by the pore radius r_{por} in (4.39).

$$D_{i,j} = 1.01323 \cdot 10^{-2} \frac{T^{1.75} \sqrt{0.001(M_i^{-1} + M_j^{-1})}}{P [V_i^{1/3} + V_j^{1/3}]^2} \quad (4.37)$$

$$D_i = \frac{1-y_i}{\sum_j \frac{y_j}{D_{i,j}}} \quad (4.38)$$

$$D_{K,i} = \frac{2}{3} r_{por} \sqrt{\frac{8RT}{\pi M_i}} \quad (4.39)$$

The effective diffusion coefficients through the electrodes are expressed by combining the above equations (Selimovic 2002), equation (4.40). Material properties porosity, ε , and tortuosity, τ , must be known for the electrodes.

$$D_{eff,i} = \frac{D_i D_{K,i} \varepsilon_{A/C}}{(D_i + D_{K,i}) \tau_{A/C}} \quad (4.40)$$

In a fuel cell the flux is directly related to the current density j and the reaction rate J for the electrochemical reactions, equation (4.41).

$$J_i = -D_{eff,i} \frac{P}{RT} \frac{dy_i}{dz} + y_i J_{tot} = \frac{j}{zF} = \frac{J}{A_{el}} \quad (4.41)$$

At the cathode side, only oxygen is diffusing since the convection of nitrogen to the TPB is zero and $J_{tot}=J_{O_2}$ in eq. (4.41). Using an ordinary diffusion coefficient in the gas volume and the effective diffusion coefficient through the cathode, we can find the concentration at the TPB, (4.42). The thickness of the air, t_{Air} , and the porous cathode, t_C , channels are necessary parameters.

$$y_{O_2,C} = 1 + (y_{O_2,B} - 1) \cdot e^{-\frac{\dot{n}_{O_2} RT 0.5 t_{Air}}{A_{el} D_{O_2} P}} \quad y_{O_2,TPB} = 1 + (y_{O_2,C} - 1) \cdot e^{-\frac{\dot{n}_{O_2} RT t_C}{A_{el} D_{eff,O_2} P}} \quad (4.42)$$

Through the anode the total convection is zero since $J_{H_2} = -J_{H_2O}$. The molar concentrations for hydrogen and water vapour at the anode surface and TPB can be found by integrating equation (4.41) assuming constant temperature and pressure (4.43).

$$\begin{aligned} y_{H_2,A} &= y_{H_2,B} - \frac{\dot{n}_{H_2} RT_{Fu} t_{Fu}}{A_{el} D_{H_2} P_{Fu} 2} y_{H_2,TPB} = y_{H_2,A} - \frac{\dot{n}_{H_2} RT_{Fu} t_A}{A_{el} D_{eff,H_2} P_{Fu}} \\ y_{H_2O,A} &= y_{H_2O,B} - \frac{\dot{n}_{H_2O} RT_{Fu} t_{Fu}}{A_{el} D_{H_2O} P_{Fu} 2} \quad y_{H_2O,TPB} = y_{H_2O,A} - \frac{\dot{n}_{H_2O} RT_{Fu} t_A}{A_{el} D_{eff,H_2O} P_{Fu}} \end{aligned} \quad (4.43)$$

Molar concentrations of the bulk volumes are used to express the reversible potential in equation (4.1). Therefore it is convenient to include the diffusion losses in the R -fields of Figure 4.10. Energy lost to the thermal model is expressed as the product of the molar flow rate and the drop in chemical potential. When temperature and pressure are assumed constant, the difference in chemical potentials can be expressed by equation (4.44). Definitions are based on the ideal gas assumption as outlined in Appendix C.

$$\Delta\mu_{diff,A} = RT_A \ln \left(\frac{y_{H_2} y_{H_2O,TPB}}{y_{H_2,TPB} y_{H_2O}} \right) \quad \Delta\mu_{diff,C} = RT_C \ln \left(\frac{y_{O_2}}{y_{O_2,TPB}} \right) \quad (4.44)$$

Additional control volumes can be included for the gas content in porous materials of anode and cathode. How this can avoid comprehensive algebraic loops will be discussed further in section 4.2.4. If such volumes are added, molar flow and not concentration is desired output from the R -fields and the above equations are rewritten. Equation (4.45) shows this for hydrogen and equivalent can be done for the oxygen and steam.

$$y_{H_2,TPB} = \frac{P^0}{P_{Fu}} \frac{e^{(\mu_{H_2} - \mu_{H_2}^0)}}{RT_A} \quad (4.45)$$

$$\dot{n}_{H_2} = (y_{H_2,B} - y_{H_2,TPB}) \frac{A_{el} P_{Fu}}{RT_{Fu}} \left(\frac{t_{Fu}}{2D_{H_2}} - \frac{t_A}{D_{eff,H_2}} \right)^{-1}$$

The control volume approach assumes a uniform gas composition in the whole volume, and molar fraction at the anode can be set equal to bulk concentration. The equations simplifies to:

$$y_{H_2,TPB} = y_{H_2,B} - \frac{\dot{n}_{H_2} RT_{Fu} t_A}{A_{el} D_{eff,H_2} P_{Fu}} \quad y_{H_2O,TPB} = y_{H_2O,B} - \frac{\dot{n}_{H_2O} RT_{Fu} t_A}{A_{el} D_{eff,H_2O} P_{Fu}} \quad (4.46)$$

$$y_{O_2,TPB} = 1 + (y_{O_2,B} - 1) \cdot e^{\frac{\dot{n}_{O_2} RT_{Air} t_c}{A_{el} D_{eff,O_2} P}}$$

$$\dot{n}_{H_2} = \frac{A_{el} D_{eff,H_2}}{t_A} \left(\frac{P_{Fu} y_{H_2,B}}{RT_{Fu}} - \frac{P_A y_{H_2,TPB}}{RT_A} \right)$$

$$\dot{n}_{H_2O} = \frac{A_{el} D_{eff,H_2O}}{t_A} \left(\frac{P_{Fu} y_{H_2O,B}}{RT_{Fu}} - \frac{P_A y_{H_2O,TPB}}{RT_A} \right) \quad (4.47)$$

$$\dot{n}_{O_2} = \frac{A_{el} D_{eff,O_2}}{t_c (y_{O_2,B} - 1)} \left(\frac{P_{Air} y_{O_2,B}}{RT_{Air}} - \frac{P_C y_{O_2,TPB}}{RT_C} \right)$$

The latter simplification will slightly underestimate the losses, but is accepted as the diffusion polarisation of an SOFC is typically very low.

Activation losses

Even when no current is drawn from the cell electrochemical reactions will take place at the electrodes. The kinetic energy of the gas components cause braking and making of bonds, and reactions will occur at an equivalent rate in both directions of equations (4.2) and (4.3). The voltage between the electrodes is the open circuit voltage, and the rate at which reactions occur is expressed by the exchange current density, j_0 . When a current larger than j_0 is drawn from the cell, more energy is needed to break additional bonds. An extra potential difference is required to drive the reactions; the activation overpotential. This potential will lower the available output voltage. SOFCs have high values of j_0 , allowing a high

electrochemical reaction rate and good fuel cell performance. Also the high temperature makes the activation losses lower in SOFCs compared to other fuel cells.

The dynamic relation for this build-up of charge can be represented by a capacitance called the “charge double layer”, (Larminie and Dicks 2003). The charge double layer acts as a capacitor between the electrodes and the electrolyte when an excess of ions of charge is present at their interface. As a result, the activation polarisation does not immediately follow a change in the current drawn from the system, but have a small time delay. For a high temperature fuel cell this delay has a marginal effect on the overall dynamic reaction and is often ignored.

When it comes to making a dynamic model without algebraic loops and with complete integral causality, different ways of implementing the activation losses and the charge double layer might be useful. Therefore, two causal ways of expressing the activation loss is presented. Physically, activation loss is related to speed of electrochemical reactions, and can be modelled both in the chemical and electrical domain. Due to frequent use of empiric relations a representation in the electric domain is chosen here.

Electron flow is limited by the speed of reactions at the boundary between gas, electrode and electrolyte, and the activation loss is controlled by the electrode reaction kinetics of the respective electrodes. The potential needed to drive reactions can be expressed through the logarithmic Tafel equation (Larminie and Dicks 2003).

$$\eta_{act} = A \ln \left(\frac{j}{j_0} \right) \quad (4.48)$$

In SOFC modelling a Butler-Volmer equation (4.49) for the cell current i is commonly used to express the slowest reaction which set the limit for current drawn from the cell. This equation is equivalent with the relations used for chemical reaction rates as for instance equation (3.24). This gives an implicit relation for the activation polarisation, η_{act} , see e.g. (Li 2006).

$$i = A_{el} j_0 \left\{ e^{\beta n F \eta_{act} / RT} - e^{-(1-\beta) n F \eta_{act} / RT} \right\} \quad (4.49)$$

Here A_{el} is the active surface area of the cell, R is the gas constant and β is the charge transfer coefficient (fraction of applied electrical energy used to change the rate of a reaction). For the SOFC with oxygen ions in the reaction $n = 2$. The exchange current density j_0 depend on materials at the reaction interface and their microstructure. As values are difficult to predict, an empiric function approximated for the tubular SOFC found in (Thorud 2005) is implemented here, eq. (4.50).

$$\begin{aligned} j_{0,A} &= \gamma_A (y_{H_2} + y_{CO})^{\beta_A} (y_{H_2O} + y_{CO_2})^{1-\beta_A} e^{-\frac{E_{act,A}}{RT_A}} \\ j_{0,C} &= \gamma_C y_{O_2}^{\beta_C} e^{-\frac{E_{act,C}}{RT_C}} \end{aligned} \quad (4.50)$$

Alternatively, (Chan, Khor et al. 2001) give an explicit relation for the activation loss in fuel cells when the transfer coefficient is $\beta = 0.5$.

$$\eta_{act} = \frac{2RT}{nF} \sinh^{-1} \left(\frac{i}{2j_0 A_{el}} \right) \quad (4.51)$$

For other values of β , simplified representations of the current-voltage relationship are applied when the activation voltage can be regarded as either sufficiently low or high (Chan, Khor et al. 2001; Noren and Hoffman 2005; Li 2006). For low voltage a Taylor expansion of (4.49), ignoring all higher order terms, gives a linear relation. For high voltage only the first term of (4.49), equivalent with the Tafel equation, is applied.

Both versions (4.49) and (4.51) were implemented for the present case giving congruent results. The alternative representations are implemented in bond graph notation and discussed in section 4.2.4. For all cases the activation polarisations are implemented in two-port R -elements. The product of the cell current and the voltage drop is output on the thermal bond of the R -element.

4.2.4 Resulting bond graph model

A main advantage of using bond graphs as a modelling tool is the simplified development of models of complete integral causality with a minimum of algebraic loops. Based on the above elements, this was straight forward for the gas supply and heat transfer models of a tubular solid oxide fuel cell. As a first approach the bond graph of Figure 4.11 was developed. In the following the electrochemical part of this model is compared to various model representations found in literature. The discussion is particularly relevant when introducing a distributed model in the following chapter.

The dotted lines of Figure 4.11 are pseudo-bonds by 20-sim notation. Green lines are hydraulic lines with total pressure and mass flow as variables on the upper (horizontal flow) or left (vertical flow) bonds. The lower or right bonds are orange thermal pseudo-bonds with temperature and heat flows as variables. Component mass fraction (alternatively partial pressure), and mass flow for each component, are the variables of the hydraulic bonds in-between. Black lines are standard power bonds. Signal bonds are included as molar fraction input to the activation losses, calculating exchange current densities, equation (4.50).

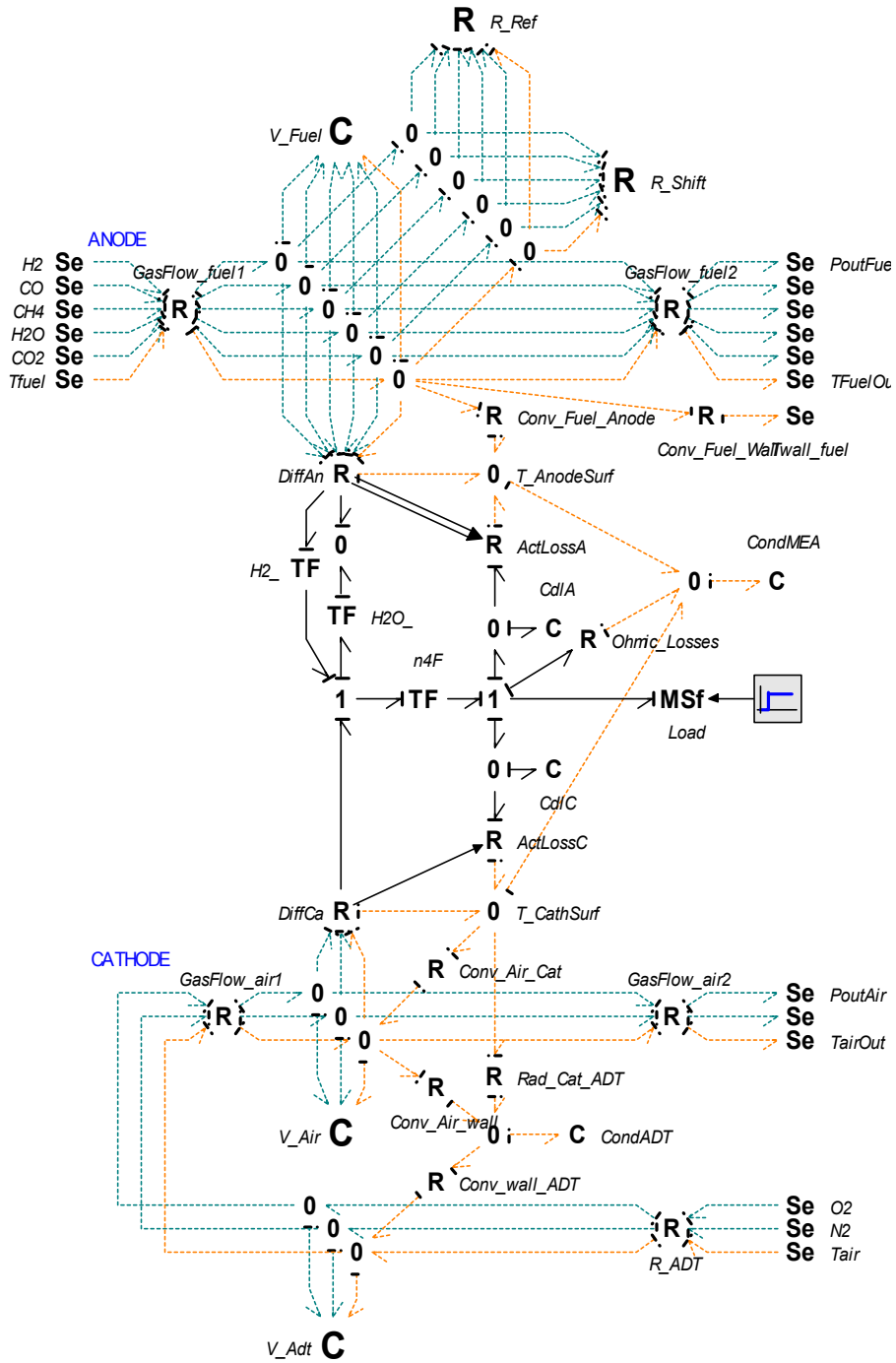


Figure 4.11 Bond graph of a lumped SOFC model

In Figure 4.11 diffusion losses are implemented assuming constant pressure and temperature across the membrane. Consequently no *C*-fields are present on the electrochemical side of the *R*-fields that represent diffusion loss between the gas volumes and the MEA. Current drawn from the cell sets the reaction rate, and only activation losses are directly delayed by the charge double layer effect of the *C*-elements. The representation is equivalent with the bond graph found in (Benbouzid, Fouquet et al. 2003). As found in (Qi, Huang et al. 2005), the effect of the charge double layer (CDL) had insignificant influence on the result. Thus the *C*-elements can be deleted, and if the conditions discussed in 4.2.3 are fulfilled, an explicit equation for the activation losses can be implemented, Figure 4.12. For a lumped model this representation is appropriate, but if extended to multiple sections of finite volumes, complicated algebraic loops between the loss-elements appear.

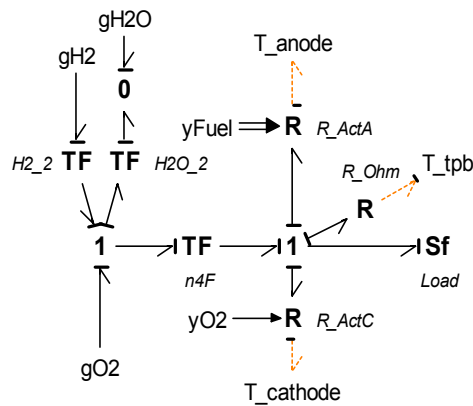


Figure 4.12 Electrochemical model with no CDL

Dynamic models of the electrochemical reactions and their corresponding losses are traditionally based on and verified by impedance measurements and resulting equivalent circuit diagrams. Such experiments measure the voltage opposition to a sinusoidal alternating electric current forced on the system. Dynamic performance and degradation rates when subject to frequent load changes can with this method be detected, and impedance measurements are therefore of great importance in fuel cell development (Singhal 2003). In overall system models the dynamics of the electrochemical reactions are for most cell designs significantly faster than the remaining dynamics modelled, and can in general be ignored. The discussion here is intended as an aid to solve algebraic loops or differential causalities in the model.

There is great variance in the literature as to whether the charge double layer effect introduced in section 4.2.3 is modelled or not, and how this effect is included. The circuit used as a first approach in the present work, Figure 4.13, is equivalent with the one shown in (Larminie and Dicks 2003), and frequently used by other authors as well. (Qi, Huang et al. 2005) questions the validity of this circuit and suggests a circuit equivalent with the one adapted in (Benbouzid, Dauphin-Tanguy et al. 2004) and (Saisset, Fontes et al. 2006), Figure 4.14. The latter circuit reflects that

the capacitive effect delays the change in electrochemical reaction rate, while in the first circuit only the effect of the activation loss is delayed.

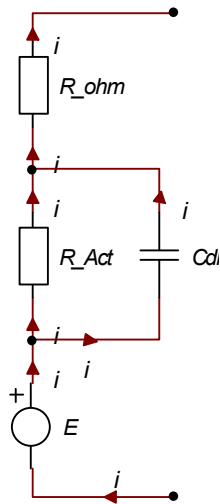


Figure 4.13 Equivalent circuit A

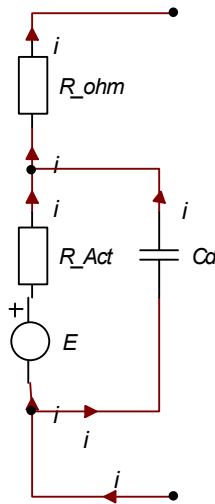


Figure 4.14 Equivalent circuit B

To implement the circuit of Figure 4.14 a bond graph proposed by (Benbouzid, Dauphin-Tanguy et al. 2004) can be used, Figure 4.15. To avoid algebraic loops a C-field must be present after the diffusion loss, representing the gas volume of the porous anode, Figure 4.16. R-fields are introduced to implement the transformation between pseudo-bonds and true bonds for the mass and energy transported to the electrochemical reactions. The energy transferred from the control volume can be represented by equation (4.28).

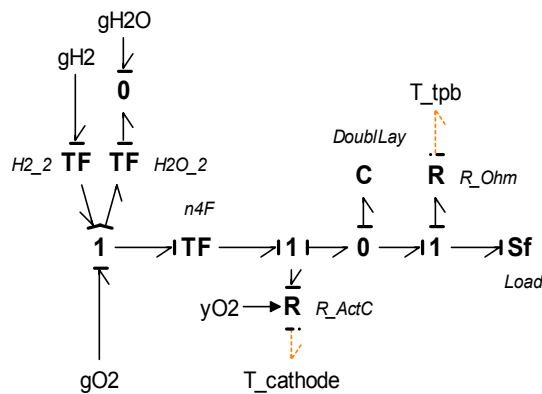


Figure 4.15 Alternative bond graph (Benbouzid, Dauphin-Tanguy et al. 2004)

In Figure 4.15 only the activation losses on the cathode side are implemented based on the assumption of these being much larger than the anode activation losses. For most fuel cells this is true. (Wagner, Schnurnberger et al. 1998) argues that due to the high operating temperature of the SOFC, the charge transfer resistances of the anode and the cathode are in the same order of magnitude.

Therefore the contribution of the anode cannot generally be neglected. Figure 4.16 shows how this might be implemented by replacing the bond graphs between the C-fields representing the anode and cathode gas volumes of Figure 4.11. (Saisset, Fontes et al. 2006) use a similar bond graph to represent the electrochemical reactions.

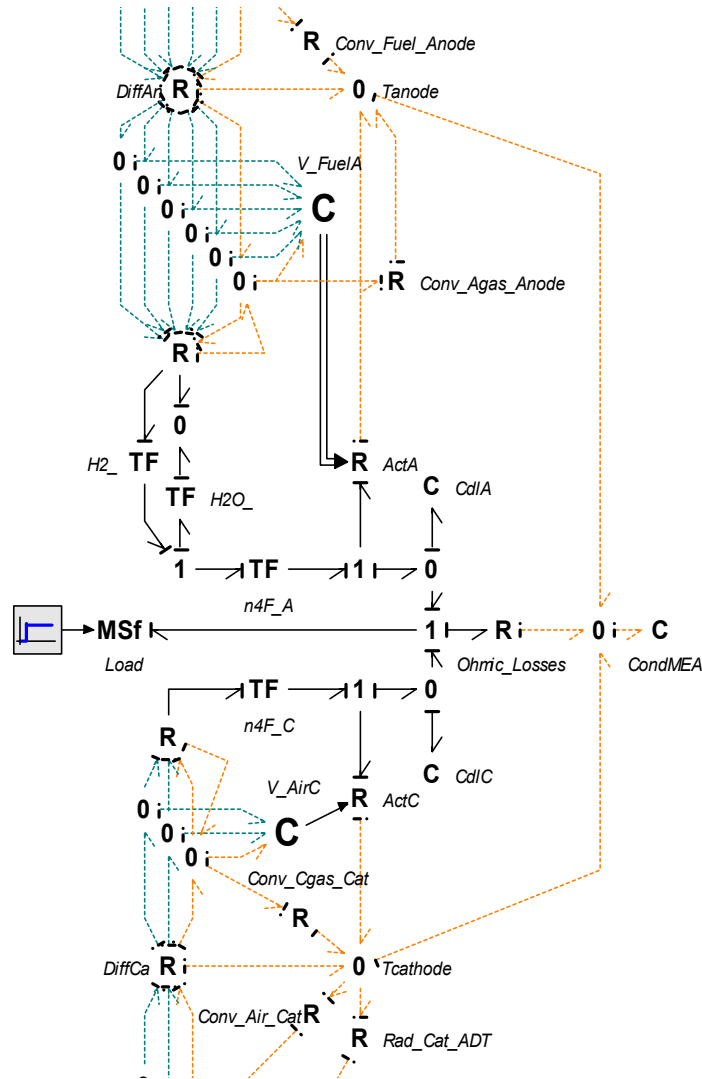


Figure 4.16 Bond graph with extra control volumes added for gas properties at TPB

Some changes and extra information is needed to implement a model according to Figure 4.16. The volumes occupied by anode and cathode gases must be estimated, and multicomponent diffusion through the membranes and a slightly different model for the heat transfer must be implemented. Proper models for multicomponent diffusion are not readily available (Cussler 1997), and simplifications are made in equations (4.38) and (4.47). The gas volumes inside the

anode and cathode are small, and especially for a distributed model of multiple control volumes the system might get too stiff. To conclude, the bond graph of Figure 4.11 is found to be a general and appropriate representation of a lumped SOFC model. If distributed characteristics are of interest Figure 4.16 is found to be more appropriate as demonstrated through simulations in chapter 5.

4.3 Distributed fuel cell model

A model of the distributed characteristics in a fuel cell can be implemented by defining repeated finite volumes in sections along the cell. For each section, control volumes for the gas channels and membranes are equivalent to the lumped model introduced above. Temperature, pressure, concentration and current density are the variables of interest in the different sections. The proper way to define the sections of such a model varies for different fuel cell designs. The number of sections must be chosen based on the desired level of details for the distributed variables. For the tubular design treated in this thesis, the distributed representation of a single cell is defined by cross sectional volumes as shown in Figure 4.17.

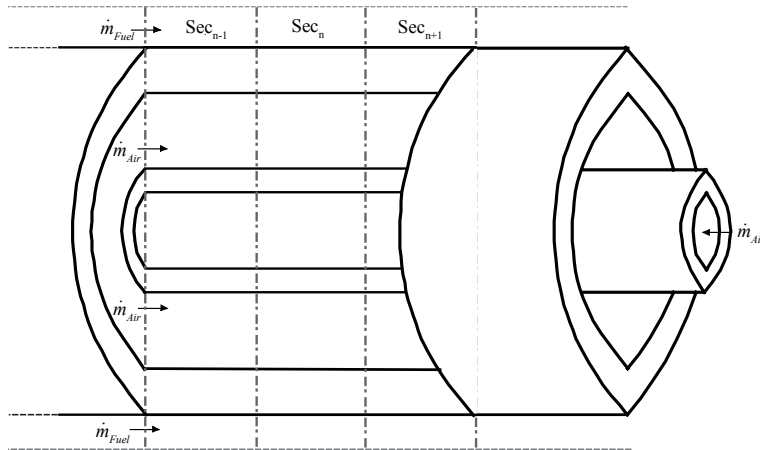


Figure 4.17 Sections of fuel cell for distributed representation.

As described in section 4.1, an overall cell voltage is delivered when current is drawn from the cell. Distributed representation of a single cell must reflect that the currents passing through each section are fractions of the total current, and that the total power delivered to the stack has effort causality representing the uniform cell voltage. The current density of each section corresponds to the number of electrochemical reactions occurring there. Electrodes are normally made of good electrode conductors implying nearly iso-potential surfaces in the cell. This potential, the fuel cell voltage, can not be higher than what the chemical potential of the gases indicates. Setting the overall voltage is therefore the part of the cell where the Nernst potential is at its minimum. Consequently, for a high fuel utility, the overall potential will be low. For a cell where both fuel and oxidant flow in the same direction the minimum potential occurs at the flow outlet (Li 2006). For

other designs such as cross flow and counter flow it is more difficult to determine the location of this minimum potential.

Figure 4.18 shows a bond graph representation of the power contribution from each section. A 0 -junction is used to sum the currents, and only one of the sections can set the uniform cell voltage as shown by the causality strokes. The Se -element $Section_n$ represents the outlet section setting the output voltage of the stack.

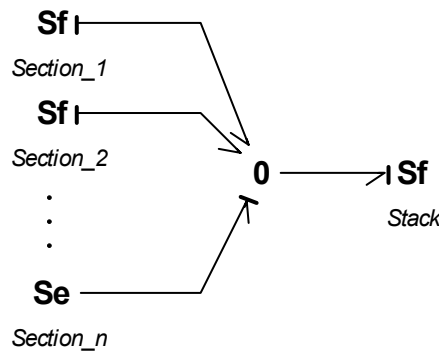


Figure 4.18 Bond graph of output causality from distributed cell model

A bond graph model of the gas flow channels are simply implemented by a repetitive use of the C - and R -fields shown in Figure 4.5. Figure 4.19 shows an example of a distributed model implemented in 20-sim. Three control volumes on the anode side and three on the cathode side represent flow of fuel and air respectively. For a more compressed figure the vertical hydraulic bonds are merged into vector bonds. The heat transfer through the membranes for each section is modelled as presented in section 4.2.2 and implemented in the submodel *HeatTrans*. As introduced above the causality distribution for the electrochemical and electrical relations are not straight forward. The bond graphs presented in 4.2.4 are used as basis to find the best representation when dividing the cell in multiple cross sectional volumes. Different variations of the electrochemical reactions and their losses are presented below, and can be implemented in the submodel *ElChem* of Figure 4.19.

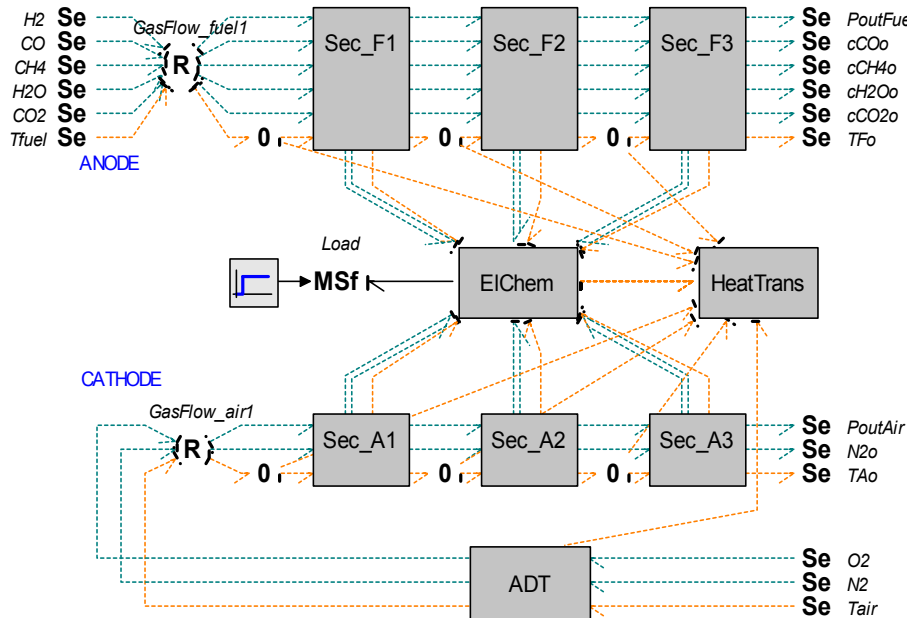


Figure 4.19 Bond graph cell model with three cross sectional volumes

For the tubular cell design with anode and cathode flow in the same direction, the last section will decide the maximum reversible voltage and can keep the causality as presented for the models in chapter 4.2.4. Algebraic loops are avoided here, as current is set externally and the fuel cell voltage is output from the model. The current distribution along the cell must be set by the remaining sections. No obvious physical inertia effects are present on the MEA of a fuel cell, and the current contribution from each remaining section must be set by an *R*-element with flow causality. Algebraic loops between the section models are therefore unavoidable, and the goal must be to make these as simple as possible.

For the most common representation of the electrochemical model, presented in Figure 4.12, algebraic loops are present between the *R*-elements inside the sections where effort is set externally. One alternative is that the distribution of current can be set by the cathode activation losses in the first two sections, see Figure 4.20. In this case either the transfer factor of the activation potential is 0,5, allowing for an explicit expression as in equation (4.51), or the losses are small enough to be treated by a linear equation. The causality can be altered as appropriate for each section model. If effort causality is preferred for all activation losses, the ohmic losses can equivalently set the current distribution by altering the causality in the first two sections. Including the charge double layer as in Figure 4.11 will require flow causality on the activation losses, and the ohmic losses set the current distribution between the sections.

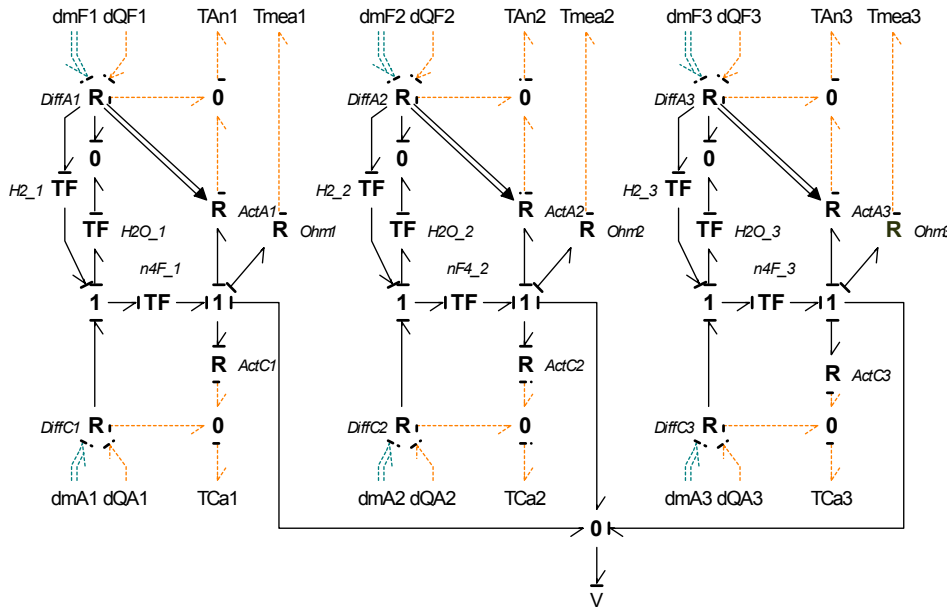


Figure 4.20 Distributed model of electrochemical phenomena

The bond graph presented in Figure 4.16, with extra control volumes for the gas properties at the reaction sites (TPB), holds a better physical representation of the charge double layer effect. When applying this bond graph, ohmic losses set the current distribution and the outlet section has the causality of Figure 4.16. No internal algebraic loops are in this case present between the R -elements of each section, and the resulting algebraic loop for the overall model is linear and more easily solved compared to Figure 4.20. The algebraic loops are solved symbolically by the solvers prior to simulation, the more linear relations the less prone to errors. The chosen representation correspond well with the electrochemical model recently presented by (Qi, Huang et al. 2008), the equivalent circuit diagram is shown in Figure 4.21.

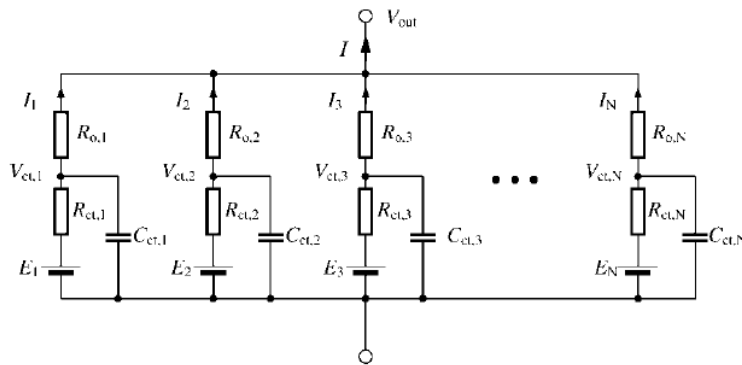


Figure 4.21 Equivalent circuit of an SOFC tube (Qi, Huang et al. 2008)

4.4 Support system models

As introduced in chapter 4.1, a fuel cell system contains several components supporting the stack of individual fuel cells, Figure 4.3. Here, each of the components is presented together with their implemented bond graph model. Only the overall characteristics of each component are modelled. If any part of the total system must be studied in greater detail, these models can be extended or replaced without changing the overall structure of the bond graph model.

In general, all gas volumes are modelled by C -fields as described in chapter 4.2.1 with R -fields modelling the gas flux between them. An alternative flux equation (4.52) is implemented when the dimensions are unknown and the friction factor is regarded as a constant, u indicates upstream values and d downstream values. The constant C is calculated from design values indicated by θ . For all elements, mass flows in the direction of decreased pressure.

$$\begin{aligned} \Delta P &= f_l \frac{1}{2} \rho(P, T, \mathbf{c}) u^2 = C \frac{\dot{m}^2}{\rho(P, T, \mathbf{c})} \\ \Rightarrow C &= \frac{\Delta P_0 \rho_0(P_0, T_0, \mathbf{c}_0)}{\dot{m}_0^2} \quad \text{and} \quad \dot{m} = \sqrt{\frac{(P_u - P_d) \rho_u(P, T, \mathbf{c})}{C}} \end{aligned} \quad (4.52)$$

4.4.1 Ejector

An ejector performs compression without moving parts. This is done by mixing a gas (drive flow) of high velocity and pressure into a gas (suction flow) whose pressure is increased. The process can be divided into four main stages. In the first stage the high pressure fuel is accelerated through a nozzle (a). In the second stage the recycled anode gas is sucked into the ejector by the drive flow (b). In the third stage momentum exchange between the two flows is carried out in a mixing section (c). The last stage is a diffuser where discharge flow is decelerated to increase the pressure (d).

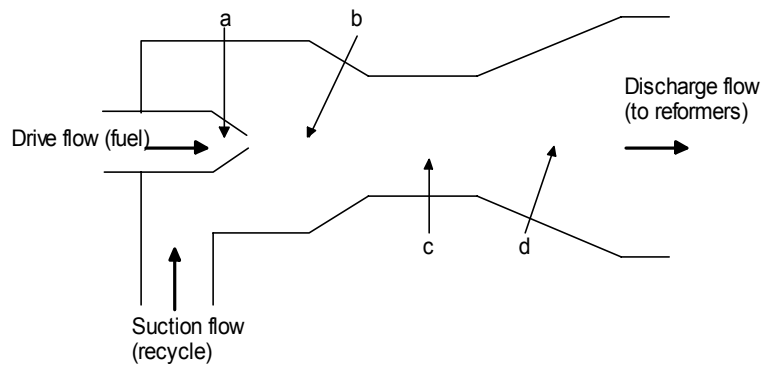


Figure 4.22 Schematic drawing of ejector

The dynamics of such a device is fast compared to the rest of the fuel system. Therefore a static (Stiller 2006) or quasi static (Ferrari, Traverso et al. 2005)

approach is common when making detailed models of the ejector. In this thesis, a static approach using tabulated values and table interpolation model the ejector. Two tables are used; one where the fuel flow is dependent on the fuel pressure, and one where the mass flow of exhaust is dependent on the fuel flow. The resulting mass flow is found by equation (4.53), with composition set by the downstream flows.

$$\begin{aligned} \dot{m}_{CH_4} &= f(P_{CH_4}) & \dot{m}_{recycle} &= f(\dot{m}_{CH_4}) \\ \dot{m}_{out} &= \dot{m}_{CH_4} + \dot{m}_{recycle} \end{aligned} \quad (4.53)$$

The composition and enthalpy values of these input flows are used to calculate the energy flow into the ejector. The energy output is found according to equation (4.54).

$$\dot{E}_{out} = \dot{E}_{CH_4} + \dot{E}_{recycle} \quad (4.54)$$

Being general relations between effort and flows, the tabulated values are implemented in a three-port *R*-field, Figure 4.23. Pressure and temperature downstream are set by a *C*-field.

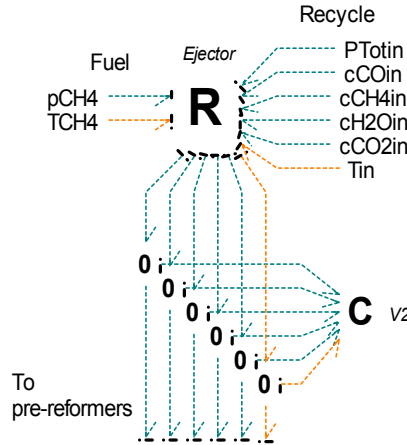


Figure 4.23 Ejector model

The approach is similar to the one used in (Paynter 1985), an approach based on tables representing available test data. In the present work it is simply assumed that there exists an ejector with the desired characteristics, an assumption that must be verified by measurements for each new design case.

4.4.2 Reformers

To achieve the desired degree of pre-reforming for the fuel entering the fuel cell, reformers are included in the support system. Reformers are designed to achieve high reaction rates allowing gases to reach equilibrium at the current pressure and temperature levels. External reformers are adiabatic and the heat needed for gases to react is supplied by the input gas flow. Because the reforming process is

endothermic, heat from the fuel cells is used to accelerate the process further in the so called indirect internal reformers. These are reformers placed inside the stack, next to a bundle of fuel cells, receiving radiation heat along the whole length of the reformer.

Both reformer types are initially modelled by a single volume approach, where the rate for the shift reaction is set according to equation (4.18). The reforming rate is also set based on equilibrium constants for the current mixture, pressure and temperature, equation (4.55). The constants, here k_{fr} , are set as high as possible to achieve equilibrium, too high values may cause simulation methods to fail. Their physical justification would be the design of the pre-reformers.

$$J = \dot{n}_{H_2} = k_{fr} \left(P_{H_2O} P_{CH_4} - \frac{P_{H_2}^3 P_{CO}}{K_{ig,e}} \right) \quad K_{ig,e} = e^{\frac{-(3\mu_{H_2} + \mu_{CO} - \mu_{H_2O} - \mu_{CH_4})}{RT}} \quad (4.55)$$

A C-field sets the pressure and composition of the volume, and a bond graph for the reformer components is shown in Figure 4.24. For the internal reformer, radiation from the fuel cells is added as a heat source to the control volume. The R-field sets the flow based on a pressure drop defined for the design case giving the constant of equation (4.52). The dynamics and extent of reactions in the internal reformer is strongly dependent on the amount of the heat transfer through its walls. A fast increase in temperature will cause a fast change in the equilibrium state for the reforming reactions. Creating a distributed model of the internal reformer by repeated control volumes may change the heat transfer characteristics and the dynamics of the pre-reformer; this is tested by simulations in chapter 5.

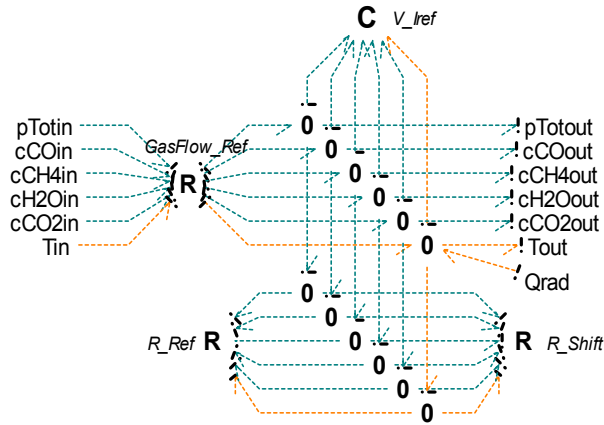


Figure 4.24 Bond graph of indirect internal reformer

4.4.3 Valve

Two controlled valves are implemented in the system model; one for air injection and one controlling the recycled gas to the ejector. The valves are assumed to be represented by the nozzle equation for ideal gas, eq. (4.56). This equation can simply replace equations (4.16) or (4.52) in a general R -field representing the mass flux between control volumes.

$$\begin{aligned}\dot{m}_{in} = \dot{m}_{out} &= C_d A \frac{P_u}{\sqrt{R_u T_u}} \Psi(\pi) \text{sign}(P_{in} - P_{out}) \\ \dot{m}_i &= \dot{m}_{in} c_i\end{aligned}\quad (4.56)$$

The function Ψ is expressed by:

$$\psi(\pi) = \begin{cases} \sqrt{\frac{2\kappa}{\kappa-1} \left(\pi^{\frac{2}{\kappa}} - \pi^{\frac{\kappa+1}{\kappa}} \right)} & , 1 \geq \pi \geq \left(\frac{2}{\kappa+1} \right)^{\frac{\kappa}{\kappa-1}} \\ \sqrt{\kappa \left(\frac{2}{\kappa+1} \right)^{\frac{\kappa+1}{\kappa-1}}} & , \pi \leq \left(\frac{2}{\kappa+1} \right)^{\frac{\kappa}{\kappa-1}} \end{cases}$$

where $\kappa = \frac{c_p}{c_v} = \frac{c_p}{c_p - R}$ og $\pi = \frac{P_d}{P_u}$ (4.57)

$$\text{linearised : } \psi(\pi) = (1.0 - \pi) \cdot 100 \cdot \sqrt{\frac{2\kappa}{\kappa-1} \left(0.99^{\frac{2}{\kappa}} - 0.99^{\frac{\kappa+1}{\kappa}} \right)}$$

The linear expression is developed to enable more robust simulation when the pressure drop over the nozzle becomes small and the curve for Ψ becomes steep (when P_u/P_d approaches 1,0). The model is adapted from (Pedersen 1999). Initial values of pressure, temperature, composition and desired mass flow are used in (4.58) to find the constant factor in the flow equation.

$$C_d A = \frac{\dot{m}_0 \sqrt{R_u T_u}}{P_u \Psi(P_{in}, P_{out})} \quad (4.58)$$

4.4.4 Afterburner

An afterburner converts the remaining fuel energy to heat. The burner is modelled as an ideal and adiabatic element. Methane, hydrogen and carbon monoxide in the anode gas are combusted with air from the cathode to form steam and carbon dioxide. Only four components remain in the exhaust from the burner; oxygen, steam, carbon dioxide and nitrogen. The constitutive equations for this reactions are shown in equation (4.59). Molar flows are calculated directly from input mass flows.

$$\begin{aligned}
 \dot{n}_{H_2O,out} &= 2\dot{n}_{CH_4,in} + \dot{n}_{H_2,in} + \dot{n}_{H_2O,in} \\
 \dot{n}_{CO_2,out} &= \dot{n}_{CH_4,in} + \dot{n}_{CO,in} + \dot{n}_{CO_2,in} \\
 \dot{n}_{O_2,out} &= \dot{n}_{O_2,in} - 2\dot{n}_{CH_4,in} - 1/2\dot{n}_{CO,in} - 1/2\dot{n}_{H_2,in}
 \end{aligned} \tag{4.59}$$

A submodel where mass and energy flows are input downstream and output upstream is required. Pressure and temperature upstream are other input variables from which the output on the power bonds can be found as listed in equation (4.60).

$$\begin{aligned}
 P_{Exh,in} &= P_{Air,in} = P_{Exh,out} \\
 T_{Exh,in} &= T_{air,in} = T_{Exh,out} \\
 c_i &= \dot{m}_{i,in} / \dot{m}_{tot,in} \\
 \dot{m}_{i,out} &= \dot{n}_{i,out} M_i & \dot{m}_{tot,out} &= \sum_i \dot{m}_i \\
 \dot{E}_{Exh,out} &= \dot{E}_{Exh,in} + \dot{E}_{Air,in}
 \end{aligned} \tag{4.60}$$

There exist several alternatives for representing these relations through pseudo-bond graphs. R -fields setting the speed of chemical reactions based on the composition in a volume were used to model the reforming reactions to an equilibrium state. Complete combustion is the goal for the afterburners, and such R -fields are not easily adaptable without an excessive use of signal bonds. Direct relation between efforts and flows are in general represented by R -fields in bond graphs. An R -field equivalent with the one used to model the ejector could therefore be used, but an equation submodel was chosen as shown in Figure 4.25.

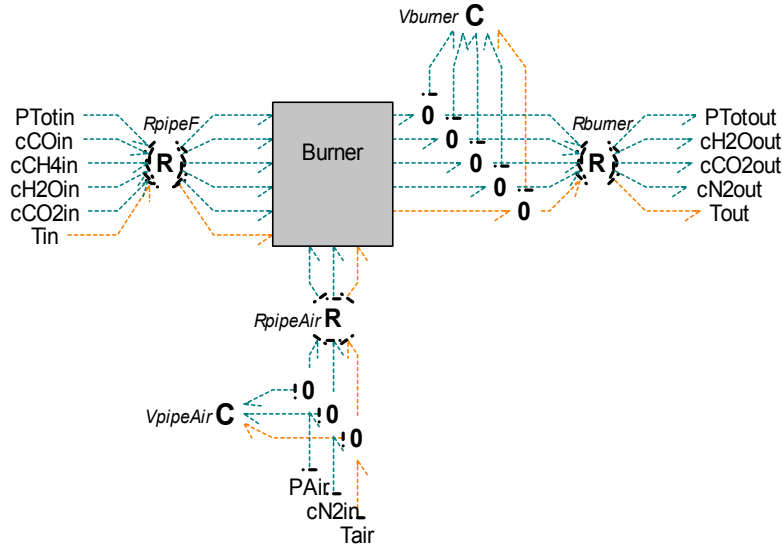


Figure 4.25 Bond graph model of afterburner

Pressure losses at design point are used to estimate flow coefficients for the three R -fields in Figure 4.25. No losses occur in these R -fields, and the energies of the

input streams to the burner submodel are equivalent with input to the R -fields. The two C -fields represent small control volumes setting the pressure and temperature of the gas streams.

An excess of oxygen needs to be present to achieve complete combustion. A check to alert when this is not the case will be a beneficial improvement to the model. This model can not represent anode backflow (air flowing into the recycled anode gas). Oxygen might poison the anode and this is therefore not accepted. An alert when pressure conditions are such that anode backflow might occur during actual operation will also improve the model.

4.4.5 Heat exchanger

The purpose of the heat exchanger is to preheat the air before it enters the fuel cell. It is designed as an extension to the air delivery tube, and the number of heat exchange surfaces equals the number of fuel cells, n_{cells} . As a simplification the heat transfer is modelled as a single heat exchange between inlet air and exhaust of the total stack. A more detailed model might be necessary depending on the dynamics of the heat exchanger compared to the rest of the system. Such a model can be found in e.g. (Engja 1986).

The heat transfer rate is calculated based on a steady state approach, equation (4.61). Thermal resistance, equation (4.62), is calculated from the heat transfer coefficients h for convection and thermal conductivity of the wall k , (Incropera and DeWitt 2002). The dimensions used are inner and outer radius of the air delivery tube and the inner radius of the shell of the heat exchangers. A factor K is included to assure high enough temperature for the air at design point.

$$\dot{Q}_{Air} = -\dot{Q}_{Exh} = K \frac{n_{cells} (T_{Exh} - T_{Air})}{R_{th}} \quad (4.61)$$

$$R_{th} = \frac{1}{h_{Exh} 2\pi r_{o,ADT} l_{HE}} + \frac{\ln(r_i/r_o)_{ADT}}{2\pi k l_{HE}} + \frac{1}{h_{Air} 2\pi r_{i,ADT} l_{HE}} \quad (4.62)$$

$$h_{Air} = \frac{Nu_{Air} \lambda_{Air}}{2r_{i,ADT}} \quad h_{Exh} = Nu_{Exh} \lambda_{Exh} \frac{r_{i,HE} - r_{o,ADT}}{2(r_{i,HE}^2 - r_{o,ADT}^2)}$$

Control volumes for the hot and cold flow are implemented by C -fields. The heat flow between them is modelled as an R -element with temperatures of each volume as the only inputs, Figure 4.26.

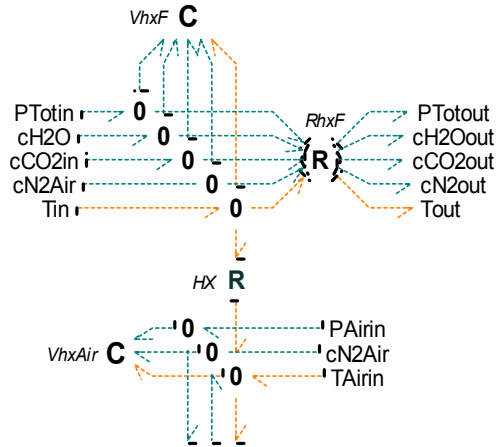


Figure 4.26 Bond graph model of heat exchange

4.4.6 Electric output power

Figure 4.2 shows how the MEA of a single cell is part of the electric circuit. As the cells are coupled in series in a fuel cell stack the same current flows through each of the individual cells. One cell can only deliver a small voltage set up by the membranes, and a summation of these contributions results in the stack output voltage. In bond graph notation the power from a cell stack can be represented by Figure 4.27.

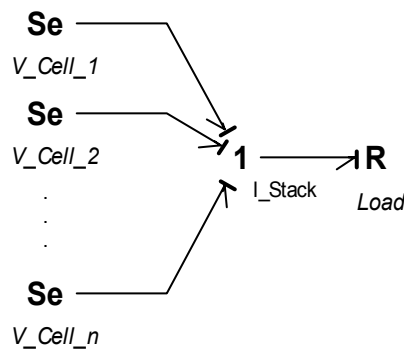


Figure 4.27 Bond graph of electric power flow in stack

To link the fuel cell stack to an overall power system DC/DC or DC/AC inverters are needed to transfer the power to the desired current or voltage level. The dynamics and power loss of such components are negligible compared to the fuel cell. (Kandepu 2007) and references therein suggests a simple model of this inverter and a typical load model.

4.5 Control of SOFC systems

The main objective of the control system is to control injection of fuel and air so the fuel cell supplies the desired amount of power at all times. To avoid damage, and to keep a high efficiency, the temperature and fuel utility of the stack is kept at a level assuring safety and durability of the system. For a SOFC this may be done by controlling the fuel and air input flows and the amount of anode recycling. (Singhal 2003) and (Stiller, Thorud et al. 2006) discuss the control of SOFCs in greater detail, (Pukrushpan, Stefanopoulou et al. 2004) gives a general overview of fuel cell control. In this thesis, the control system is kept as simple as possible, just showing some possibilities of the purposed model.

When controlling output from an SOFC stack the goal is to keep the temperature inside the cells as constant as possible to avoid material degradation. To keep a high voltage and efficiency, maximum and minimum fuel utility is also defined according to equation (4.63). The factor 8 is included because two electrons are charged per hydrogen molecule reacting, and using methane as fuel gives 4 hydrogen molecules per mole fuel.

$$FU = \frac{i}{8F\dot{n}_{Fu}} = 0,85 \quad \begin{cases} FU_{\min} = 0,75 \\ FU_{\max} = 0,9 \end{cases} \quad (4.63)$$

Adjusting the fuel flow into the stack will control the power obtainable from a fuel cell. For a chosen fuel utility, equation (4.63) gives a direct relation between the current and the fuel flow setpoint. At these setpoints, air flow is controlled to keep the desired operating temperature. At stationary conditions the voltage is set as a result of this air flow, the fuel flow and input current, resulting in desired power supplied from the cell. Also the recirculation of anode gas must be controlled in order to keep a desired steam to carbon ratio, defined for methane as fuel in equation (4.64).

$$SC = \frac{\dot{n}_{H_2O}}{\dot{n}_{CH_4} + \dot{n}_{CO}} > 2,0 \quad (4.64)$$

In this model the above requirements may be achieved using two regulators; one for the fuel flow and one for the air flow corresponding to the desired current setpoint. Air flow may be controlled through a valve or a compressor adjusting the input pressure. The first regulator then controls valve opening or compressor setpoint. Table values from stationary runs are implemented relating input current to the required air flow, this defines the regulator setpoint.

Due to simplified modelling of the ejector, no fuel valve is used for control. The ejector uses a table to set the fuel flow as function of fuel pressure and a relation between current and fuel pressure decides the regulator setpoint. Tabulated values of fuel flow as function of pressure is set to assure the desired degree of fuel utility. The integration time constant of the controller can be used to test the effect of time delay caused by valve adjustments. Since the ejector model is based on

tabulated values setting the mass flow of recycled gas, control of the throttle valve is redundant.

The presented control strategy is very dependent on accurate stationary runs defining the air flow table to hold a constant mean fuel cell temperature. To oppose changes in ambient conditions a slow temperature controller may be implemented adjusting the air flow setpoint according to measured temperature. To obtain a faster fuel cell response (Haynes 2002) lets the fuel cell operate at a lower fuel utility. Then the fuel processing will not limit a possible load increase, but system efficiency might be lower. In (Iora, Aguiar et al. 2005) the air and fuel flow is controlled to keep a constant fuel utility and air excess rate, the temperature is not measured in the control loop. These are just a few examples of the possibilities of SOFC control. In the model of the system simulated in chapter 5 no regulators are included. Instantaneous change in fuel and air flow is implemented by tables being functions of the input current. The model may therefore serve as a basis for controller design.

Chapter 5

Simulations

A range of models for prediction of steady state and transient performance of an SOFC power plant was developed in chapter 4. In this chapter simulations are carried out to predict the behaviour of a system implemented applying these models. No detailed test-data was obtainable, thus the results are compared to similar approaches in the literature. In chapter 4 both lumped and distributed model representations were presented. In the simulations of this chapter four different models of the single cell are verified, two lumped and two distributed variants. Different ways of implementing distributed cell models in a total system are also presented to see the difference in transient behaviour of the system simulations. Table 5.1 sums up the representations and assign model names used in the documentation and simulation plots of this chapter. The cell models are named I, II, III and four, while the different system models are named A, B and C.

Table 5.1 Names of the different simulation models

Fuel cell representation	Model	System integration	Model
Lumped model, Figure 4.11	I	None	
Lumped model with extra control volumes for electrode gas, Figure 4.16	II		
Distributed model of anode gas, cathode gas and MEA. Six repeated sections of model II, Figure 5.2	III	Bulk heat transfer to internal reformer	C
Distributed model of anode gas, cathode gas, MEA and ADT. The ADT volume of model III split in six sections, Figure 5.4	IV	Bulk heat transfer to internal reformer	A
		Distributed heat transfer to internal reformer	B

A design case with main system parameters is presented first. In section 5.2 results from steady state simulations at design point verify different model representations of a single SOFC. Response of the single cell model to transient load changes is shown in 5.3.1. Simulations of a model including the most important components of the total power plant are presented in section 5.3.2.

5.1 The design case

The design cases presented in (Stiller 2006) and (Thorud 2005) are used as basis for the model implementation and verification in this thesis. Their models were based on data obtained and estimated from published data for the Siemens Westinghouse fuel cell plant, a hybrid system combining the SOFC stack with a gas turbine. For comparative reasons, the same operational design point for the SOFC stack was chosen in the present work, approximately four bars. A plant operating at ambient pressure is more likely for a free-standing fuel cell, but the design point is kept to simplify verification of results. Main dimensions and design point parameters for each cell can be found in Table 5.2. Main variables for the total plant at design conditions can be found in Figure 5.1. All remaining parameters used in the simulations can be found in Appendix B.

Table 5.2 Main parameters single cell simulation

Parameter	Value
Length of fuel cell	1.5 m
Active surface area of cell	0.0834 m ²
Hydraulic diameter anode channel, cathode channel and ADT.	0.001 m, 0.00932 m and 0.0033 m
Thickness anode, cathode and electrolyte	0.0001 m, 0.0022 m and 0.00004 m
Fuel and air inlet temperature	1000 K and 1154 K
Fuel and air inlet pressure	3.831 bar and 3.8356 bar
Fuel and air outlet pressure	3.822 bar and 3.820 bar
Mass fraction inlet fuel [H ₂ , CO, CH ₄ , H ₂ O, CO ₂]	[0.0443, 0.2594, 0.0206, 0.2698, 0.4059]
Mass fraction inlet air [O ₂ , N ₂]	[0.23, 0.77]
Mass flow fuel	5.28e ⁻⁵ kg/s
Mass flow air	3.28e ⁻⁴ kg/s

In (Stiller 2006), no pressure drop and constant speed of mass flows were set across the fuel cell. In the present implementation this cell pressure is set to be the outlet pressure from the cell. Inlet pressure must be estimated to achieve the design values of fuel and air mass flows through the cell. For the total system, fuel flow is dimensioned in order to achieve a fuel utility of 85% at steady state and a steam to carbon ratio of two at the inlet of the first reformer. An air excess ratio of 3,25 sets the air flow at design point. Composition of the fuel entering the single cell models is estimated assuming 80% pre-reforming of the methane. The resulting mass flow for the given pressure difference and tube dimensions are as listed above; 5.28e⁻⁵ kg/s or 0.369 m/s in the anode channel and 3.28e⁻⁴ kg/s or 1.747 m/s in the cathode channel. This gives Reynolds numbers of around 7 for

fuel and 350 for air, values well within the laminar flow area. Values in the same range are also documented by (Iora, Aguiar et al. 2005).

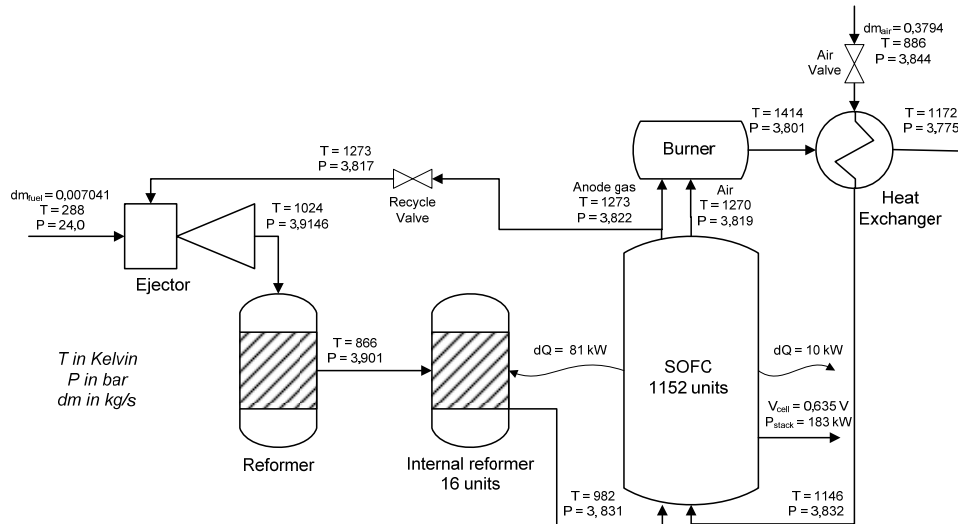


Figure 5.1 The SOFC power plant; process flow and design case variables

The heat transfer from each cell is approximately 70 W at design point. This results in a total of 80 kW for a stack of 1152 cells. Some of the heat is utilised by the internal reformers and the rest (~ 10 kW) is lost to the surroundings, see Figure 5.1. The figure also illustrates how mass and energy flows of the fuel and air, together with heat transfer and electric work, are the only inputs/outputs from the SOFC stack model. A description of the functionality and level of details for the different submodels of Figure 5.1 are documented in chapter 4. Some important assumptions of the system model are repeated here.

- Gases obey the ideal gas law, and perfect gas behaviour can be assumed around the operating temperature. This results in simplified relations for finding thermal properties, outlined in Appendix C.
- Laminar flow in gas channels; justified by low Reynolds numbers.
- Only a single cell is modelled. Inlet flow is divided and outlet flow is multiplied by the number of cells. Interaction between the different cells and indirect internal reformers of a stack is therefore not represented.
- Bulk heat exchange for the total stack replaces the tubular heat exchangers of each cell.
- Complete combustion occurs in the afterburner.
- Dynamics of the ejector model are ignored; the model is based on performance tables.

5.2 Steady state performance

A design point load of 250 A (3000 A/m²) was applied to the four different models of a single SOFC described in Table 5.1, and steady state values were compared. The two lumped model implementations (model I and II) presented in section 4.2.4 are compared verifying that they both represent the physical cell in a proper manner. Simulations of a model where each lumped volume is divided into six sections (model III) demonstrate the ability to model distributed characteristics of the fuel cell. Finally, a distributed model of the air delivery tube is included to see whether this affects the temperature distribution inside the cell.

5.2.1 Lumped model

As discussed in chapter 2 models used for control purposes and in overall system simulations typically represent the anode and cathode gas volumes by single lumped volumes. Their simplicity allows for efficient simulations while still showing the most important dynamics. Two lumped models are compared here. In model I the losses are implemented in a traditional way. According to the discussion in section 4.2.4 model II improves the causal representation both for distributed and single section characteristics. The main model variables at design point are shown in Table 5.3 for model I and in Table 5.4 for model II. The last four values of Table 5.4 are only found in this model where extra anode and cathode volumes are included.

Table 5.3 Main variables at design point, model I

Variable	Value
Fuel, air and MEA temperatures	1317 K, 1315 K and 1317 K
Fuel and air pressure	3.83 bar and 3.82 bar
Molar fractions [H ₂ : CO: CH ₄ : H ₂ O: CO ₂]	[0.1106: 0.0889: 0.00009: 0.5559: 0.2445]
Molar fraction O ₂ in air	0.1594
Activation losses, anode and cathode	0.00777 V and 0.03326 V
Diffusion losses, anode and cathode	0.000956 V and 0.001637 V
Ohmic losses	0.1613 V
Voltage output per cell	0.5967 V
Molar fraction O ₂ at TPB	0.1505
Molar fraction H ₂ at TPB	0.1095
Temperature ADT	1306 K

Table 5.4 Main variables at design point, model II

Variable	Value
Fuel, air and MEA temperatures	1318 K, 1316 K and 1318 K
Fuel and air pressure	3.83 bar and 3.82 bar
Molar fractions [H ₂ : CO: CH ₄ : H ₂ O: CO ₂]	[0.1105: 0.0889: 0.00009: 0.5560: 0.2445]
Molar fraction O ₂ in air	0.1594
Activation losses, anode and cathode	0.00775 V and 0.03369 V
Diffusion losses, anode and cathode	0.000956 V and 0.001553 V
Ohmic losses	0.1611 V
Voltage output per cell	0.5943 V
Molar fraction O ₂ at TPB	0.1519
Molar fraction H ₂ at TPB	0.1091
Temperature ADT	1307 K
Anode and cathode gas pressures	3.84 bar and 3.79 bar
Anode and cathode gas temperatures	1317 K and 1318 K

There are two main differences between the bond graphs of model I and model II. The latter includes an extra gas volume for each porous electrode and a more realistic placement of the charge double layer capacitance. The tables below show that none of these changes had significant effect on stationary values. Model I consists of 528 variables and 16 independent states and model II consists of 687 variables and 27 independent states when implemented in 20-sim.

As expected the temperature, pressure and composition of the main gas volumes are equivalent for the two models. Also the losses are near identical, but still the output voltage deviates slightly between the two representations (0.0024 V higher in Table 5.3). This is a result of the pressure and temperature differences across the porous anode and cathode, only present in model II. These values have an effect on the calculated chemical potential of each component in the electrochemical reaction, giving a lower open circuit voltage for model II. Changes done to the implementation of diffusion through the membranes also gives a slight difference in the concentration at TPB for the two models. Exact values were not available, neither for internal variables nor the resulting output. Deviations between the models are small and the implementation of diffusion in model II is kept. Special attention must be paid to these values if verification towards real test data is carried out. Energy and mass balances were calculated for both models. The largest deviation was in the area of 0,003 % and considered to be negligible and most likely due to normal numerical errors.

The temperature profile over the fuel, anode, MEA, cathode, air and ADT volumes (1318, 1317, 1316, 1318, 1318 and 1307 K) is a result of entropy production and mass flows in the cell. The production of oxygen ions at the cathode results in high entropy production and a large asymmetry in the heat production inside the cell (Ratkje and Moller-Holst 1993). A high mass flow of air provides cooling for the stack. The relative temperature differences between the volumes are affected by the heat transfer coefficients, the heat capacity of the solid materials, and the quantity of gas flowing along the membranes. Heat transfer coefficients are a function of thermal conductivity and Nusselt number, equation (4.22). In the model they are implemented as constants, and a small sensitivity study was carried out to verify the assumption.

For the present case, values of the thermal conductivities for the gas composition found throughout various sections of the cell and operating temperatures between 1000 K and 1300 K were calculated. Values varied between 0,3 and 0,8 W/mK for the fuel. Inserted in the model this changed air and fuel temperatures by less than 0,1 K. For air, values varied between 0,065 and 0,085 W/mK. A change from 0,065 to 0,1 W/mK increased temperature in the air delivery tube by 5 K and decreased the temperature difference between fuel and air channel by 0,5 K. It was therefore found reasonable to use a fixed value for both conductivities. The heat transfer coefficient is also a function of the Nusselt number, but this is regarded constant for the operating conditions (Stiller 2006). The formulas used to calculate thermal conductivity of a gas mixture can be found in Appendix C.

The temperatures of the above models are about 30 K higher than the outlet values of the equivalent, but distributed, model of (Stiller 2006). The voltage delivered is approximately 0,06 V lower. It is believed that since the present model uses a higher activation energy value than reported by (Stiller 2006), this causes higher loss reducing the output voltage and producing thermal energy. The value for the activation energy is taken from (Thorud 2005). In the present model methane is not fully reformed in the fuel channel, and this also causes a slightly lower voltage output due to the lower hydrogen concentration.

5.2.2 Distributed model

To include the possibility of representing changing conditions throughout the cell the bond graph of model II is adapted to represent a cross section of the fuel cell as described in section 4.3. The bond graph of Figure 4.16 is imploded into submodels and repeated in six sections as shown in Figure 5.2. Steady state results at design conditions (Table 5.2) are compared with results based on similar parameter sets and operating conditions published in (Thorud 2005) and (Campanari and Iora 2004). Both publications show distributed characteristics in a tubular SOFC fed by methane and hydrogen fuel. As outlined in Table 5.1, two different single cell models are compared. First the ADT is modelled as a lumped volume, model III, secondly a distributed model of the ADT, model IV, is presented.

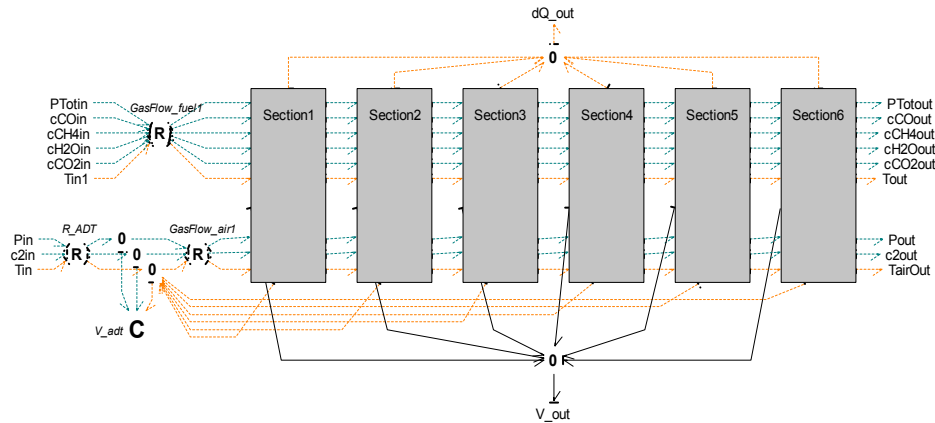


Figure 5.2.6 section model of a SOFC, single volume ADT and reformer, model III

At design point of 250 A the voltage output from the cell (model III) is 0,6306 V, and the outlet temperatures of fuel and air are 1287 and 1284 K respectively. The temperature distribution in the gas channels along the six sections of the cell are shown in Figure 5.3. The inlet temperature of the fuel is 1000 K, while the inlet temperature of the air corresponds to the temperature in the ADT volume (1260 K). Inlet conditions correspond to section 0, section 1 to 6 hold variables of control volumes for each section of the fuel cell.

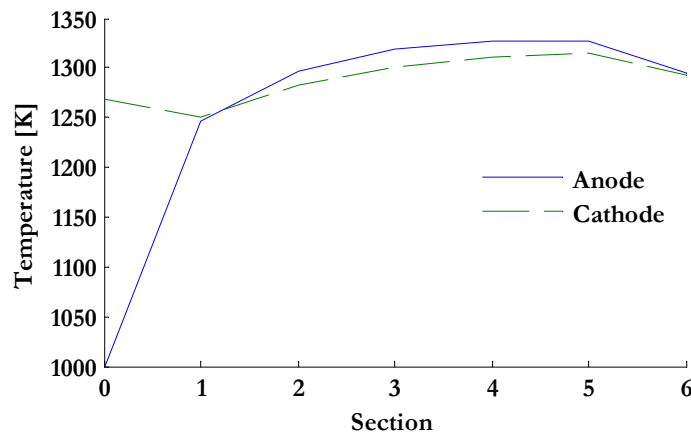


Figure 5.3 Temperature distribution in gas flows, model III

The temperature deviations between the ADT-volume and various sections of the cathode gas necessitate an investigation of whether the air delivery tube should also be modelled in a distributed manner. This can be done by modifying the lower part of Figure 5.2 by inserting the bond graph of Figure 5.4 dividing the ADT-volume in six sections. The input pressure of air is slightly modified to assure that an equivalent mass flow is kept. The voltage output of this model (model IV) is 0,6313 V and the outlet temperatures of fuel and air are 1290 and 1286 K respectively. These values are almost identical to results based on the original

model of Figure 5.2. Multiple sections in the ADT can therefore be omitted if these are the main values of interest to a system simulation.

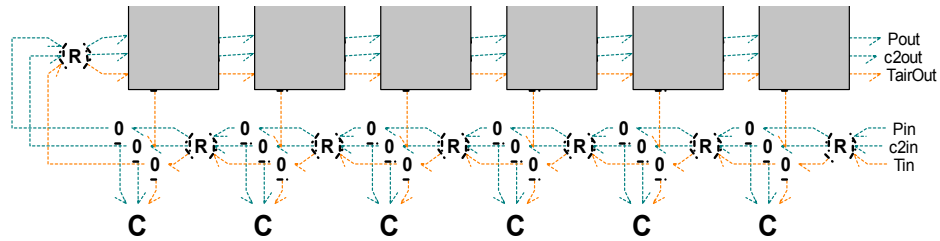


Figure 5.4 Bond graph of ADT in 6 sections, model IV

In Figure 5.5 the temperature distributions of the three gas channels are shown for the modified model. Although the output temperatures are almost identical, the internal temperature distribution differs from Figure 5.3. Figure 5.6 shows that the difference between the minimum and maximum temperature of the sections is larger in the model including sections of the ADT, model IV. The difference is $\sim 90\text{K}$ for model III and $\sim 130\text{K}$ for model IV.

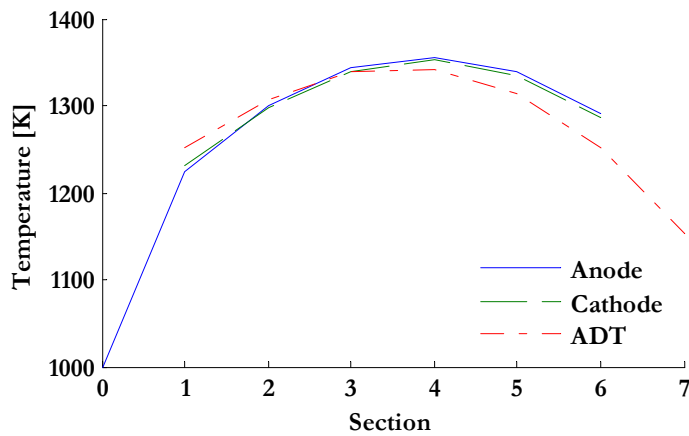


Figure 5.5 Temperature distribution in gas flows, model IV

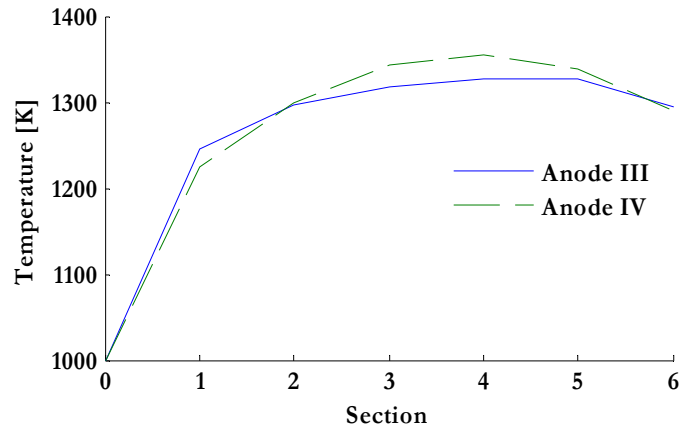


Figure 5.6 Temperature in anode gas, with (IV) and without (III) distributed ADT model

One main objective for dividing the lumped model in several sections is to monitor the temperature gradients inside the cell. Model IV is therefore chosen for the simulations in the remainder of this section. Another important factor when choosing model implementation is that they may result in different transient characteristics, this will be treated in section 5.3.

Figure 5.7 shows how the molar fractions of each component at the anode and the oxygen at the cathode change from inlet conditions (section 0) and through the six fuel cell sections. A high degree of pre-reforming assures that most of the methane is converted to hydrogen in the first two sections. The hydrogen and oxygen concentration falls along the tube, and Figure 5.8 shows how the current density of each lump changes accordingly. In general the current density will change according to the molar concentration of hydrogen. However, the high degree of pre-reforming in the first section lowers the temperature significantly, and the losses become higher reducing the number of reactions to occur here.

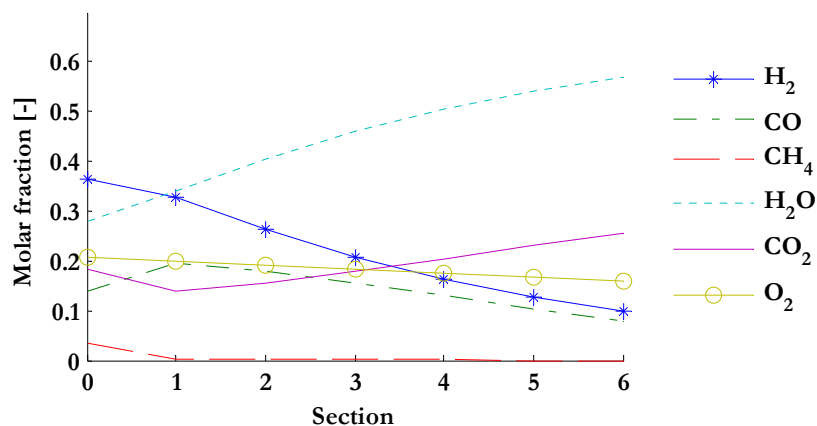


Figure 5.7 Distributed values of molar fractions for each gas component

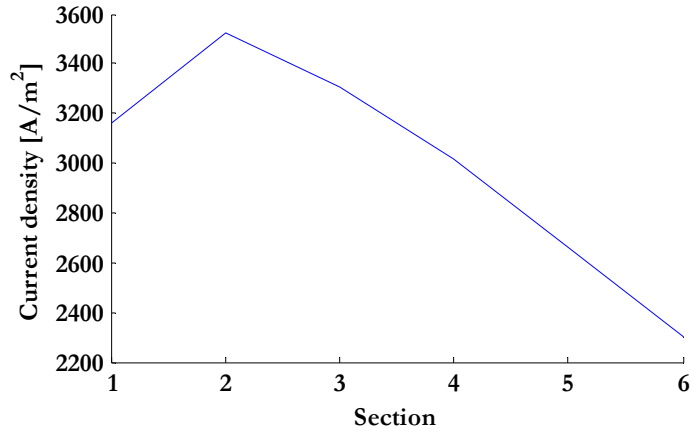


Figure 5.8 Current distribution inside fuel cell

The model was also run with an inlet composition for the fuel after a much lower degree of pre-reforming ($\sim 22\%$), similar to values found in (Campanari and Iora 2004). Since more methane reforming occurs inside the cell, even lower temperatures occur in the first sections, resulting in few electrochemical reactions and low current density here, see Figure 5.9. High activation losses are the main reasons causing the low current density in these sections.

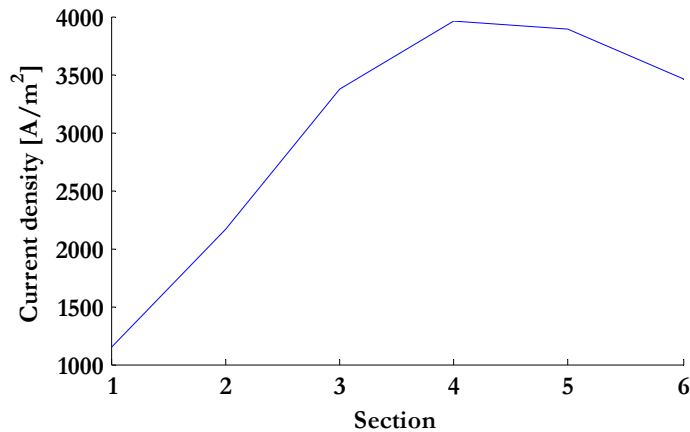


Figure 5.9 Current distribution with low degree of pre-reforming

Figure 5.5 and Figure 5.10 show how the temperature distribution along the tube develops for a high ($\sim 80\%$) and low ($\sim 22\%$) degree of pre-reforming respectively. Since the SOFC materials can be damaged by large temperature-gradients a high degree of pre-reforming is preferred (Thorud 2005).

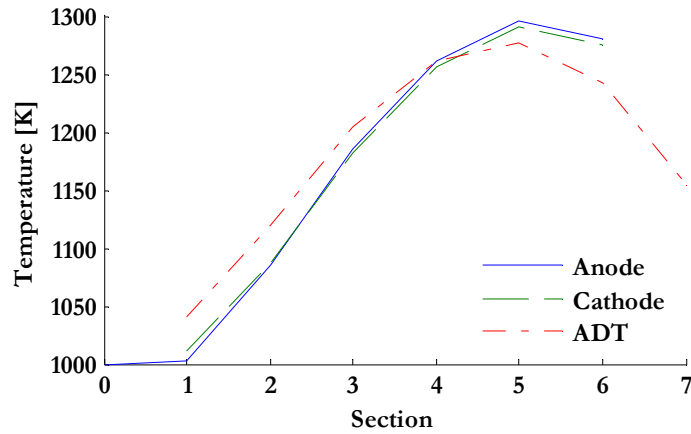


Figure 5.10 Temperature distribution with a low degree of pre-reforming

Losses will also vary with changing temperatures and current density along the cell tube. In Figure 5.11 losses of each section for the model with a high degree of pre-reforming is shown. If the ohmic losses were only dependent on current density the upper plot would show the same characteristics as the plot in Figure 5.8. Since the material resistance values are temperature dependent this increases the loss in the first lump where the temperature is low. Values for the ohmic losses range between 0,128 and 0,196 V.

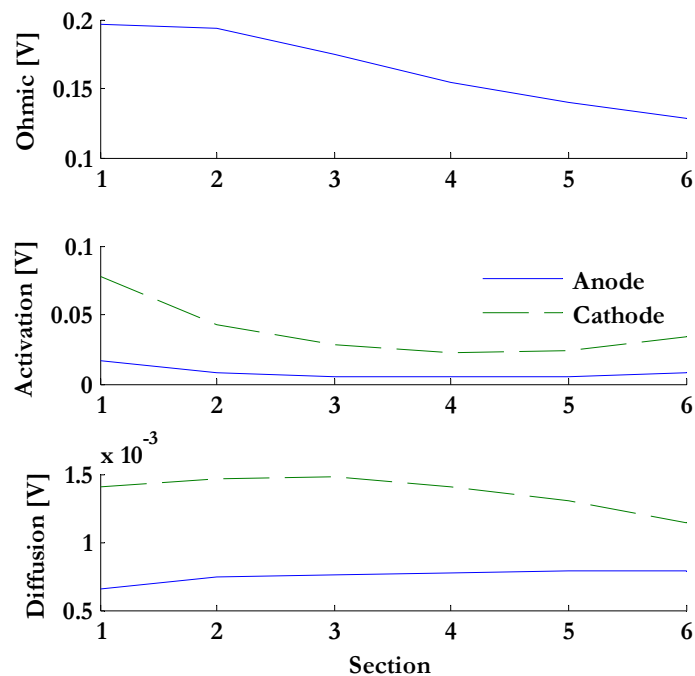


Figure 5.11 Distribution of losses

The activation losses vary between 0,005 and 0,016 V at the anode, and between 0,023 and 0,078 V at the cathode. Due to differences in temperatures, current density, material properties and molar concentration, all influencing activation losses, it is difficult to compare values directly with other implementations. The reference case of (Thorud 2005) shows values between 0.015 and 0.04 V for the anode activation losses, the cathode losses are said to be higher but no values are given.

(Thorud 2005) and (Campanari and Iora 2004) both conduct sensitivity studies on a range of model parameters, claiming that the activation losses are the main uncertainty of the model. Parameters for the activation losses are thus difficult to estimate. In (Thorud 2005) parameter estimation of the activation losses is used to match simulated results to actual results of output voltage from SOFC test runs. With values for the activation energy adapted from (Stiller 2006) the cathode activation losses of the present model became almost ignorable and the voltage output higher than expected. According to (Wagner, Schnumberger et al. 1998) the high operating temperature of the SOFC gives charge transfer resistances of the anode and the cathode to be within the same order of magnitude, and to achieve this the estimated values from (Thorud 2005) were adopted.

According to (Singhal 2003), the binary diffusion coefficient of steam and hydrogen at the anode is four times the one for oxygen at the cathode. The diffusion loss is therefore highest at the cathode, if thickness and material properties of the electrode materials are similar, and will be increased even further when the cell is cathode supported as in the present case. Although (Campanari and Iora 2004) shows the opposite effect in their model (largest loss at the anode) the current implementation is believed to be reasonable. (Thorud 2005) only shows values for the anode diffusion in the area of 0.004 V, somewhat higher than results given in Figure 5.11. As stated in section 4.2.3 the diffusion losses are slightly underestimated by assumptions done to simplify the implementation. The diffusion losses are too small to have a significant effect on the output voltage and are often ignored (Campanari and Iora 2004), (Chan, Khor et al. 2001). Thus no further modifications to the implementation are found beneficial at this stage.

5.3 Transient simulations

With all system boundary parameters and initial values for the control volumes set, the system is simulated to steady state before a step-change in current is applied. First the dynamic response of a single cell model will be presented, followed by the behaviour of the cell in the total power plant system of Figure 5.1. Two main cases are used to investigate transient behaviour. First load is increased by a step-change in current from 190 A (2280 A/m²) to the design point of 250 A (3000 A/m²). The second case is the reverse behaviour of load decrease from 250 A to 190 A.

5.3.1 Behaviour of single cell models

For the first two bond graph models presented in chapter 5.2, model I and model II, a step change was enforced increasing the current drawn from the fuel cell by 60 A. All other parameters were kept constant during simulations, optimised for the design point at 250 A. Figure 5.12 shows the voltage drop for the models both without, model I, and with, model II, extra control volumes on the anode and cathode. Results are nearly identical and indicate that the extra control volumes and the different implementations of the charge double layer do not affect the dynamic response.

The immediate voltage drop in Figure 5.12 is caused by the increase in fuel utilisation and the corresponding decrease in Nernst voltage. An increased number of reactions occur and more thermal energy is released. The following increase in output voltage is caused by the increased temperature that reduces losses, and the slow stabilisation is caused by the long stabilisation times for the temperatures.

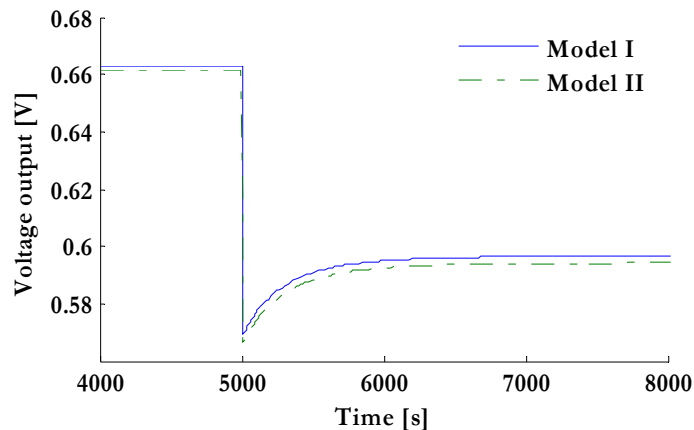


Figure 5.12 Voltage output, load increase of 60 A at 5000 s

Figure 5.13 shows the temperature development for the anode gas control volumes of the two models. It shows a time to steady state at around 3000 s, and a time constant of about 600 s. In (Qi, Huang et al. 2006) a cell of same dimensions is simulated giving a time constant of about 200 s for a similar load increase. Material properties for the MEA (density and heat capacity) were slightly different, but

changing to similar values had minimal effect. However, increasing the inlet pressure to obtain the same gas velocity reduced the time constant, and the results were comparable.

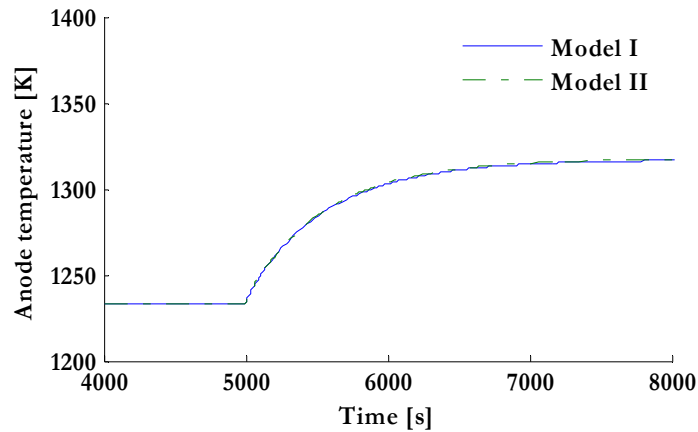


Figure 5.13 Temperature in anode channel, load increase of 60 A at 5000 s

In addition to the magnitude of gas flowing through the system, the material properties and heat transfer coefficients will influence temperature dynamics. The value of the heat transfer coefficient for convection from the electrode material to the gas volumes inside the porous electrodes of model II are difficult to predict. Heat transfer coefficients are kept constant due to a small variation found within the operating area (discussed in chapter 5.2.1). All considered, the gas velocities proved to be the single most important variables when it came to time response of the various models. There are no dynamics related directly to the diffusion, and the charge double layer effects are too fast to influence overall dynamic response.

For control development lumped models are usually preferred. Thus it is important to see how the above model behaves as opposed to the more detailed models representing distributed values within the fuel cells. The dynamic response of the output voltage and anode gas temperature for a model with six sections (model III, Figure 5.2) is shown in Figure 5.14 and Figure 5.15. Only the steady state values differ from results of model II presented above, the dynamic response is near identical. Steady state values differ by less than 5 %, considered as an acceptable value.

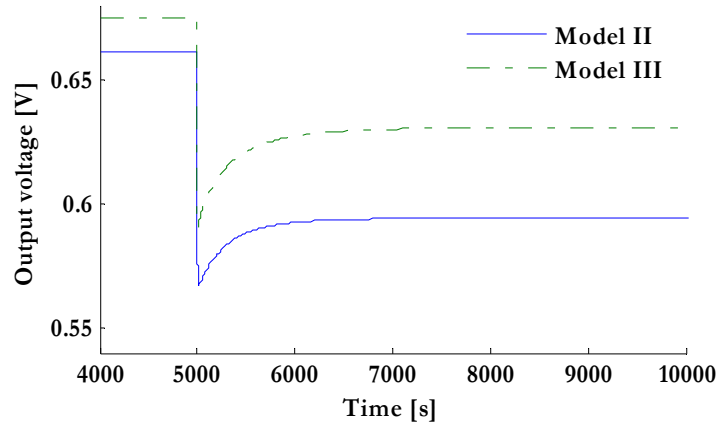


Figure 5.14 Voltage response to increased load, lumped (II) and distributed (III) model

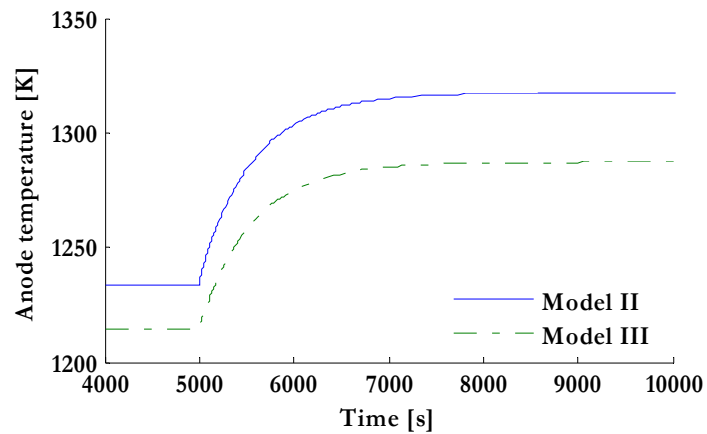


Figure 5.15 Temperature response to increased load, lumped (II) and distributed (III) model

Figure 5.16 shows how the pressure level in the small cathode volume and the corresponding diffusion losses of model II are affected by load increase. The diffusion rate is not fast enough to compensate for increased use of O_2 , and result in a drop in pressure level and increased diffusion loss. Pressure in the air supply volume is unaffected. With very large changes in the capacitance value of the charge double layer, it is possible to detect some effects of changing the dynamics of the activation loss as discussed in chapter 4.2.3. With time constant of less than 2 seconds it does not affect the other variables. The small peak in pressure in the cathode volume is the only place where it is visible (can barely be seen in Figure 5.16).

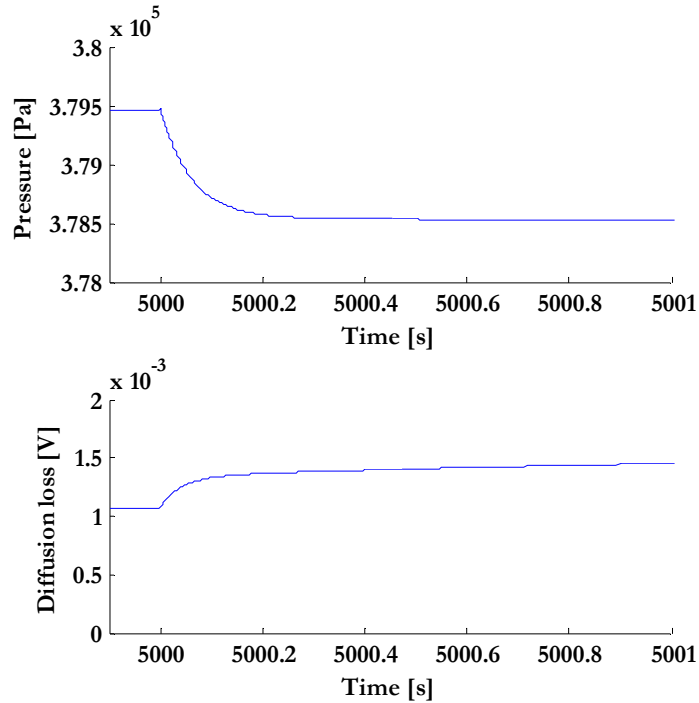


Figure 5.16 Pressure and diffusion loss at cathode for model II, load increase

A slight change in the dynamic response is found when the air delivery tube is also modelled by six sections, model IV. Figure 5.17 shows the voltage response and Figure 5.18 the temperature response comparing a model without (model III) and with (model IV) sectioned representation of the ADT volume. The dynamic response is slower for Model IV due to smaller temperature differences between the adjacent volumes and thereby a slower heat exchange.

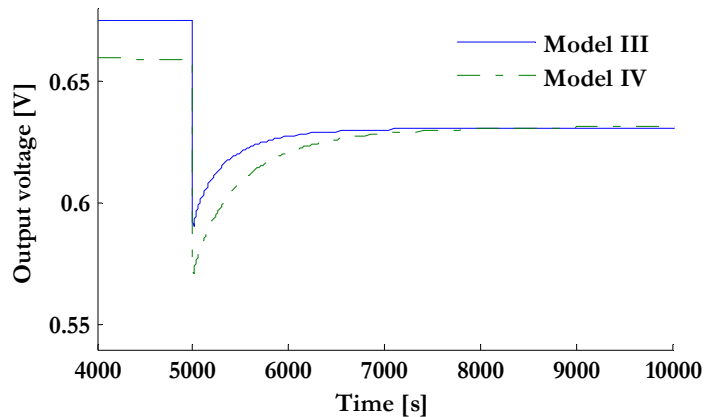


Figure 5.17 Voltage response, model with(IV) and without(III) distributed ADT

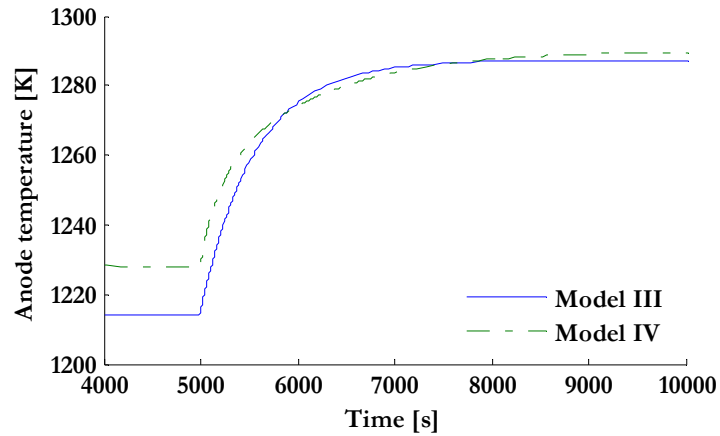


Figure 5.18 Temperature response, model with(IV) and without(III) distributed ADT

Steady state values prior to load change are slightly different for the above models. This is because gas velocities are equal at design point, but slightly different at off design values. Pressure drop is one of the factors of equation (4.16) setting the gas flow rate in the R -fields, and with a larger number of lumps this factor gets smaller and the flow decreases. The inlet pressure of model IV was increased to achieve the desired gas velocities at design point, but values at off design do not change equally for the two models. When these models are included in a total system simulation the mass flows and pressure levels are adjusted based on system behaviour, and off design simulations will have more comparable conditions.

Voltage losses due to activation are strongly affected by temperatures, reactant concentration and current density. Figure 5.19 shows the development in the first and last section along the fuel cell model when load is increased from 190 A to 250 A. The immediate response is caused by increased current, and the long term decrease is caused by higher temperatures. The corresponding current distribution between the two sections is shown in Figure 5.20, the temperature increase in Figure 5.21.

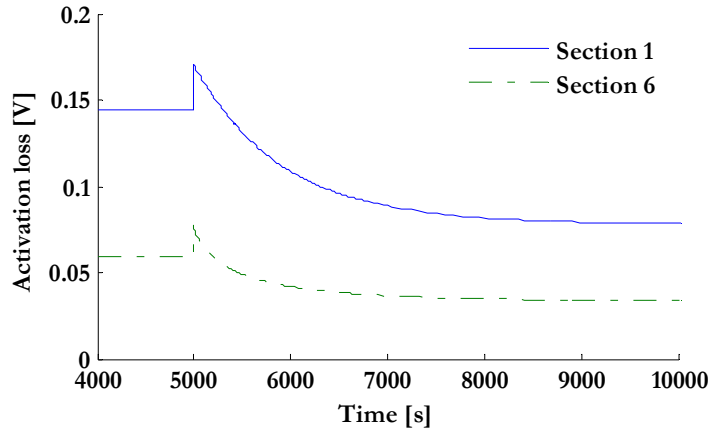


Figure 5.19 Activation losses at anode during load increase

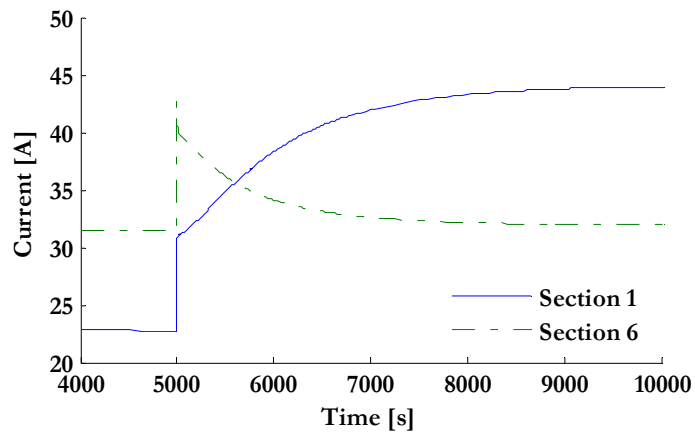


Figure 5.20 Current in section 1 and 6 during load increase

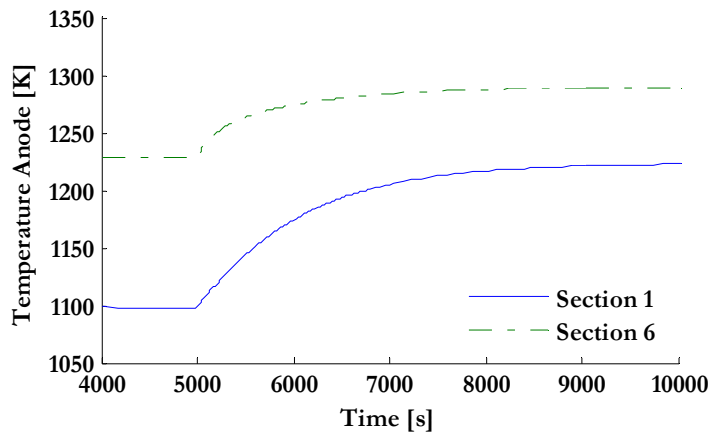


Figure 5.21 Temperature in section 1 and 6 during load increase

Figure 5.22 shows how a load increase results in a step like change in molar fraction of hydrogen. Due to the temperature effect on the reaction rates, it takes some time to reach a final steady state. The change of shift reaction rate is dominated by the Gibbs free energy which is affected by change in composition and slightly by the temperature. The reforming reaction is only dependent on the partial pressure of methane, not by the other molar fractions. It is also exponentially dependent on the inverse of temperature and this result in a long time for the reforming rate to reach steady state.

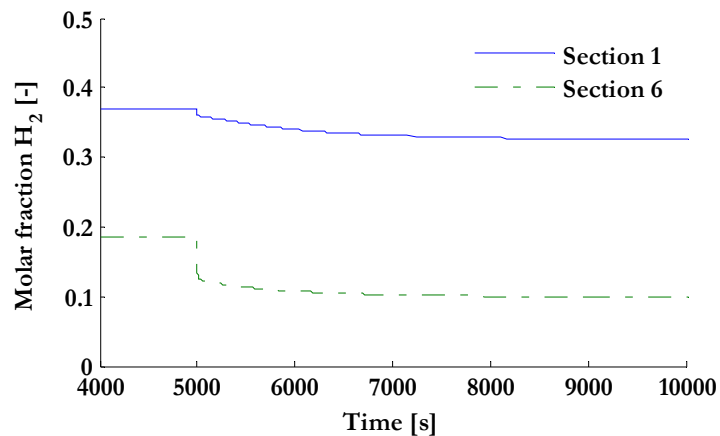


Figure 5.22 Molar fraction of hydrogen in section 1 and 6 during load increase

Above, the cells reaction to load increase is investigated by four different model implementations. A load decrease from 250 A to 190 A at 5000 s is also simulated using model II and model IV. Figure 5.23 shows the temperature development and Figure 5.24 the voltage development, as expected showing opposite characteristics of the load increase case.

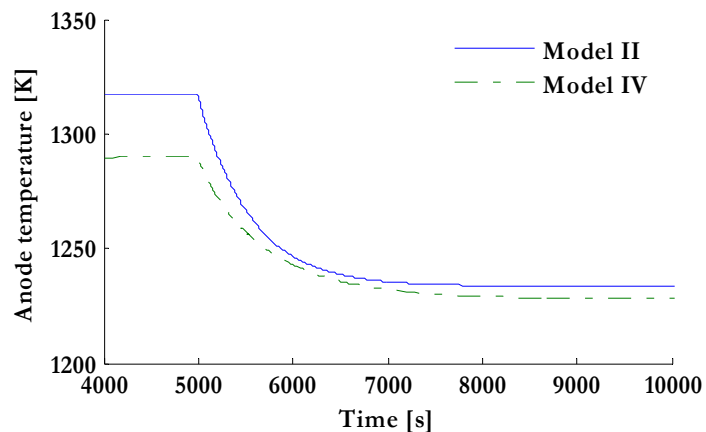


Figure 5.23 Temperature response after load decrease, Model II and Model IV

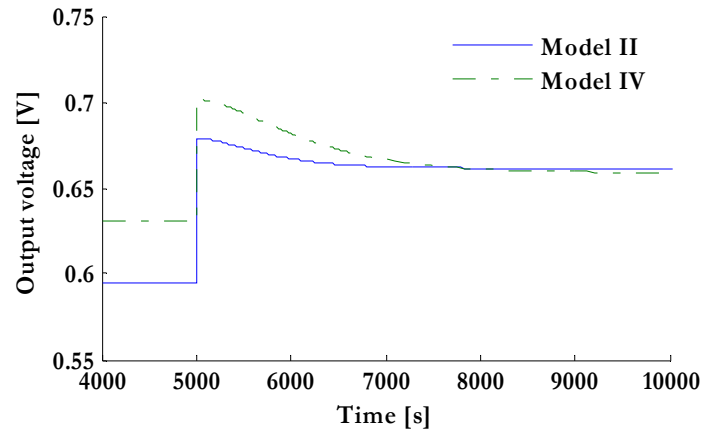


Figure 5.24 Voltage response after load decrease, Model II and Model IV

For the fuel cells included in a total system simulation the aim is to keep temperatures and fuel utility constant at off design conditions (part load). The following section shows how this result in slightly different behaviours of the model variables.

5.3.2 Total system behaviour

A model of the total SOFC power plant is implemented by pseudo bond graphs in 20-sim. Figure 5.25 shows how the subsystems presented in chapter 4 are assembled to a system model. Load steps are enforced by a signal input setting the current, and no controllers are included in this model. Tables set the corresponding air valve opening and fuel input pressure that result in proper values for air flow and fuel flow respectively. For all simulations the operational pressure is kept at approximately 3,8 bar. If the cell is to be integrated in a hybrid power system, or a compressor adjusts the air flow, the pressure level will not be constant. The model is fully capable of handling such variations.

As presented in section 4.2.2, one seek to minimise temperature variations inside the solid oxide fuel cell. To keep the efficiency as high as possible by a high fuel utility and constant steam to carbon ratio, the preferred option is to control the temperature by adjusting the air flow through the system. The design point is chosen as close as possible to the model presented in (Stiller 2006) with respect to input values for pressures, temperatures and mass flows. Since it is difficult to measure the mean value of the MEA temperature (although obtainable from the model) air flow is dimensioned to keep the output temperature of the anode flow close to the design point value of 1273 K.

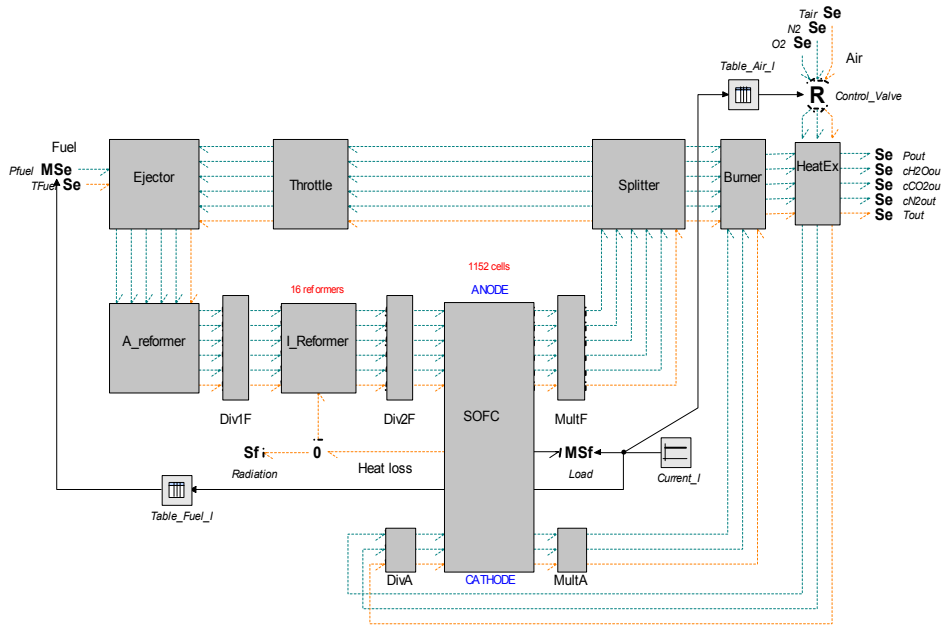


Figure 5.25 Total SOFC system, submodels connected by pseudo bond graphs.

Table 5.5 shows some important steady state values for load steps from 125 A to 275 A. For lower values the mass flow of air must be very low in order to keep the high temperature of the fuel cell, and the model easily becomes unstable. For a load of 275 A an increased mass flow from the one presented in the table makes the model unstable, a higher steady state temperature was therefore allowed. Figure 5.26 shows the voltage-current density plot for values from Table 5.5.

Table 5.5 Steady state values for different loads (PR is the degree of prereforming)

I	\dot{m}_{fuel}	\dot{m}_{air}	V	T_{split}	PR	W_{cell}	W_{total}
125	2.64	1	0.725	1280	0.999	90.6	104414
150	3.17	1.35	0.714	1278	0.929	107.1	123345
175	3.7	1.76	0.699	1275	0.956	122.3	140898
200	4.22	2.23	0.680	1272	0.888	135.9	156580
225	4.75	2.76	0.657	1271	0.823	147.9	170372
250	5.28	3.29	0.635	1273	0.776	158.8	182880
275	5.81	3.56	0.620	1298	0.783	170.6	196511

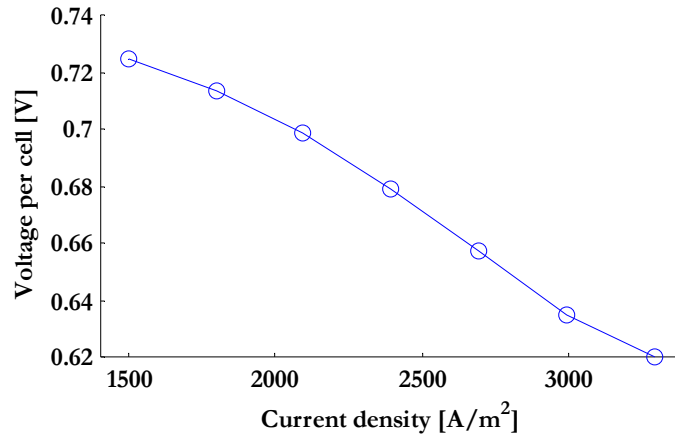


Figure 5.26 Voltage-current density plot for a single cell

Based on results from chapter 5.3.1, a model where the cell is represented by six sections of lumped volumes, including a distributed ADT, is chosen for implementation in total system simulations, model IV. Results from two different ways of linking the fuel cells with the internal reformer are compared, model A and model B. It is assumed that the reformers are placed in-between the fuel cells and receive heat from the whole length of the cells. The reformer consists of a supply tube transporting the fuel internally from the bottom of the stack to the top allowing counter flow between the anode gas and the reformer gas, see Figure 4.3. The exchange of heat between the supply tube and the outer tube is not included in the model.

Figure 5.27 shows temperature development of three different system models presented in Table 5.1. In model A heat flows from each section of the fuel cell is summed by a θ -junction; dQ_{out} in Figure 5.2. This heat is transferred to the internal reformer and the reformer temperature sets the rate of heat transfer from each section. In model B the reformer model is split in six sections. Heat transfer between fuel cell and reformer is represented by six separate bonds exchanging temperature and heat flow between corresponding sections of the two components. Model C does not have a distributed representation of the ADT and is included to show how the temperature peak is underestimated using this model. The characteristics of models A and B are fairly close, but the steady state temperature of model B is lower than for model A.

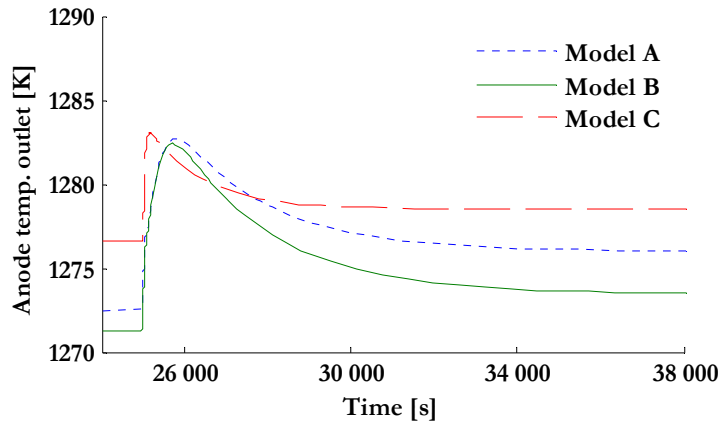


Figure 5.27 Temperature in anode output flow, load increase

The voltage drops for the same simulations are plotted in Figure 5.28. They show how the effort to keep a constant temperature cause the “dip” below steady state values to almost disappear compared to the simulations with constant air flow, Figure 5.14. A close-up of the transient around 25000 s is found in Figure 5.30. A small decrease in the voltage due to increasing losses is seen until the system reaches the steady state temperature. As expected the lower temperature of model B corresponds to a higher voltage output. This model is believed to give the best physical representation and therefore chosen for the remaining simulations of this chapter.

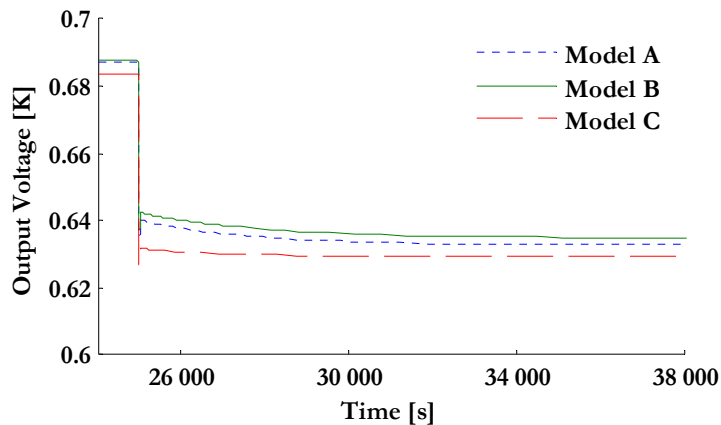


Figure 5.28 Voltage output, load increase

Temperature development during a load decrease from 250 A and back to 190 A is shown in Figure 5.29 together with the corresponding increase. The transient development shows opposite characteristics, the response after a load decrease being somewhat slower. This is due to slower gas velocities at lower load resulting in slower transport of heat and a lower number of reactions releasing heat. Figure

5.30 shows a close-up of the voltage response for the same model, both for increase and decrease.

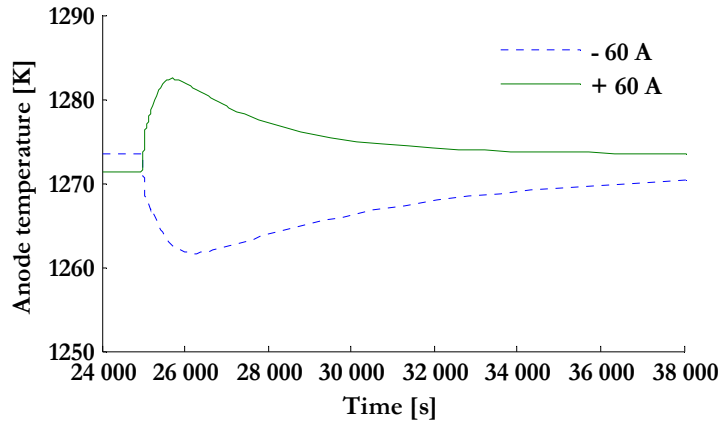


Figure 5.29 Temperature response to load increase and decrease, model B

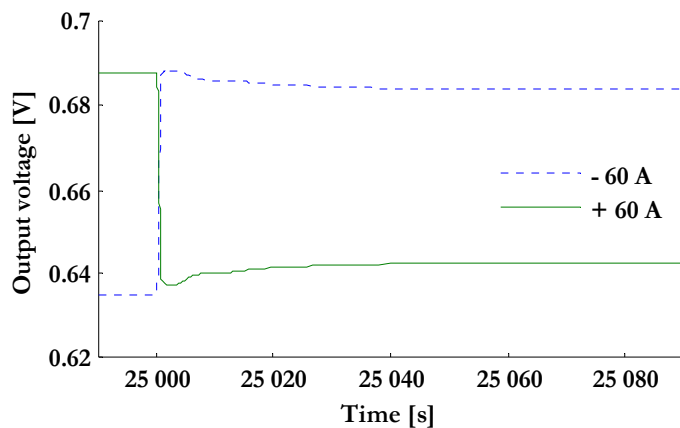


Figure 5.30 Close-up of voltage response to load increase and decrease

Fuel input is controlled by the same step changes as the load, providing a fuel utility of 85% at all steady state conditions. The molar fraction of fuel at the fuel cell outlet is shown in Figure 5.31 for both load increase and decrease. This explains why the voltage dips slightly below steady state although the temperature rises the first 1000 seconds after load increase. The dip reflects the time it takes for an increased or decreased amount of hydrogen to get from the fuel input valve to the fuel cell. Size and configuration of piping and reformer will govern the time constant for this phenomena, and must be verified for each system design.

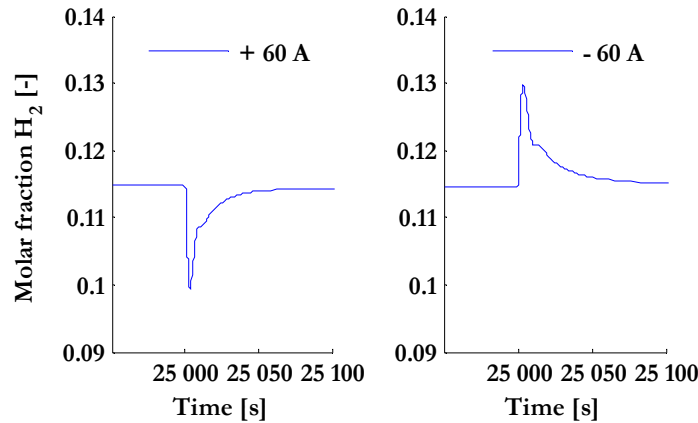


Figure 5.31 Molar fraction of hydrogen at anode outlet, load increase and decrease

As mentioned in chapter 4 the model can serve as a basis for further control development. As an example the system response may be altered by choosing a lower fuel utility setpoint possibly reducing the peaks in Figure 5.31. A change in air to fuel ratio may speed up or slow down the thermal response. For all cases simulated above, an immediate step change in current is applied to the cell. In a true physical system different effects of the electrical load may impose a different characteristic of the current and voltage relations of the external circuit, this is discussed in for instance (Zenith and Skogestad 2007). The model is perfectly adaptable to these kind of applications.

5.3.3 Distributed characteristics at part load

Due to the importance of reducing temperature gradients inside the cell and across membranes it might be useful to monitor some important parameters at off design conditions also for the total system models (model B). The temperature distributions in the fuel cell and reformer are shown for two different steady states; Figure 5.32 at 250 A and Figure 5.33 at 190 A.

The degree of pre-reforming is higher in the off design case, 190 A, due to a higher temperature in the internal reformer, Figure 5.33. Heat flows between the different tubes are driven mainly by the relative differences in temperatures. Fuel cell temperature and inlet temperature of injected fuel is kept constant; this results in small changes of inlet temperature to the reformer, and nearly constant heat input from the fuel cell to the reformer. A lower mass flow makes temperatures rise in the reformer, resulting in a high degree of pre-reforming and higher temperature in the first section of the fuel cell, as found in Figure 5.33.

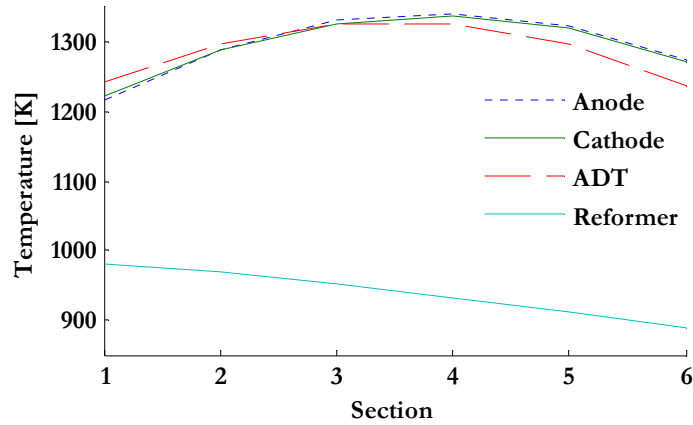


Figure 5.32 Temperature at steady state, 250 A, fuel cell and reformer

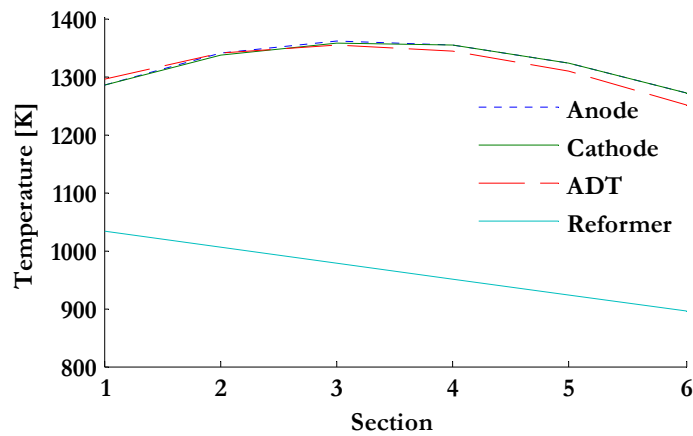


Figure 5.33 Temperature at steady state, 190 A, fuel cell and reformer

Figure 5.34 shows how the current is distributed for the design case and at part load. The internal reforming is almost ignorable at part load, resulting in lower temperature gradients. Current density distribution is monotonically decreasing along the cell, caused mainly by the fall in Nernst voltage.

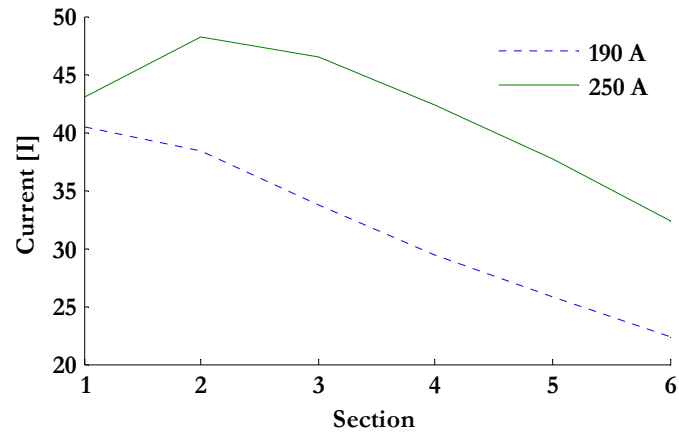


Figure 5.34 Current per section at steady state, 190 and 250 A

A more refined model may be obtained by splitting the fuel cell tube in a larger number of sections. For the present fuel cell, more than six sections gave no significant change in output voltage or gas temperatures, and therefore this number was regarded sufficient. For other operating conditions or cell designs a different number of sections may be appropriate. The proper number of sections to include, and how section borders are defined, must be adapted for each new fuel cell design.

Chapter 6

Conclusions and further work

6.1 Conclusions

In this thesis a bond graph template for modelling of fuel cells has been developed. The template is verified through modelling and simulation of a solid oxide fuel cell stack.

The project was motivated by the increased attention towards emissions from the shipping industry, resulting in a search for cleaner energy sources on board. A market assessment for fuel cells in marine applications carried out in chapter 1 revealed the SOFC as a possible future component in marine power plant systems.

Chapter 1 and the outline of previous work in chapter 2 describe the need for a consistent framework for structuring existing fuel cell knowledge in proper simulation models. The tool will enhance design and analysis of future marine power plant solutions. A method suitable for creating such models applicable for system simulations was developed in chapter 3, and applied when implementing a model of a SOFC stack in chapter 4. The implemented models were verified through simulations in chapter 5. Main findings of this thesis are;

- Bond graphs were identified as a good tool for the multi-domain nature of fuel cell modelling. Pseudo-bond graphs were chosen to model thermofluid properties while true bond graphs were the choice for electrochemical and electrical domains.
- A new R -field was developed enabling a straight forward conversion between the thermofluid and electrochemical domains. Conservation of energy is assured by accounting for the entropy production causing generation of heat.
- By expanding the lumped model approach to represent multiple sections, a new model was developed enabling simulations of distributed characteristics inside the fuel cell.
- The bond graph tool strongly supported the model implementation process when evaluating different ways of representing the electrochemical losses. The resulting models were of complete integral causality, lending themselves to computationally efficient system simulations.

- Component models of the gas supply system were developed and implemented, enabling simulations of the fuel cell stack under realistic operating conditions.

Data from a specific tubular SOFC was applied to develop a design case. Simulations were used to compare different model implementations both at single cell and system level. Steady state conditions were comparable for the different implementations, although distributed characteristics were only represented in cell models built up by multiple sections. Dynamic properties differed slightly between lumped and distributed models and the distributed models are assumed to be closer to resembling actual physical behaviour.

6.2 Further work

The implemented models are developed with the purpose of allowing for reuse and further refinements or adaptations depending on relevant application. Possible future use and potential improvements of the models are summarised here.

The presented method is a general framework for fuel cell modelling. Gas composition both on anode and cathode, and the nature of chemical and electrochemical reactions, vary between different fuel cell types. This must be reflected in new models. Parameters in the relations implementing losses must be adapted for the current materials and reactions. Variation in operating temperature and pressure affect thermal properties of gases, and it must be assured that these are calculated in a correct manner. As an example, formation of liquid water requires two-phase modelling in PEM fuel cells. Also the stack support systems will vary with fuel cell type, for example affected by the need for gas recycle or by the exhaust properties. All of the above changes are possible as modifications using the existing framework models.

A possible extension of the model will be to implement control procedures allowing for simulation of start-up and shut-down of the power production from the fuel cell. For a high temperature fuel cell there are sequential procedures for each specific installation. The fuel cell must be heated before reactions can occur, and there are limitations to the allowed heating and cooling rates to avoid high temperature gradients. All submodels must be reviewed to see that they will result in a realistic physical behaviour in such operating conditions. This may also require changes to operating range of support system models, such as the after-burners and heat exchangers. Expanding the operating area will also require implementation of thermal property packages for improved estimation of component and mixture properties in off-design conditions. These changes will increase the robustness of the model implementation.

In order to explore interactions with the remainder of the ship power system, the models should be included in system simulations based on a component library such as developed in (Pedersen 2009). This will help to demonstrate the quality of power production from fuel cells in a ship machinery system. Depending on the

complexity of the total power plant, the level of details included can be reduced for more efficient simulation. For many cases a lumped fuel cell model may be sufficient in demonstrating the system behaviour.

Results from simulations of the numerical models will indicate which operating conditions that might cause problems for a power plant, and help understanding the connection between physical variables of the different components. Using the models for parameter estimations will aid processes such as finding the optimal materials, gas flows and fuel cell dimensions. Still, models are based on a number of estimations, and further refinement and interpretation of results will have higher value if compared to real test data. Acquiring relevant results from physical testing would be the next step for further verification and refinement of the solid oxide fuel cell models presented in this thesis.

CONCLUSIONS AND FURTHER WORK

Bibliography

- Achenbach, E. (1994). *Three-dimensional and time-dependent simulation of a planar solid oxide fuel cell stack*. Journal of Power Sources 49(1-3): 333-348.
- Adamson, K.-A. (2005). *Fuel Cell Market Survey: Niche Transport (Part 2)* www.fuelcelltoday.com.
- AEA (2008). *Greenhouse gas emissions from shipping: trends, projections and abatement potential*. Final report to the Committee on Climate Change (CCC), AEA Energy & Environment, <http://www.aeat.co.uk/cms/>.
- Aesoy, V. and H. Engja (1994). *Pseudo Bond Graph Representation of Transient Heat Conduction in a Cylindrical Coordinate System Using a Modal Decoupling of the "Bessel Equation"*. International Conference on Bond Graph Modelling and Simulation, SCS.
- Auslander, D. M., G. F. Oster, et al. (1972). *On Systems With Coupled Chemical Reaction and Diffusion*. Journal of Dynamic Systems, Measurement and Control, Transactions of the ASME 94 Ser G(3): 239-248.
- Bejan, A. (2006). *Advanced engineering thermodynamics*. Hoboken, N.J., Wiley.
- Benbouzid, S., G. Dauphin-Tanguy, et al. (2004). *Electrochemical Phenomena Modelling in PEM Fuel Cell with Bond Graph Approach*. IEEE Vehicular Power & Propulsion, Paris.
- Benbouzid, S., N. Fouquet, et al. (2003). *Bond graph approach for pem fuel cell modelling*. 3rd Congress Computational Engineering in Systems Applications. Lille.
- Blunier, B. and A. Miraoui (2008). *Modelling of fuel cells using multi-domain VHDL-AMS language*. Journal of Power Sources 177(2): 434-450.
- Boot, P., J. Klein Woud, et al. (1991). *A mathematical model for a turbocharged 4-stroke diesel engine*. 4th International Marine Systems Design Conference, Kobe, Japan.
- Borutzky, W. (2002). *Bond graphs and object-oriented modelling—a comparison*. Proceedings of the Institution of Mechanical Engineers, Part I: Journal of Systems and Control Engineering 216(1): 21-33.
- Broenink, J. F. (1997). *Bond-graph modeling in Modelica™*. 9th European Simulation Symposium (ESS'97), Passau, Germany.
- Brown, F. T. (1991). *Convection bonds and bond graphs*. Journal of the Franklin Institute 328(5-6): 871-886.

-
- Brown, F. T. (2002). *Non-iterative evaluation of multiphase thermal compliances in bond graphs*. Proceedings of the Institution of Mechanical Engineers. Part I: Journal of Systems and Control Engineering 216(1): 13-19.
- Brown, F. T. (2006). *Engineering system dynamics: a unified graph-centered approach*. Boca Raton, Fla., Taylor & Francis.
- Bruun, K. and E. Pedersen (2007). *Bond graph model of a high temperature fuel cell*. International Conference on Bond Graph Modeling and Simulation, ICBGM '07, San Diego, SCS.
- Bruun, K., E. Pedersen, et al. (2005). *Modelling for transient torsional vibration analysis in marine power train systems*. International Conference on Bond Graph Modeling and Simulation, ICBGM'05, New Orleans, SCS.
- Butler, J. (2008). *Fuel Cell Market Survey: Niche Transport Volume 2*, www.fuelcelltoday.com.
- Campanari, S. and P. Iora (2004). *Definition and sensitivity analysis of a finite volume SOFC model for a tubular cell geometry*. Journal of Power Sources 132(1-2): 113-126.
- Campora, U. and M. Figari (2003). *Numerical simulation of ship propulsion transients and full-scale validation*. Proceedings of the Institution of Mechanical Engineers, Part M: Journal of Engineering for the Maritime Environment 217(1): 41-52.
- Carrera, G. and E. Rizzuto (1997). *Simulation of mechanical and thermodynamic performances of a ship propulsion plant in transient conditions*, New York, American Society of Mechanical Engineers.
- Cellier, F. E. (1991). *Continuous system modeling*. New York, Springer-Verlag.
- Cellier, F. E., Greifender, J. (2008). *ThermoBondLib - A New Modelica Library for Modeling Convective Flows*. 6th International Modelica Conference, Bielefeld, Germany.
- Chan, S. H., K. A. Khor, et al. (2001). *Complete polarization model of a solid oxide fuel cell and its sensitivity to the change of cell component thickness*. Journal of Power Sources 93(1-2): 130-140.
- Chase, M. W., Jr., C. A. Davies, et al. (1986). *JANAF thermochemical tables* Journal of Physical and Chemical Reference Data 14, Suppl. 1.
- Chesse, P., D. Chalet, et al. (2004). *Real-Time Performance Simulation of Marine Diesel Engines for the Training of Navy Crews*. Marine Technology 41(3): 95-101.
- Christen, E. and K. Bakalar (1999). *VHDL-AMS - a hardware description language for analog and mixed-signal applications*. IEEE Transactions on Circuits and Systems II: Analog and Digital Signal Processing 46(10): 1263-1272.
- Couenne, F., C. Jallut, et al. (2008). *Bond graph for dynamic modelling in chemical engineering*. Chemical Engineering and Processing: Process Intensification 47(11): 1994-2003.

-
- Cussler, E. L. (1997). *Diffusion: mass transfer in fluid systems*. Cambridge, Cambridge University Press.
- DNV (2008). *Rules for Ships, Part 6, Chapter 23, "Fuel cell installations"* Det Norske Veritas AS. JULY 2008.
- DOE, U. S. (2008). *Comparison of fuel cell technologies*, by U.S. Department of Energy. Retrieved January, 2009, from http://www1.eere.energy.gov/hydrogenandfuelcells/fuelcells/pdfs/fc_comparison_chart.pdf.
- EE-AES (2003). *Application for KMB within the area energy-efficient all electric ship*. Trondheim, NTNU.
- EG&G, I. (2004). *Fuel Cell Handbook*, U.S. Department of Energy. 7th edition.
- Egeland, O. and J. T. Gravdahl (2002). *Modeling and simulation for automatic control*. Trondheim, Marine Cybernetics.
- Engja, H. (1985). *Bond graph model of a reciprocating compressor*. Journal of the Franklin Institute 319(1-2): 115-124.
- Engja, H. (1986). *Modeling and simulation of heat exchanger dynamics using bond graphs*. European Simulation Congress, Antwerpen, Simulation Councils, Inc.
- Engja, H. H. (1985). *Pseudo bond graph representation of unsteady state heat conduction*. IMACS World Congress on Systems Simulation and Scientific Computation, Oslo.
- Fahrenthold, E. P. and J. D. Wargo (1994). *Lagrangian bond graphs for solid continuum dynamics modeling*. Journal of Dynamic Systems, Measurement and Control, Transactions of the ASME 116(2): 178-192.
- FCSHIP (2004). *Fuel Cells in Ships – Synthesis of open problems and Roadmap for future RTD*, European Commission. Final Report.
- FELICITAS (2006). *FELICITAS - fuel cells for heavy duty applications*. Warship Technology. May: 12-13.
- FellowSHIP. (2009). *Developing maritime fuel cells...* Retrieved Feb, 2009, from <http://www.fuelcellship.com>.
- Ferrari, M. L., A. Traverso, et al. (2005). *Influence of the anodic recirculation transient behaviour on the SOFC hybrid system performance*. Journal of Power Sources 149(SUPPL): 22-32.
- Fritzson, P., P. Aronsson, et al. (2007). *OpenModelica - A free open-source environment for system modeling, simulation, and teaching*, Munich, Germany, Institute of Electrical and Electronics Engineers Inc., Piscataway, NJ 08855-1331, United States.
- Gawthrop, P. J. (1999). *Thermal modelling using mixed energy and pseudo bond graphs*. Proceedings of the Institution of Mechanical Engineers. Part I: Journal of Systems and Control Engineering 213(3): 201-216.

-
- Gawthrop, P. J. and G. P. Bevan (2007). *Bond-graph modeling*. IEEE Control Systems Magazine 27(2): 24-45.
- Gjerde, O. (1999). *Systemanalyser av skipstekniske anlegg (in Norwegian)*. Dr.ing. avhandling. Trondheim, NTNU.
- GL (2003). "Guidelines for the Use of Fuel Cell Systems on Board of Ships and Boats" VI - Part 3, Chapter 11. G. Lloyd. Rules and Guidelines 2008.
- Greifeneder, J., Cellier, F.E. (2001). *Modeling convective flows using bond graphs*. 5'th International Conference on Bond Graph Modeling and Simulation, Phoenix, Arizona, SCS.
- Greig, A. (2003). *Fuel cells and issues for their use in warships*. Proceedings of the IMarEST. Part B, Journal of marine design and operations B3: 9-19.
- Haberman, B. A. and J. B. Young (2006). *Diffusion and chemical reaction in the porous structures of solid oxide fuel cells*. Journal of Fuel Cell Science and Technology 3(3): 312-321.
- Haller, C. (2001). *Transient simulation of an intergrated diesel-electric propulsion system with podded electric propulsors for engine selection*. 23rd CIMAC World Congress on Combustion Engine Technology, Hamburg: 1224-1236.
- Hansen, J. F., A. K. Ådnanes, et al. (2001). *Mathematical Modelling of Diesel-Electric Propulsion Systems for Marine Vessels*. Mathematical and Computer Modelling of Dynamical Systems 7(3): 323-355.
- Haynes, C. (2002). *Simulating process settings for unslaved SOFC response to increases in load demand*. Journal of Power Sources 109(2): 365-376.
- Heny, C., D. Simanca, et al. (2000). *Pseudo-bond graph model and simulation of a continuous stirred tank reactor*. Journal of the Franklin Institute 337(1): 21-42.
- Hetet, J. F., B. Inozu, et al. (1999). *Performance Simulation of Marine Diesel Engines with SELENDIA*. Journal of Ship Research 43(4): 201-217.
- Hung, Y. H., P. H. Lin, et al. (2008). *Real-time dynamic modeling of hydrogen PEMFCs*. Journal of the Franklin Institute 345(2): 182-203.
- Incropera, F. P. and D. P. DeWitt (2002). *Fundamentals of heat and mass transfer*. New York, Wiley.
- Iora, P., P. Aguiar, et al. (2005). *Comparison of two IT DIR-SOFC models: Impact of variable thermodynamic, physical, and flow properties. Steady-state and dynamic analysis*. Chemical Engineering Science 60(11): 2963-2975.
- Kandepu, R., L. Imsland, et al. (2007). *Modeling and control of a SOFC-GT-based autonomous power system*. Energy 32(4): 406-417.
- Karnopp, D. (1978). *Bond graph modeling philosophy for thermofluid systems*. Journal of Dynamic Systems, Measurement and Control, Transactions of the ASME 100(1): 70-75.

-
- Karnopp, D. (1979). *State variables and pseudo bond graphs for compressible thermofluid systems*. Journal of Dynamic Systems, Measurement and Control, Transactions of the ASME 101(3): 201-204.
- Karnopp, D. (1990). *Bond graph models for electrochemical energy storage. Electrical, chemical and thermal effects*. Journal of the Franklin Institute 327(6): 983-992.
- Karnopp, D. C., Donald L. Margolis, Ronald C. Rosenberg (2000). *System dynamics : modeling and simulation of mechatronic systems*. New York, John Wiley & Sons, Inc.
- Krummrich, S., B. Tuinstra, et al. (2006). *Diesel fuel processing for fuel cells-DESIRE*. Journal of Power Sources 160(1): 500-504.
- Kyrtatos, N. P., P. Theodossopoulos, et al. (1999). *Simulation of the overall ship propulsion plant for performance prediction and control*. MarPower '99 (Advanced Marine Power conference), Newcastle-upon-Tyne, UK.
- Kyrtatos, N. P., G. Theotokatos, et al. (2001). *Transient operation of large-bore two-stroke marine diesel engine power plants: measurements and simulations*. 23rd World Congress on Combustion Engine Technology for Ship Propulsion, Power Generation, Rail Traction, Hamburg, Germany, CIMAC.
- Larminie, J. and A. Dicks (2003). *Fuel cell systems explained* Chichester, Wiley.
- Lefèvre, J. and J. Barreto (1985). *A mixed block diagram bond graph approach for biochemical models with mass action and rate law kinetics*. Journal of the Franklin Institute 319(1-2): 201-215.
- Levander, O. (2001). *Continuing economic advantage for diesel-electric cruise ships*. Marine News. Helsinki, Wärtsilä Corporation: 18-22.
- Li, X. (2006). *Principles of fuel cells*. New York, Taylor & Francis Group.
- Little, G. T., S. S. Young, et al. (2003). *The electric warship VII - the reality*. Journal of Marine Design and Operations B2.
- Mangset, L. E., Longva, T., Tronstad, T. (2008). *Analysis of the Economy of Fuel Cells Used in Merchant Ships*. 30th Propulsion & Emissions Conference, Gothenburg.
- MarineProp (2008a). *Reheat raises hopes of steam propulsion revival*. Marine Propulsion & Auxiliary Machinery. April/May: 33.
- MarineProp (2008b). *Countdown to seagoing debuts for fuel cells*. Marine Propulsion & Auxiliary Machinery. April/May: 55-56.
- Mattsson, S. E., H. Elmqvist, et al. (1998). *Physical system modeling with Modelica*. Control Engineering Practice 6(4): 501-510.
- METAPHU. (2009). *Validation of renewable methanol based auxiliary power system for commercial vessels*. Retrieved 10 Jan, 2009, from <http://www.methapu.eu/>.

-
- Moksnes, P. O. (1997). *Modeling two-phase thermo-fluid systems using bond graphs*. Trondheim, Norwegian University of Science and Technology, Faculty of Marine Technology. Doktor Ingeniør 1997:116.
- Moran, M. J., Howard N. Shapiro (1998). *Fundamentals of engineering thermodynamics*. Chichester, Wiley.
- NavalArch (2004a). *Queen Mary 2: Genesis of a Queen*. The Naval Architect: 50-52.
- NavalArch (2004b). *Wider horizons for gas turbine propulsion*. The Naval Architect: 14-16.
- Nickens, A. (2006). *U.S. Navy's advanced shipboard fuel cell program*. USFCC Fuel Cell Seminar, Honolulu.
- Noren, D. A. and M. A. Hoffman (2005). *Clarifying the Butler-Volmer equation and related approximations for calculating activation losses in solid oxide fuel cell models*. Journal of Power Sources 152: 175-181.
- Paynter, H. M. (1961). *Analysis and Design of Engineering Systems*. Cambridge, Massachusetts, The M.I.T. Press.
- Paynter, H. M. (1985). *Representation of Measured Ejector Characteristics by Simple Eulerian Bond Graph Models*. Journal of Dynamic Systems, Measurement and Control, Transactions ASME 107(4): 258-261.
- Pedersen, E. (1999). *Modelling Thermodynamic Systems With Changing Gas Mixtures*. Proc. of the 4'th International Conference on Bond Graph Modeling, San Francisco, SCS.
- Pedersen, E. (2001). *Modelling gas turbine systems for transient performance using bond graphs*. European Simulation Symposium and Exhibition/Bond Graph Workshop Marseille, SCS.
- Pedersen, E. (2001). *Modelling multicomponent two-phase thermodynamic systems using pseudo-bond graphs*. Proc. of the 5'th International Conference on Bond Graph Modeling, Phoenix, SCS.
- Pedersen, E. and H. Engja (2000). *A bond graph model library for modelling diesel engine transient performance*. Proceedings of the 6th International Symposium on Marine Engineering, Tokyo, Marine Engineering Society in Japan.
- Pedersen, E. and H. Engja (2008). *Mathematical modelling and simulation of physical systems: lecture notes in course TMR4275 Modelling, simulation and analysis of dynamic systems*. Trondheim, Department of Marine Technology, Norwegian University of Science and Technology.
- Pedersen, T. A. (2009). *Bond graph modeling of marine power systems*. Trondheim, Norwegian University of Science and Technology, Faculty of Engineering Science and Technology, Department of Marine Technology. 2009:56.
- Poling, B. E., J. P. O'Connell, et al. (2001). *The properties of gases and liquids*. New York, McGraw-Hill.

-
- Pukrushpan, J. T., A. G. Stefanopoulou, et al. (2004). *Control of fuel cell power systems: principles, modeling, analysis and feedback design*. London, Springer.
- Qi, Y., B. Huang, et al. (2005). *Dynamic modeling of solid oxide fuel cell: The effect of diffusion and inherent impedance*. *Journal of Power Sources* 150(1-2): 32-47.
- Qi, Y., B. Huang, et al. (2006). *Dynamic modeling of a finite volume of solid oxide fuel cell: The effect of transport dynamics*. *Chemical Engineering Science* 61(18): 6057-6076.
- Qi, Y., B. Huang, et al. (2008). *1-D dynamic modeling of SOFC with analytical solution for reacting gas-flow problem*. *AIChE Journal* 54(6): 1537-1553.
- Radan, D. (2008). *Integrated control of marine electrical power systems*. Trondheim, Norwegian University of Science and Technology, Faculty of Engineering Science & Technology, Department of Marine Technology. PhD 2008:37.
- Ratkje, S. K. and S. Moller-Holst (1993). *Exergy efficiency and local heat production in solid oxide fuel cells*. *Electrochimica Acta* 38(2-3): 447-453.
- Saisset, R., G. Fontes, et al. (2006). *Bond Graph model of a PEM fuel cell*. *Journal of Power Sources* 156(1): 100-107.
- Saisset, R., C. Turpin, et al. (2002). *Study of thermal imbalances in arrangements of solid oxide fuel cells by mean of bond graph modelling*, Cairns, Australia, Institute of Electrical and Electronics Engineers Inc.
- Samantaray, A. K. and B. O. Bouamama (2008). *Model-based Process Supervision: A Bond Graph Approach*. London, Springer-Verlag London Limited.
- Sattler, G. (2000). *Fuel cells going on-board*. *Journal of Power Sources* 86(1-2): 61-67.
- Sedghisigarchi, K. and A. Feliachi (2004). *Dynamic and transient analysis of power distribution systems with fuel cells - Part I: Fuel-cell dynamic model*. *IEEE Transactions on Energy Conversion* 19(2): 423-428.
- Selimovic, A. (2002). *Modelling of Solid Oxide Fuel Cells Applied to the Analysis Of Integrated Systems with Gas Turbines*. Lund, Lund Institute of Technology. Doctoral Thesis.
- Siemens, P. G. (2007, 2007). *Solid Oxide Fuel Cells Introduction*. from <http://www.powergeneration.siemens.com/products-solutions-services/products-packages/fuel-cells/>.
- Singhal, S. C., K. Kendall (2003). *High temperature solid oxide fuel cells : fundamentals, design, and applicatons*. Oxford, Elsevier Ltd.
- Siuru, B. (2007). *Greener Ships on the Horizon*. Diesel & gas turbine worldwide, Diesel & Gas Turbine Publications. 39: 10-13.
- Smith, J. J. M., H.C. Van Ness, M.M. Abbott (2005). *Introduction to chemical engineering thermodynamics*. Boston, McGraw-Hill.
- Smogeli, Ø. N. (2006). *Control of marine propellers: from normal to extreme conditions*. Trondheim, Norwegian University of Science and Technology, Faculty of

-
- Engineering Science & Technology, Department of Marine Technology.
PhD 2006:187.
- Stapersma, D. (1999). *The potential of gas turbines with complex cycles*. MarPower'99 (Advanced Marine Power conference), Newcastle-upon-Tyne, UK.
- Stiller, C. (2006). *Design, operation and control modelling of SOFC/GT hybrid systems*. Trondheim, Norwegian University of Science and Technology, Faculty of Engineering Science and Technology, Department of Energy and Process Engineering. PhD 2006:28.
- Stiller, C., B. Thorud, et al. (2006). *Control strategy for a solid oxide fuel cell and gas turbine hybrid system*. Journal of Power Sources 158(1): 303-315.
- Sødal, S. (2003). *Fuel cells in shipping: higher capital costs and reduced flexibility*. Bergen, Institute for research in economics and business administration.
- Thoma, J. U. (1971). *Bond graphs for thermal energy transport and entropy flow*. Journal of the Franklin Institute 292(2): 109-120.
- Thoma, J. U. and B. Ould-Bouamama (2000). *Modelling and simulation in thermal and chemical engineering: a bond graph approach*. Berlin ; New York, Springer.
- Thorud, B. (2005). *Dynamic modelling and characterisation of a solid oxide fuel cell integrated in a gas turbine cycle*. Trondheim, Norwegian University of Science and Technology, Faculty of Engineering Science and Technology, Department of Energy and Process Engineering. Doktor Ingeniør 2005:176: XII, 163, [100] s. ill.
- Todd, B. and J. B. Young (2002). *Thermodynamic and transport properties of gases for use in solid oxide fuel cell modelling*. Journal of Power Sources 110(1): 186-200.
- Tronstad, T. and J. Byrknes (2003). *Fuel cells in ships: safety & reliability*. 1st European Hydrogen Energy Conference. Grenoble, France, Association Française de l'Hydrogène.
- Vijay, P., A. K. Samantaray, et al. (2008). *Bond graph model of a solid oxide fuel cell with a C-field for mixture of two gas species*. Proceedings of the Institution of Mechanical Engineers. Part I: Journal of Systems and Control Engineering 222(4): 247-259.
- Wagner, N., W. Schnurnberger, et al. (1998). *Electrochemical impedance spectra of solid-oxide fuel cells and polymer membrane fuel cells*. Electrochimica Acta 43(24): 3785-3793.
- Winkler, W. and H. Lorenz (2002). *The design of stationary and mobile solid oxide fuel cell-gas turbine systems*. Journal of Power Sources 105(2): 222-227.
- Woodward, J. B. and R. G. Latorre (1984). *Modeling of Diesel Engine Transient Behavior in Marine Propulsion Analysis*. SNAME Transactions 92: 33-49.
- WWM. (2008). *Zero emission tug speeds up!* Press release from WorldWide Marine Engineering Retrieved December, 2008, from <http://www.worldwisemarine.com/greentug1.html>.

-
- Xi, H., J. Sun, et al. (2007). *A control oriented low order dynamic model for planar SOFC using minimum Gibbs free energy method*. Journal of Power Sources 165(1): 253-266.
- Young, J. B. (2007). *Thermofluid Modeling of Fuel Cells*. Annual Review of Fluid Mechanics 39(1): 193-215.
- Yuan, J., J. Sun, et al. (2004). *Marine applications of fuel cell technology*. Fuel Cell Science, Engineering and Technology, Rochester, NY, United States, American Society of Mechanical Engineers.
- Zenith, F. and S. Skogestad (2007). *Control of fuel cell power output*. Journal of Process Control 17(4): 333-347.
- Øverli, J. M. (1978). *Strømningsmaskiner (in Norwegian)*. Trondheim, Tapir.
- Ådnes, A. K. (2003). *Maritime electrical installations and diesel electric propulsion*. Tutorial report. Oslo, ABB.

Appendix A

The bond graph method

A bond graph is essentially a mathematical model of the energetic structure of a system presented in a graphical notation form. The elemental physical properties of a system is identified and represented by ideal elements representing sources, accumulation, transfer and dissipation of energy. These elements are connected by graphical lines representing energy flow of the system. Having this graphical representation, a set of first order differential equations for the system can be derived appropriate for numerical simulation. Bond graphs were invented by H.M. Paynter (Paynter 1961) and since developed further mainly by Karnopp and co-workers (Karnopp 2000). A brief introduction to the method is given below, further details can be found in (Karnopp 2000), (Cellier 1991), (Brown 2006) and (Gawthrop and Bevan 2007).

The unifying concept for dynamic systems is the exchange of energy. In a bond graph this exchange is described by graphical lines defined as power bonds. The bond transmits power between two elements instantaneously and without losses, se Figure A.1.

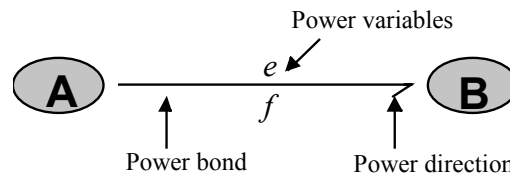


Figure A.1 Power bond between systems A and B

Two variables are needed to accurately define the power transfer between the elements, generally called effort, e , and flow, f . The relation between effort, flow and power, P , is given in (A.1).

$$P(t) = e(t)f(t) \quad (\text{A.1})$$

In a bond graph model the energy, E , is the time integral of power flowing in or out of an element, (A.2). Energy relations within the elements are described by generalised momentum variable, p , and the generalised displacement variable, q , (A.3).

$$E(t) = \int_0^t P(t)dt \quad (\text{A.2})$$

$$p(t) = \int_0^t e(t)dt + p(0) \quad q(t) = \int_0^t f(t)dt + q(0) \quad (\text{A.3})$$

Table A.1 shows the physical energy domains involved in typical power plant systems with identification of the generalised power variables, their symbols and SI units.

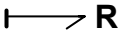
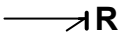
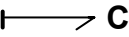
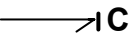
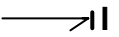
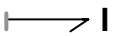

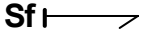




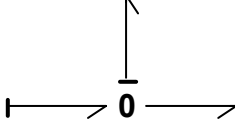
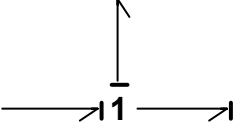
Table A.1 Power variables for different energy domains

Systems	Effort	Flow
Mechanical	Force [N]	Velocity [m/s]
	Torque [Nm]	Angular velocity [rad/s]
Electrical	Voltage [V]	Current [A]
Hydraulic	Pressure [Pa]	Volume flow rate [m ³ /s]
Thermal	Temperature [K]	Entropy change rate [J/Ks]
	Pressure [Pa]	Volume change rate [m ³ /s]
Chemical	Chemical potential [J/mol]	Mole flow rate [mol/s]
Magnetic	Magneto-motive force [A]	Magnetic flux [Wb/s]

Nine basic ideal bond graph elements and their symbols are listed in Table A.2. Energy is supplied to or withdrawn from a system by source elements Se and Sf . Energy storage is counted for by the capacitor element, C , and the inertia element, I . The resistance element, R , handles energy dissipation. The two-port transformer, TF , and gyrator, GY , transmit power instantaneously, often between elements of different energy domains. If more than two elements are connected, the relations between efforts and flows are represented by multi-port θ - and I -junctions. The linear relations between the power variables possible in each element are also given in Table A.2. Nonlinear relations between the generalised variables are also common (except for the junction elements).

No causal information is given from the basic bond graph definition, and bond graphs are essentially an acausal modelling technique. To enable development of mathematical equations from bond graphs in a systematic manner it is possible to apply information about computational causality to the graph. In Table A.2 causal strokes in the form of vertical lines are applied to the power bonds. These lines define which power variable is the input (cause) and which is the output (effect) from an element. The effort variable flows in the direction of the causal stroke. When an input variable is integrated to generate the output we have integral causality. From a physical point of view this is the preferred causality as information about the past is used to calculate the present state. Differential causality causes increased complexity when it comes to simulation and one seek to represent the system with integral causality for all elements.

Table A.2 Basic bond graph elements

Element	Symbol	Causal relations
Resistance		$e = Rf$
		$f = \frac{e}{R}$
Capacitance		$e = \frac{1}{C} \int f dt$
		$f = \frac{d}{dt}(Ce)$
Inertia		$f = I \int e dt$
		$e = \frac{d}{dt}(If)$
Effort source	Se 	$e(t) = \text{given}$
Flow source	Sf 	$f(t) = \text{given}$
Transformer		$e_1 = m e_2, \quad f_2 = m f_1$
		$e_2 = m^{-1} e_1, \quad f_1 = m^{-1} f_2$
Gyrator		$e_1 = r f_2, \quad e_2 = r f_1$
		$f_1 = r^{-1} e_2, \quad f_2 = r^{-1} e_1$
0-junction		$e_1 = e_2, \quad e_3 = e_2$ $f_1 = f_2 + f_3$
1-junction		$f_1 = f_3, \quad f_2 = f_3$ $e_1 = e_2 + e_3$

State space equations are written by finding expression for the derivative of each state variable. According to (A.3) the energy variables p and q are the state variables in a bond graph model and the time derivatives can be found as the effort or flow variable of the bond number i connected to a storage element (A.4). An expression for e and f in terms of the state variables can be found directly from the graph.

$$\dot{p}_i = e_i \quad \dot{q}_i = f_i \quad (\text{A.4})$$

Equations can be written manually, but for larger complex systems software that generates equations automatically is preferred. In this thesis 20-sim (www.20sim.com) is used to generate equations.

Bond graphs are developed mainly for lumped parameter representation of systems, resulting in a set of ordinary differential equations. This method is believed to be appropriate for models used to analyse total system behaviours with interaction over several domains and for control purposes. Bond graphs have also been successfully implemented for system descriptions based on partially differential equations models based, se e.g. (Karnopp 1978), (Engja 1985) and (Fahrenthold and Wargo 1994), extending their applicability to incorporate a distributed system representation.

Appendix B

Model parameters

Symbol	Description	Value	Unit
Fuel cell dimensions			
l_{tube}	length fuel cell tube	1.5	m
$d_{hyd,A}$	hydraulic diameter anode channel	0.001	m
A_A	cross sectional area anode channel	0.000176	m ²
$d_{hyd,C}$	hydraulic diameter cathode channel	0.00932	m
A_C	cross sectional area cathode channel	1.8534 e ⁻⁴	m ²
$d_{hyd,ADT}$	hydraulic diameter ADT	0.005	m
A_{ADT}	cross sectional area anode channel	1.96e ⁻⁵	m ²
$r_{ADT,o}$	outer radius ADT	0.004	m
r_i	inner radius MEA	0.0025	m
Gas volumes in fuel cell			
V_{ADT}	gas volume ADT	2.9e ⁻⁵	m ³
V_{Air}	volume cathode air channel	0.000278	m ³
V_{Fu}	volume anode fuel channel	0.000266	m ³
V_A	estimated volume porous anode	4.1e ⁻⁵	m ³
V_C	estimated volume porous cathode	0.000101	m ³
Chemical reactions			
A_{el}	active surface of the fuel cell	0.0834	m ²
n_e	number of electrons per O ₂ molecule	4	-
F	Faradays number	96485.3	C/mol
ν_{H_2}	TF coefficient to elchem	0.5	-

v_{H_2O}	TF coefficient to elchem	2	-
$k_{f,s}$	coefficient reforming (cell)	1e6	-
$k_{f,r}$	coefficient reforming (reformers)	10000	-
$k_{f,s}$	coefficient reforming (reformers)	10000	-

Loss relations

r_d	degradation coefficient	0	-
$\rho\delta_l$	Product of density and thickness, interconnect	$2e^{-7}$	kg/m ²
l_l	circumferential length interconnect	0.006	m
l_E	circumferential length electrolyte	0.0616	m
δ_E	thickness electrolyte	0.00004	m
δ_A	thickness anode	0.0001	m
δ_C	thickness cathode	0.0022	m
γ_{act}	estimated constant for activation polarisation	$1.956e^{10}$	A/m ²
$\beta_{A/C}$	Butler-Volmer constant, anode and cathode	0.5	-
$E_{act,A}$	activation energy anode	140000	J/mol
γ_C	estimated constant for activation polarisation	$1.026e^{10}$	A/m ²
$E_{act,C}$	activation energy cathode	149000	J/mol
ε_A	porosity anode	0.4	-
τ_A	tortuosity anode	3	-
$r_{p,A}$	pore radius anode	0.00001	m
ε_C	porosity cathode	0.5	-
τ_C	tortuosity cathode	1.5	-
$r_{p,C}$	pore radius cathode	$4e^{-6}$	m
V_{H_2}	diffusion volume hydrogen	6.12	10 ⁻³ m ³
V_{CO}	diffusion volume carbon monoxide	18	10 ⁻³ m ³
V_{CH_4}	diffusion volume methane	25.14	10 ⁻³ m ³
V_{H_2O}	diffusion volume steam	13.1	10 ⁻³ m ³
V_{CO_2}	diffusion volume carbon dioxide	26.9	10 ⁻³ m ³
V_{O_2}	diffusion volume oxygen	16.3	10 ⁻³ m ³
V_{N_2}	diffusion volume nitrogen	18.5	10 ⁻³ m ³
C_{CDL}	CDL coefficient anode and cathode	0.003	F

Material dimensions and properties, heat transfer

V_{MEA}	volume MEA	0.000199	m ³
ρ_{MEA}	density MEA	2809	kg/m ³
$c_{v,MEA}$	heat capacity MEA	376	J/kgK
A_{MEA}	conduction area MEA	0.085	m ²
l_{MEA}	conduction length MEA	0.0023	m
k_{MEA}	thermal conductivity MEA	9.06	W/mK
V_{ADT}	volume ADT	4.6e ⁻⁵	m ³
ρ_{ADT}	density ADT	3970	kg/m ³
$c_{v,ADT}$	heat capacity ADT	1167	J/kgK
Nu_{ADT}	Nusselt number ADT flow	10	-
Nu_C	Nusselt number cathode flow	7	-
Nu_A	Nusselt number anode flow	1.8	-
λ_{Air}	vapour thermal conductivity, air	0.1	W/mK
λ_{Fuel}	vapour thermal conductivity, fuel	1.0	W/mK
ε	radiative emittance, cathode and ADT	0.85	-
σ_B	Boltzmann constant	5.6697e ⁻⁸	W/m ² K ⁴
$A_{conv,Fu,wall}$	area convection fuel to “surroundings”	0.141	m ²
$h_{conv,Fu,wall}$	heat transfer coeff convection fuel to wall	1.4	W/m ² K
$A_{conv,Air,wall}$	area convection air to wall	0.0307	m ²
$d_{conv,Air,wall}$	diameter convection air to wall	0.0022	m
A_{conA_W}	area convection ADT to wall	0.0307	m ²
$d_{conv,ADT,wall}$	diameter convection ADT wall	0.0015	m
$A_{rad,C,ADT}$	area radiation cathode ADT	0.0816	m ²
$A_{conv,Air,C}$	area convection air cathode	0.092	m ²
$d_{conv,Air,C}$	diameter convection air cathode	0.0022	m
$A_{conv,Fu,A}$	area convection fuel anode	0.1032	m ²
$d_{conv,Fu,A}$	diameter convection fuel anode	0.0001	m

Properties heat exchanger

$r_{i,HE}$	inner radius heat exchanger	0.0055	m
l_{HE}	length heat exchanger tube	0.4776	m
λ_{hot}	vapour thermal conductivity, hot	0.15	W/mK
λ_{cold}	vapour thermal conductivity, cold	0.1	W/mK

K	coefficient heat exchanger	10	-
$V_{Air,HE}$	air volume heat exchanger	0.0108	m ³
$V_{Exh,HE}$	exhaust volume heat exchanger	0.02463	m ³
k_{HE}	thermal conductivity heat exchanger	11.8	W/mK
Nu_{Exh}	Nusselt number exhaust tube	10	-
Nu_{Air}	Nusselt number air tube	4.364	-

Plant properties

N_{cells}	number of cells in stack	1152	-
N_{ref}	number of indirect internal reformers	16	-
V_{I_ref}	volume internal prereformer	0.018	m ³
V_{E_ref}	volume external prereformer	0.008	m ³
V	volumes splitter, burner and air pipe -estimate	0.001	m ³

Appendix C

Thermodynamic relations

Solid oxide fuel cells operate with constant volume and at pressure and temperatures that allow for using the ideal gas assumption to relate thermodynamic state variables according to the relation of equation (C.1) where R is the gas constant of the mixture. This is confirmed in (Todd and Young 2002).

$$\begin{aligned} pV &= mRT \\ T &= \frac{Q}{c_v(T)m} \end{aligned} \quad (C.1)$$

Disregarding start-up and shut-down that requires special procedures a SOFC system operates in a limited temperature and pressure area. The model is therefore implemented based on the perfect gas assumption. This means that constant heat capacities around the operating temperature are also assumed, avoiding the iterative temperature equation (perfect gas).

C.1 Thermal properties

The basic parameters are taken from tabulated values (Chase, Davies et al. 1986) and by applying general mixing rules for ideal gas mixtures. The reference state for all thermal properties are chosen at $T=0K$ and $p=0.1MPa$.

The enthalpy or total heat content of a gas flow component is expressed by eq. (C.2). It includes the enthalpy of formation, h_f , at the reference state, the enthalpy change, Δh , from the reference state and the heat capacity, c_p , from tabulated values at the temperature T_{0h} (in this case 1200K).

$$\begin{aligned} h_i &= h_{f,i}^0 + \Delta h_i(T_{0h}) + c_{p,i}(T_{0h})(T - T_{0h}) \\ h_{mix} &= \sum_{i=1}^{n_c} y_i h_i \quad [J / mol] \end{aligned} \quad (C.2)$$

The entropy is used in order to find the energy fraction not obtainable as work from a gas flow component. For a component in a gas mixture the entropy can be found according to eq. (C.3).

$$\begin{aligned}
s_i(T, p_{ref}) &= s_i(T_{ref}, p_{ref}) + \int_{T_{ref}}^T \frac{c_{pi}}{T} dT \\
s_i(T, p) &= s_i(T, p_{ref}) - R_m \ln \frac{y_i p}{p_{ref}} \\
\Rightarrow s_i(T, p) &= s(T_{0h}, p_{ref}) + c_p(T_{0h}) \ln \frac{T}{T_{0h}} - R_m \ln \frac{y_i p}{p_{ref}}
\end{aligned} \tag{C.3}$$

Gibbs energy or chemical potential describes the maximum available work from a chemical or electrochemical reaction involving the specific component. It can be found by eq. (C.4).

$$g_i = h_i - Ts_i = \mu_i \tag{C.4}$$

Where required density is found by using the ideal gas law, eq. (C.5).

$$\left. \begin{aligned} pV &= mRT \\ \rho &= m/V \end{aligned} \right\} \Rightarrow \rho = \frac{p}{T \sum_{i=1}^N c_i R_i} \tag{C.5}$$

The method of Wilke, equation (C.6), is used to find the viscosity in a gas mixture (Poling2001). No significant variation in the viscosity is experienced in the model, but it is still implemented as a variable in the elements inside the fuel cell. For other components it is assumed constant.

$$\begin{aligned}
\mu_m &= \frac{\sum_{i=1}^n y_i \mu_i}{\sum_{j=1}^n y_j \phi_{ij}} = \frac{\sum_{i=1}^n \mu_i}{1 + \frac{1}{y_i} \sum_{j=1, j \neq i}^n y_j \phi_{ij}} \\
\phi_{ij} &= \frac{[1 + (\mu_i / \mu_j)^{1/2} (M_j / M_i)^{1/4}]^2}{[8(1 + (M_i / M_j))]^{1/2}}
\end{aligned} \tag{C.6}$$

Thermal conductivity is used in the heat transfer equations. The Wassiljewa equation with the modification of Mason and Saxena (Poling, O'Connell et al. 2001) can be used to express the conductivity of a gas mixture, eq. (C.7). In the present model the small conductivity changes had no significant impact on the overall heat transfer. The conductivities were therefore taken as constants estimated by finding the result of eq. (C.7) at different operating conditions.

$$\begin{aligned}
\lambda_m &= \frac{\sum_{i=1}^n y_i \lambda_i}{\sum_{j=1}^n y_j \phi_{ij}} = \frac{\sum_{i=1}^n \lambda_i}{1 + \frac{1}{y_i} \sum_{j=1, j \neq i}^n y_j \phi_{ij}} \\
\phi_{ij} &= \frac{\varepsilon [1 + (\lambda_i / \lambda_j)^{1/2} (M_j / M_i)^{1/4}]^2}{[8(1 + (M_i / M_j))]^{1/2}}
\end{aligned} \tag{C.7}$$

As the thermal properties are expressed on a molar basis while the mass flow is used as a system variable some general relations are frequently in use, eq. (C.8).

$$c_i = \frac{m_i}{m} \quad n_i = \frac{m_i}{M_i} \quad (C.8)$$

$$y_i = \frac{n_i}{n} = c_i \frac{1}{M_i \sum_{j=1}^N (c_j / M_j)}$$

Table C.1 Thermodynamic parameters used in simulations

Gas Comp.	M kg/mol	R J/kgK	$c_p(T_{0h})$ J/molK	$c_v(T_{0h})$ J/kgK	$s(T_{0h}, p_{ref})$ J/molK	$-h_f \theta$ J/mol	$\Delta h(T_{0h})$ J/mol	μ kg/ms
H_2	0,002016	4120	30,992	11238	171,79	0	35264	2,25
CO	0,02801	297	34,175	923	240,679	113805	37101	4,04
CH_4	0,016043	518	78,833	4396	261,287	66911	63294	2,01
H_2O	0,018015	461	43,768	1967	240,485	238921	44410	4,51
CO_2	0,044009	189	56,342	1091	279,39	393151	53837	4,17
O_2	0,032	260	35,667	855	250,01	0	38444	4,92
N_2	0,02802	297	33,723	907	234,226	0	36779	4,68
								*10 ⁻⁵
$p_{ref} = 1 \text{ bar}$		$T_{ref} = 0 \text{ K}$			$R_m = 8,314 \text{ J/molK}$			

R A P P O R T E R
UTGITT VED
INSTITUTT FOR MARIN TEKNIKK
(tidligere: FAKULTET FOR MARIN TEKNIKK)
NORGES TEKNISK-NATURVITENSKAPELIGE UNIVERSITET

Report No.	Author	Title
	Kavlie, Dag	Optimization of Plane Elastic Grillages, 1967
	Hansen, Hans R.	Man-Machine Communication and Data-Storage Methods in Ship Structural Design, 1971
	Gisvold, Kaare M.	A Method for non-linear mixed -integer programming and its Application to Design Problems, 1971
	Lund, Sverre	Tanker Frame Optimalization by means of SUMT-Transformation and Behaviour Models, 1971
	Vinje, Tor	On Vibration of Spherical Shells Interacting with Fluid, 1972
	Lorentz, Jan D.	Tank Arrangement for Crude Oil Carriers in Accordance with the new Anti-Pollution Regulations, 1975
	Carlsen, Carl A.	Computer-Aided Design of Tanker Structures, 1975
	Larsen, Carl M.	Static and Dynamic Analysis of Offshore Pipelines during Installation, 1976
UR-79-01	Brigt Hatlestad, MK	The finite element method used in a fatigue evaluation of fixed offshore platforms. (Dr.Ing. Thesis)
UR-79-02	Erik Pettersen, MK	Analysis and design of cellular structures. (Dr.Ing. Thesis)
UR-79-03	Sverre Valsgård, MK	Finite difference and finite element methods applied to nonlinear analysis of plated structures. (Dr.Ing. Thesis)
UR-79-04	Nils T. Nordsve, MK	Finite element collapse analysis of structural members considering imperfections and stresses due to fabrication. (Dr.Ing. Thesis)
UR-79-05	Ivar J. Fylling, MK	Analysis of towline forces in ocean towing systems. (Dr.Ing. Thesis)
UR-80-06	Nils Sandsmark, MM	Analysis of Stationary and Transient Heat Conduction by the Use of the Finite Element Method. (Dr.Ing. Thesis)
UR-80-09	Sverre Haver, MK	Analysis of uncertainties related to the stochastic modeling of ocean waves. (Dr.Ing. Thesis)
UR-81-15	Odland, Jonas	On the Strength of welded Ring stiffened cylindrical Shells primarily subjected to axial Compression

UR-82-17	Engesvik, Knut	Analysis of Uncertainties in the fatigue Capacity of Welded Joints
UR-82-18	Rye, Henrik	Ocean wave groups
UR-83-30	Eide, Oddvar Inge	On Cumulative Fatigue Damage in Steel Welded Joints
UR-83-33	Mo, Olav	Stochastic Time Domain Analysis of Slender Offshore Structures
UR-83-34	Amdahl, Jørgen	Energy absorption in Ship-platform impacts
UR-84-37	Mørch, Morten	Motions and mooring forces of semi submersibles as determined by full-scale measurements and theoretical analysis
UR-84-38	Soares, C. Guedes	Probabilistic models for load effects in ship structures
UR-84-39	Aarsnes, Jan V.	Current forces on ships
UR-84-40	Czujko, Jerzy	Collapse Analysis of Plates subjected to Biaxial Compression and Lateral Load
UR-85-46	Alf G. Engseth, MK	Finite element collapse analysis of tubular steel offshore structures. (Dr.Ing. Thesis)
UR-86-47	Dengody Sheshappa, MP	A Computer Design Model for Optimizing Fishing Vessel Designs Based on Techno-Economic Analysis. (Dr.Ing. Thesis)
UR-86-48	Vidar Aanesland, MH	A Theoretical and Numerical Study of Ship Wave Resistance. (Dr.Ing. Thesis)
UR-86-49	Heinz-Joachim Wessel, MK	Fracture Mechanics Analysis of Crack Growth in Plate Girders. (Dr.Ing. Thesis)
UR-86-50	Jon Taby, MK	Ultimate and Post-ultimate Strength of Dented Tubular Members. (Dr.Ing. Thesis)
UR-86-51	Walter Lian, MH	A Numerical Study of Two-Dimensional Separated Flow Past Bluff Bodies at Moderate KC-Numbers. (Dr.Ing. Thesis)
UR-86-52	Bjørn Sortland, MH	Force Measurements in Oscillating Flow on Ship Sections and Circular Cylinders in a U-Tube Water Tank. (Dr.Ing. Thesis)
UR-86-53	Kurt Strand, MM	A System Dynamic Approach to One-dimensional Fluid Flow. (Dr.Ing. Thesis)
UR-86-54	Arne Edvin Løken, MH	Three Dimensional Second Order Hydrodynamic Effects on Ocean Structures in Waves. (Dr.Ing. Thesis)
UR-86-55	Sigurd Falch, MH	A Numerical Study of Slamming of Two-Dimensional Bodies. (Dr.Ing. Thesis)
UR-87-56	Arne Braathen, MH	Application of a Vortex Tracking Method to the Prediction of Roll Damping of a Two-Dimension

		Floating Body. (Dr.Ing. Thesis)
UR-87-57	Bernt Leira, MK	Gaussian Vector Processes for Reliability Analysis involving Wave-Induced Load Effects. (Dr.Ing. Thesis)
UR-87-58	Magnus Småvik, MM	Thermal Load and Process Characteristics in a Two-Stroke Diesel Engine with Thermal Barriers (in Norwegian). (Dr.Ing. Thesis)
MTA-88-59	Bernt Arild Bremdal, MP	An Investigation of Marine Installation Processes – A Knowledge - Based Planning Approach. (Dr.Ing. Thesis)
MTA-88-60	Xu Jun, MK	Non-linear Dynamic Analysis of Space-framed Offshore Structures. (Dr.Ing. Thesis)
MTA-89-61	Gang Miao, MH	Hydrodynamic Forces and Dynamic Responses of Circular Cylinders in Wave Zones. (Dr.Ing. Thesis)
MTA-89-62	Martin Greenhow, MH	Linear and Non-Linear Studies of Waves and Floating Bodies. Part I and Part II. (Dr.Techn. Thesis)
MTA-89-63	Chang Li, MH	Force Coefficients of Spheres and Cubes in Oscillatory Flow with and without Current. (Dr.Ing. Thesis)
MTA-89-64	Hu Ying, MP	A Study of Marketing and Design in Development of Marine Transport Systems. (Dr.Ing. Thesis)
MTA-89-65	Arild Jæger, MH	Seakeeping, Dynamic Stability and Performance of a Wedge Shaped Planing Hull. (Dr.Ing. Thesis)
MTA-89-66	Chan Siu Hung, MM	The dynamic characteristics of tilting-pad bearings
MTA-89-67	Kim Wikstrøm, MP	Analysis av projekteringen for ett offshore projekt. (Licenciat-avhandling)
MTA-89-68	Jiao Guoyang, MK	Reliability Analysis of Crack Growth under Random Loading, considering Model Updating. (Dr.Ing. Thesis)
MTA-89-69	Arnt Olufsen, MK	Uncertainty and Reliability Analysis of Fixed Offshore Structures. (Dr.Ing. Thesis)
MTA-89-70	Wu Yu-Lin, MR	System Reliability Analyses of Offshore Structures using improved Truss and Beam Models. (Dr.Ing. Thesis)
MTA-90-71	Jan Roger Hoff, MH	Three-dimensional Green function of a vessel with forward speed in waves. (Dr.Ing. Thesis)
MTA-90-72	Rong Zhao, MH	Slow-Drift Motions of a Moored Two-Dimensional Body in Irregular Waves. (Dr.Ing. Thesis)
MTA-90-73	Atle Minsaas, MP	Economical Risk Analysis. (Dr.Ing. Thesis)
MTA-90-74	Knut-Aril Farnes, MK	Long-term Statistics of Response in Non-linear Marine Structures. (Dr.Ing. Thesis)
MTA-90-	Torbjørn Sotberg, MK	Application of Reliability Methods for Safety

75		Assessment of Submarine Pipelines. (Dr.Ing. Thesis)
MTA-90-76	Zeuthen, Steffen, MP	SEAMAID. A computational model of the design process in a constraint-based logic programming environment. An example from the offshore domain. (Dr.Ing. Thesis)
MTA-91-77	Haagensen, Sven, MM	Fuel Dependant Cyclic Variability in a Spark Ignition Engine - An Optical Approach. (Dr.Ing. Thesis)
MTA-91-78	Løland, Geir, MH	Current forces on and flow through fish farms. (Dr.Ing. Thesis)
MTA-91-79	Hoen, Christopher, MK	System Identification of Structures Excited by Stochastic Load Processes. (Dr.Ing. Thesis)
MTA-91-80	Haugen, Stein, MK	Probabilistic Evaluation of Frequency of Collision between Ships and Offshore Platforms. (Dr.Ing. Thesis)
MTA-91-81	Sødahl, Nils, MK	Methods for Design and Analysis of Flexible Risers. (Dr.Ing. Thesis)
MTA-91-82	Ormberg, Harald, MK	Non-linear Response Analysis of Floating Fish Farm Systems. (Dr.Ing. Thesis)
MTA-91-83	Marley, Mark J., MK	Time Variant Reliability under Fatigue Degradation. (Dr.Ing. Thesis)
MTA-91-84	Krokstad, Jørgen R., MH	Second-order Loads in Multidirectional Seas. (Dr.Ing. Thesis)
MTA-91-85	Molteberg, Gunnar A., MM	The Application of System Identification Techniques to Performance Monitoring of Four Stroke Turbocharged Diesel Engines. (Dr.Ing. Thesis)
MTA-92-86	Mørch, Hans Jørgen Bjelke, MH	Aspects of Hydrofoil Design: with Emphasis on Hydrofoil Interaction in Calm Water. (Dr.Ing. Thesis)
MTA-92-87	Chan Siu Hung, MM	Nonlinear Analysis of Rotordynamic Instabilities in Highspeed Turbomachinery. (Dr.Ing. Thesis)
MTA-92-88	Bessason, Bjarni, MK	Assessment of Earthquake Loading and Response of Seismically Isolated Bridges. (Dr.Ing. Thesis)
MTA-92-89	Langli, Geir, MP	Improving Operational Safety through exploitation of Design Knowledge - an investigation of offshore platform safety. (Dr.Ing. Thesis)
MTA-92-90	Sævik, Svein, MK	On Stresses and Fatigue in Flexible Pipes. (Dr.Ing. Thesis)
MTA-92-91	Ask, Tor Ø., MM	Ignition and Flame Growth in Lean Gas-Air Mixtures. An Experimental Study with a Schlieren System. (Dr.Ing. Thesis)
MTA-86-92	Hessen, Gunnar, MK	Fracture Mechanics Analysis of Stiffened Tubular

		Members. (Dr.Ing. Thesis)
MTA-93-93	Steinebach, Christian, MM	Knowledge Based Systems for Diagnosis of Rotating Machinery. (Dr.Ing. Thesis)
MTA-93-94	Dalane, Jan Inge, MK	System Reliability in Design and Maintenance of Fixed Offshore Structures. (Dr.Ing. Thesis)
MTA-93-95	Steen, Sverre, MH	Cobblestone Effect on SES. (Dr.Ing. Thesis)
MTA-93-96	Karunakaran, Daniel, MK	Nonlinear Dynamic Response and Reliability Analysis of Drag-dominated Offshore Platforms. (Dr.Ing. Thesis)
MTA-93-97	Hagen, Arnulf, MP	The Framework of a Design Process Language. (Dr.Ing. Thesis)
MTA-93-98	Nordrik, Rune, MM	Investigation of Spark Ignition and Autoignition in Methane and Air Using Computational Fluid Dynamics and Chemical Reaction Kinetics. A Numerical Study of Ignition Processes in Internal Combustion Engines. (Dr.Ing. Thesis)
MTA-94-99	Passano, Elizabeth, MK	Efficient Analysis of Nonlinear Slender Marine Structures. (Dr.Ing. Thesis)
MTA-94-100	Kvålsvold, Jan, MH	Hydroelastic Modelling of Wetdeck Slamming on Multihull Vessels. (Dr.Ing. Thesis)
MTA-94-102	Bech, Sidsel M., MK	Experimental and Numerical Determination of Stiffness and Strength of GRP/PVC Sandwich Structures. (Dr.Ing. Thesis)
MTA-95-103	Paulsen, Hallvard, MM	A Study of Transient Jet and Spray using a Schlieren Method and Digital Image Processing. (Dr.Ing. Thesis)
MTA-95-104	Hovde, Geir Olav, MK	Fatigue and Overload Reliability of Offshore Structural Systems, Considering the Effect of Inspection and Repair. (Dr.Ing. Thesis)
MTA-95-105	Wang, Xiaozhi, MK	Reliability Analysis of Production Ships with Emphasis on Load Combination and Ultimate Strength. (Dr.Ing. Thesis)
MTA-95-106	Ulstein, Tore, MH	Nonlinear Effects of a Flexible Stern Seal Bag on Cobblestone Oscillations of an SES. (Dr.Ing. Thesis)
MTA-95-107	Solaas, Frøydis, MH	Analytical and Numerical Studies of Sloshing in Tanks. (Dr.Ing. Thesis)
MTA-95-108	Hellan, Øyvind, MK	Nonlinear Pushover and Cyclic Analyses in Ultimate Limit State Design and Reassessment of Tubular Steel Offshore Structures. (Dr.Ing. Thesis)
MTA-95-109	Hermundstad, Ole A., MK	Theoretical and Experimental Hydroelastic Analysis of High Speed Vessels. (Dr.Ing. Thesis)
MTA-96-110	Bratland, Anne K., MH	Wave-Current Interaction Effects on Large-Volume Bodies in Water of Finite Depth. (Dr.Ing. Thesis)

MTA-96-111	Herfjord, Kjell, MH	A Study of Two-dimensional Separated Flow by a Combination of the Finite Element Method and Navier-Stokes Equations. (Dr.Ing. Thesis)
MTA-96-112	Æsøy, Vilmar, MM	Hot Surface Assisted Compression Ignition in a Direct Injection Natural Gas Engine. (Dr.Ing. Thesis)
MTA-96-113	Eknes, Monika L., MK	Escalation Scenarios Initiated by Gas Explosions on Offshore Installations. (Dr.Ing. Thesis)
MTA-96-114	Erikstad, Stein O., MP	A Decision Support Model for Preliminary Ship Design. (Dr.Ing. Thesis)
MTA-96-115	Pedersen, Egil, MH	A Nautical Study of Towed Marine Seismic Streamer Cable Configurations. (Dr.Ing. Thesis)
MTA-97-116	Moksnes, Paul O., MM	Modelling Two-Phase Thermo-Fluid Systems Using Bond Graphs. (Dr.Ing. Thesis)
MTA-97-117	Halse, Karl H., MK	On Vortex Shedding and Prediction of Vortex-Induced Vibrations of Circular Cylinders. (Dr.Ing. Thesis)
MTA-97-118	Igland, Ragnar T., MK	Reliability Analysis of Pipelines during Laying, considering Ultimate Strength under Combined Loads. (Dr.Ing. Thesis)
MTA-97-119	Pedersen, Hans-P., MP	Levendefiskteknologi for fiskefartøy. (Dr.Ing. Thesis)
MTA-98-120	Vikestad, Kyrre, MK	Multi-Frequency Response of a Cylinder Subjected to Vortex Shedding and Support Motions. (Dr.Ing. Thesis)
MTA-98-121	Azadi, Mohammad R. E., MK	Analysis of Static and Dynamic Pile-Soil-Jacket Behaviour. (Dr.Ing. Thesis)
MTA-98-122	Ulltang, Terje, MP	A Communication Model for Product Information. (Dr.Ing. Thesis)
MTA-98-123	Torbergesen, Erik, MM	Impeller/Diffuser Interaction Forces in Centrifugal Pumps. (Dr.Ing. Thesis)
MTA-98-124	Hansen, Edmond, MH	A Discrete Element Model to Study Marginal Ice Zone Dynamics and the Behaviour of Vessels Moored in Broken Ice. (Dr.Ing. Thesis)
MTA-98-125	Videiro, Paulo M., MK	Reliability Based Design of Marine Structures. (Dr.Ing. Thesis)
MTA-99-126	Mainçon, Philippe, MK	Fatigue Reliability of Long Welds Application to Titanium Risers. (Dr.Ing. Thesis)
MTA-99-127	Haugen, Elin M., MH	Hydroelastic Analysis of Slamming on Stiffened Plates with Application to Catamaran Wetdecks. (Dr.Ing. Thesis)
MTA-99-128	Langhelle, Nina K., MK	Experimental Validation and Calibration of Nonlinear Finite Element Models for Use in Design of Aluminium Structures Exposed to Fire. (Dr.Ing. Thesis)

		Thesis)
MTA-99-129	Berstad, Are J., MK	Calculation of Fatigue Damage in Ship Structures. (Dr.Ing. Thesis)
MTA-99-130	Andersen, Trond M., MM	Short Term Maintenance Planning. (Dr.Ing. Thesis)
MTA-99-131	Tveiten, Bård Wathne, MK	Fatigue Assessment of Welded Aluminium Ship Details. (Dr.Ing. Thesis)
MTA-99-132	Søreide, Fredrik, MP	Applications of underwater technology in deep water archaeology. Principles and practice. (Dr.Ing. Thesis)
MTA-99-133	Tønnessen, Rune, MH	A Finite Element Method Applied to Unsteady Viscous Flow Around 2D Blunt Bodies With Sharp Corners. (Dr.Ing. Thesis)
MTA-99-134	Elvekrok, Dag R., MP	Engineering Integration in Field Development Projects in the Norwegian Oil and Gas Industry. The Supplier Management of Norne. (Dr.Ing. Thesis)
MTA-99-135	Fagerholt, Kjetil, MP	Optimeringsbaserte Metoder for Ruteplanlegging innen skipsfart. (Dr.Ing. Thesis)
MTA-99-136	Bysveen, Marie, MM	Visualization in Two Directions on a Dynamic Combustion Rig for Studies of Fuel Quality. (Dr.Ing. Thesis)
MTA-2000-137	Storteig, Eskild, MM	Dynamic characteristics and leakage performance of liquid annular seals in centrifugal pumps. (Dr.Ing. Thesis)
MTA-2000-138	Sagli, Gro, MK	Model uncertainty and simplified estimates of long term extremes of hull girder loads in ships. (Dr.Ing. Thesis)
MTA-2000-139	Tronstad, Harald, MK	Nonlinear analysis and design of cable net structures like fishing gear based on the finite element method. (Dr.Ing. Thesis)
MTA-2000-140	Kroneberg, André, MP	Innovation in shipping by using scenarios. (Dr.Ing. Thesis)
MTA-2000-141	Haslum, Herbjørn Alf, MH	Simplified methods applied to nonlinear motion of spar platforms. (Dr.Ing. Thesis)
MTA-2001-142	Samdal, Ole Johan, MM	Modelling of Degradation Mechanisms and Stressor Interaction on Static Mechanical Equipment Residual Lifetime. (Dr.Ing. Thesis)
MTA-2001-143	Baarholm, Rolf Jarle, MH	Theoretical and experimental studies of wave impact underneath decks of offshore platforms. (Dr.Ing. Thesis)
MTA-2001-144	Wang, Lihua, MK	Probabilistic Analysis of Nonlinear Wave-induced Loads on Ships. (Dr.Ing. Thesis)
MTA-2001-145	Kristensen, Odd H. Holt, MK	Ultimate Capacity of Aluminium Plates under Multiple Loads, Considering HAZ Properties. (Dr.Ing. Thesis)

MTA-2001-146	Greco, Marilena, MH	A Two-Dimensional Study of Green-Water Loading. (Dr.Ing. Thesis)
MTA-2001-147	Heggelund, Svein E., MK	Calculation of Global Design Loads and Load Effects in Large High Speed Catamarans. (Dr.Ing. Thesis)
MTA-2001-148	Babalola, Olusegun T., MK	Fatigue Strength of Titanium Risers – Defect Sensitivity. (Dr.Ing. Thesis)
MTA-2001-149	Mohammed, Abuu K., MK	Nonlinear Shell Finite Elements for Ultimate Strength and Collapse Analysis of Ship Structures. (Dr.Ing. Thesis)
MTA-2002-150	Holmedal, Lars E., MH	Wave-current interactions in the vicinity of the sea bed. (Dr.Ing. Thesis)
MTA-2002-151	Rognebakke, Olav F., MH	Sloshing in rectangular tanks and interaction with ship motions. (Dr.Ing. Thesis)
MTA-2002-152	Lader, Pål Furset, MH	Geometry and Kinematics of Breaking Waves. (Dr.Ing. Thesis)
MTA-2002-153	Yang, Qinzhen, MH	Wash and wave resistance of ships in finite water depth. (Dr.Ing. Thesis)
MTA-2002-154	Melhus, Øyvind, MM	Utilization of VOC in Diesel Engines. Ignition and combustion of VOC released by crude oil tankers. (Dr.Ing. Thesis)
MTA-2002-155	Ronæss, Marit, MH	Wave Induced Motions of Two Ships Advancing on Parallel Course. (Dr.Ing. Thesis)
MTA-2002-156	Økland, Ole D., MK	Numerical and experimental investigation of whipping in twin hull vessels exposed to severe wet deck slamming. (Dr.Ing. Thesis)
MTA-2002-157	Ge, Chunhua, MK	Global Hydroelastic Response of Catamarans due to Wet Deck Slamming. (Dr.Ing. Thesis)
MTA-2002-158	Byklum, Eirik, MK	Nonlinear Shell Finite Elements for Ultimate Strength and Collapse Analysis of Ship Structures. (Dr.Ing. Thesis)
IMT-2003-1	Chen, Haibo, MK	Probabilistic Evaluation of FPSO-Tanker Collision in Tandem Offloading Operation. (Dr.Ing. Thesis)
IMT-2003-2	Skaugset, Kjetil Bjørn, MK	On the Suppression of Vortex Induced Vibrations of Circular Cylinders by Radial Water Jets. (Dr.Ing. Thesis)
IMT-2003-3	Chezian, Muthu	Three-Dimensional Analysis of Slamming. (Dr.Ing. Thesis)
IMT-2003-4	Buhaug, Øyvind	Deposit Formation on Cylinder Liner Surfaces in Medium Speed Engines. (Dr.Ing. Thesis)
IMT-2003-5	Tregde, Vidar	Aspects of Ship Design: Optimization of Aft Hull with Inverse Geometry Design. (Dr.Ing. Thesis)
IMT-2003-6	Wist, Hanne Therese	Statistical Properties of Successive Ocean Wave

		Parameters. (Dr.Ing. Thesis)
IMT-2004-7	Ransau, Samuel	Numerical Methods for Flows with Evolving Interfaces. (Dr.Ing. Thesis)
IMT-2004-8	Soma, Torkel	Blue-Chip or Sub-Standard. A data interrogation approach of identity safety characteristics of shipping organization. (Dr.Ing. Thesis)
IMT-2004-9	Ersdal, Svein	An experimental study of hydrodynamic forces on cylinders and cables in near axial flow. (Dr.Ing. Thesis)
IMT-2005-10	Brodtkorb, Per Andreas	The Probability of Occurrence of Dangerous Wave Situations at Sea. (Dr.Ing. Thesis)
IMT-2005-11	Yttervik, Rune	Ocean current variability in relation to offshore engineering. (Dr.Ing. Thesis)
IMT-2005-12	Fredheim, Arne	Current Forces on Net-Structures. (Dr.Ing. Thesis)
IMT-2005-13	Heggernes, Kjetil	Flow around marine structures. (Dr.Ing. Thesis)
IMT-2005-14	Fouques, Sebastien	Lagrangian Modelling of Ocean Surface Waves and Synthetic Aperture Radar Wave Measurements. (Dr.Ing. Thesis)
IMT-2006-15	Holm, Håvard	Numerical calculation of viscous free surface flow around marine structures. (Dr.Ing. Thesis)
IMT-2006-16	Bjørheim, Lars G.	Failure Assessment of Long Through Thickness Fatigue Cracks in Ship Hulls. (Dr.Ing. Thesis)
IMT-2006-17	Hansson, Lisbeth	Safety Management for Prevention of Occupational Accidents. (Dr.Ing. Thesis)
IMT-2006-18	Zhu, Xinying	Application of the CIP Method to Strongly Nonlinear Wave-Body Interaction Problems. (Dr.Ing. Thesis)
IMT-2006-19	Reite, Karl Johan	Modelling and Control of Trawl Systems. (Dr.Ing. Thesis)
IMT-2006-20	Smogeli, Øyvind Notland	Control of Marine Propellers. From Normal to Extreme Conditions. (Dr.Ing. Thesis)
IMT-2007-21	Storhaug, Gaute	Experimental Investigation of Wave Induced Vibrations and Their Effect on the Fatigue Loading of Ships. (Dr.Ing. Thesis)
IMT-2007-22	Sun, Hui	A Boundary Element Method Applied to Strongly Nonlinear Wave-Body Interaction Problems. (PhD Thesis, CeSOS)
IMT-2007-23	Rustad, Anne Marthine	Modelling and Control of Top Tensioned Risers. (PhD Thesis, CeSOS)
IMT-2007-24	Johansen, Vegar	Modelling flexible slender system for real-time simulations and control applications
IMT-2007-25	Wroldsen, Anders Sunde	Modelling and control of tensegrity structures. (PhD

		Thesis, CeSOS)
IMT-2007-26	Aronsen, Kristoffer Høye	An experimental investigation of in-line and combined inline and cross flow vortex induced vibrations. (Dr. avhandling, IMT)
IMT-2007-27	Gao, Zhen	Stochastic Response Analysis of Mooring Systems with Emphasis on Frequency-domain Analysis of Fatigue due to Wide-band Response Processes (PhD Thesis, CeSOS)
IMT-2007-28	Thorstensen, Tom Anders	Lifetime Profit Modelling of Ageing Systems Utilizing Information about Technical Condition. (Dr.ing. thesis, IMT)
IMT-2008-29	Berntsen, Per Ivar B.	Structural Reliability Based Position Mooring. (PhD-Thesis, IMT)
IMT-2008-30	Ye, Naiquan	Fatigue Assessment of Aluminium Welded Box-stiffener Joints in Ships (Dr.ing. thesis, IMT)
IMT-2008-31	Radan, Damir	Integrated Control of Marine Electrical Power Systems. (PhD-Thesis, IMT)
IMT-2008-32	Thomassen, Paul	Methods for Dynamic Response Analysis and Fatigue Life Estimation of Floating Fish Cages. (Dr.ing. thesis, IMT)
IMT-2008-33	Pákozdi, Csaba	A Smoothed Particle Hydrodynamics Study of Two-dimensional Nonlinear Sloshing in Rectangular Tanks. (Dr.ing.thesis, IMT)
IMT-2007-34	Grytøyr, Guttorm	A Higher-Order Boundary Element Method and Applications to Marine Hydrodynamics. (Dr.ing.thesis, IMT)
IMT-2008-35	Drummen, Ingo	Experimental and Numerical Investigation of Nonlinear Wave-Induced Load Effects in Containerships considering Hydroelasticity. (PhD thesis, CeSOS)
IMT-2008-36	Skejjic, Renato	Maneuvering and Seakeeping of a Singel Ship and of Two Ships in Interaction. (PhD-Thesis, CeSOS)
IMT-2008-37	Harlem, Alf	An Age-Based Replacement Model for Repairable Systems with Attention to High-Speed Marine Diesel Engines. (PhD-Thesis, IMT)
IMT-2008-38	Alsos, Hagbart S.	Ship Grounding. Analysis of Ductile Fracture, Bottom Damage and Hull Girder Response. (PhD-thesis, IMT)
IMT-2008-39	Graczyk, Mateusz	Experimental Investigation of Sloshing Loading and Load Effects in Membrane LNG Tanks Subjected to Random Excitation. (PhD-thesis, CeSOS)
IMT-2008-40	Taghipour, Reza	Efficient Prediction of Dynamic Response for Flexible amd Multi-body Marine Structures. (PhD-thesis, CeSOS)
IMT-2008-41	Ruth, Eivind	Propulsion control and thrust allocation on marine vessels. (PhD thesis, CeSOS)

IMT-2008-42	Nystad, Bent Helge	Technical Condition Indexes and Remaining Useful Life of Aggregated Systems. PhD thesis, IMT
IMT-2008-43	Soni, Prashant Kumar	Hydrodynamic Coefficients for Vortex Induced Vibrations of Flexible Beams, PhD thesis, CeSOS
IMT-2009-43	Amlashi, Hadi K.K.	Ultimate Strength and Reliability-based Design of Ship Hulls with Emphasis on Combined Global and Local Loads. PhD Thesis, IMT
IMT-2009-44	Pedersen, Tom Arne	Bond Graph Modelling of Marine Power Systems. PhD Thesis, IMT
IMT-2009-45	Kristiansen, Trygve	Two-Dimensional Numerical and Experimental Studies of Piston-Mode Resonance. PhD-Thesis, CeSOS
IMT-2009-46	Ong, Muk Chen	Applications of a Standard High Reynolds Number Model and a Stochastic Scour Prediction Model for Marine Structures. PhD-thesis, IMT
IMT-2009-47	Hong, Lin	Simplified Analysis and Design of Ships subjected to Collision and Grounding. PhD-thesis, IMT
IMT-2009-48	Koushan, Kamran	Vortex Induced Vibrations of Free Span Pipelines, PhD thesis, IMT
IMT-2009-49	Korsvik, Jarl Eirik	Heuristic Methods for Ship Routing and Scheduling. PhD-thesis, IMT
IMT-2009-50	Lee, Jihoon	Experimental Investigation and Numerical in Analyzing the Ocean Current Displacement of Longlines. Ph.d.-Thesis, IMT.
IMT-2009-50	Vestbøstad, Tone Gran	A Numerical Study of Wave-in-Deck Impact usin a Two-Dimensional Constrained Interpolation Profile Method, Ph.d.thesis, CeSOS.